

# Development of a vital signs monitoring wireless ear probe

by  
André Bestbier

*Thesis presented in partial fulfilment of the requirements for the degree  
of Master of Engineering (Mechatronic) in the Faculty of Engineering at  
Stellenbosch University*



Supervisor: Prof. Pieter Rousseau Fourie

December 2017

# Declaration

By submitting this thesis electronically, I declare that the entirety of the work contained therein is my own, original work, that I am the sole author thereof (save to the extent explicitly otherwise stated), that reproduction and publication thereof by Stellenbosch University will not infringe any third party rights and that I have not previously in its entirety or in part submitted it for obtaining any qualification.

Date: December 2017

Copyright © 2017 Stellenbosch University  
All rights reserved.

# Abstract

## Development of a vital signs monitoring wireless ear probe

A. Bestbier

*Department of Mechanical and Mechatronic Engineering,  
University of Stellenbosch,  
Private Bag X1, Matieland 7602, South Africa.*

Thesis: MEng (Mechatronic)

December 2017

The need exists for a mobile and unobtrusive way to continuously monitor vital signs in everyday life. Wearable devices are rapidly advancing in terms of technology, functionality, and size, with more real-time applications becoming available every day. This thesis investigates the external ear as a novel location for a wearable device. The ear allows for the monitoring of multiple vital signs from one location, making the device an ideal mobile solution for non-clinical applications, without compromising the quality of life of the wearer. An application example is the monitoring of infants at home for sudden infant death syndrome risk factors. The main purpose of the device is to measure vital signs, including core temperature, heart rate, respiratory rate and blood oxygen saturation ( $\text{SpO}_2$ ). The device transmits collected data through a wireless connection to a computer for analyses and storage.

A proof of concept, called the Ear-Monitor, was designed and built. It consists of a silicone ear probe with embedded sensors connected to a head-band containing a microcontroller, battery, and Bluetooth modem. A trial was conducted in which the Ear-Monitor was tested on a group of 16 participants. Measurements were compared to benchmark measurements recorded by commercially available devices.

The following results were obtained: core temperature was measured with a mean error of  $0.02 \pm 0.52$  °C through an infrared sensor pointed at the tympanic membrane. Heart rate was determined through an infrared photoplethysmogram measured from the ear canal wall. A beat detection algorithm identifies heart beats and heart rate was calculated with a mean error of  $0.03 \pm 0.72$

beats per minute. Respiratory rate was determined through analysing respiratory sinus arrhythmia. The respiratory rate was measured with a mean error of  $-0.56 \pm 1.41$  breaths per minute. Finally, SpO<sub>2</sub> was measured through pulse oximetry conducted against the ear canal wall. The different absorption spectra of oxygenated and deoxygenated blood were used to calculate the percentage oxygen saturation of blood in peripheral blood vessels with a mean error of  $-0.22 \pm 1.50\%$ .

All measurements showed statistically significant correlation with their respective benchmark measurements ( $p < 0.05$ ), except for SpO<sub>2</sub>. The latter is due to the absence of measurable SpO<sub>2</sub> variations in healthy individuals during the trial. It is concluded that the external ear is a suitable location for measuring core temperature, heart rate, and respiratory rate. Further testing is needed to evaluate the SpO<sub>2</sub> measurement capabilities of the device. This thesis produced valuable insights into the feasibility of measuring multiple vital signs through the external ear and lays the foundation towards a commercial version of the Ear-Monitor.

# Uittreksel

## Ontwikkeling van n draadlose vitale parameter monitering oor probe

*(“Development of a vital signs monitoring wireless ear probe”)*

A. Bestbier

*Departement Meganiese en Megatroniese Ingenieurswese,  
Universiteit van Stellenbosch,  
Privaatsak X1, Matieland 7602, Suid Afrika.*

Tesis: MIng (Megatronies)

Desember 2017

Daar is ’n konstante behoefte na ’n mobiele en onopvallende manier om vitale parameters in die alledaagse lewe te monitor. Draagbare toestelle ontwikkel teen ’n hoë tempo in terme van tegnologie, funksionaliteit en grootte, met meer intydse toepassings elke dag. Hierdie tesis ondersoek die eksterne oor as ’n alternatiewe ligging vir ’n draagbare toestel. Die ligging maak dit moontlik om verskeie vitale parameters vanaf een posisie te meet. Verder dien dit ook as ideale mobiele oplossing in nie-kliniese situasies, sonder om die lewensgehalte van die draer in gedrang te bring. ’n Voorbeeld van toepassing is die monitering van babas by die huis vir skielike infantiedood sindroom risiko faktore. Die hoofdoel van hierdie toestel is om vitale parameters, insluitend kerntemperatuur, hartklop, respiratoriese tempo en bloed suurstofversadiging ( $\text{SpO}_2$ ) te meet. Die toestel stuur versamelde data deur ’n draadlose verbinding na ’n rekenaar vir analiese en berging.

’n Bewys van konsep, genaamd die *Ear-Monitor*, was ontwerp en gebou. Dit bestaan uit ’n silikoon oorprop met ingeboude sensors wat aan ’n kopband gekoppel is. Die kopband bevat ’n mikrokontrolleerder, battery en Bluetooth-modem. ’n Eksperiment is uitgevoer waarin die *Ear-Monitor* op ’n groep van 16 individue getoets was. Metings is vergelyk met maatstafmetings, wat deur kommersiële toestelle opgeneem is.

Die volgende resultate was verkry: kerntemperatuur was gemeet met ’n gemiddelde foutsyfer van  $0.02 \pm 0.52^\circ\text{C}$  deur ’n infrarooi sensor wat op die tympaniese membraan gerig is. Hart tempo was bepaal deur ’n infrarooi fotoplethysmogram gemeet vanaf die oorkanaalmuur. ’n Klopdeteksie-algoritme

identifiseer hartkloppe en die hart tempo was bereken met 'n gemiddelde fout-syfer van  $0.03 \pm 0.72$  slae per minuut. Respiratoriese tempo was bepaal deur die ontleding van respiratoriese sinus-aritmie. Respiratoriese tempo was gemeet met 'n gemiddelde foutsyfer van  $-0.56 \pm 1.41$  asemhalings per minuut. Laastens, was  $\text{SpO}_2$  gemeet deur middel van polsoksimetrie wat teen die oorkanaalmuur uitgevoer word. Die verskillende absorpsiespektra van geoksigeneerde en gedeoksigeneerde bloed word gebruik om die persentasie suurstofversadiging van bloed in perifere bloedvate te bereken. Dit het gelei tot 'n gemiddelde foutsyfer van  $-0.22 \pm 1.50\%$ .

Die statistiese ontleding van die resultate dui aan dat 'n definitiewe korrelasie gevind is tussen die mates ( $p < 0.05$ ), behalwe vir  $\text{SpO}_2$ . Laasgenoemde is as gevolg van die afwesigheid van meetbare  $\text{SpO}_2$ -variasies in gesonde individue tydens die eksperiment. Die huidige bewyse ondersteun die gebruik van die eksterne oor om kerntemperatuur, hartklop en respiratoriese tempo te meet. Addisionele toetsing is nodig om die  $\text{SpO}_2$  metingsvermoë van die toestel te evalueer. Hierdie tesis het waardevolle insig gelewer in die lewensvatbaarheid van die meet van verskeie vitale parameters in die eksterne oor en lê die grondslag vir 'n kommersiële weergawe van die *Ear-Monitor*.

# Acknowledgements

I would like to express my sincere gratitude to the following people: Firstly, to my supervisor, Prof. Pieter Fourie, for his guidance throughout the course of this project. Secondly, to all the members of the BERG research group. Your intellectual and moral support through long days and late nights have made this period worth so much more. Lastly, I would like to thank my family for their unwavering support and love.

# Contents

<b>Declaration</b>	<b>i</b>
<b>Abstract</b>	<b>ii</b>
<b>Uittreksel</b>	<b>iv</b>
<b>Acknowledgements</b>	<b>vi</b>
<b>Contents</b>	<b>vii</b>
<b>List of Figures</b>	<b>x</b>
<b>List of Tables</b>	<b>xii</b>
<b>Nomenclature</b>	<b>xiii</b>
<b>1 Introduction</b>	<b>1</b>
1.1 Background . . . . .	1
1.2 Aim and objectives . . . . .	2
1.3 Motivation . . . . .	2
1.4 Document outline . . . . .	3
<b>2 Literature review</b>	<b>4</b>
2.1 Ear anatomy . . . . .	4
2.1.1 Auricle . . . . .	4
2.1.2 Ear canal . . . . .	5
2.1.3 Tympanic membrane . . . . .	6
2.2 Vital sign physiology . . . . .	6
2.2.1 Core temperature . . . . .	7
2.2.2 Heart rate . . . . .	8
2.2.3 Respiratory rate . . . . .	8
2.2.4 Blood oxygen saturation . . . . .	9
2.3 Vital signs measurement theory . . . . .	9
2.3.1 Core temperature . . . . .	10
2.3.2 Heart rate . . . . .	14



2.3.3	Respiratory rate . . . . .	20
2.3.4	Blood oxygen saturation . . . . .	22
2.4	Conclusion . . . . .	25
<b>3</b>	<b>Concept selection</b>	<b>26</b>
3.1	Engineering specifications . . . . .	26
3.2	Core temperature . . . . .	26
3.2.1	Measurement method . . . . .	27
3.2.2	Sensor selection . . . . .	28
3.3	Heart rate . . . . .	29
3.3.1	Measurement method . . . . .	29
3.3.2	Sensor selection . . . . .	32
3.4	Respiratory rate . . . . .	34
3.4.1	Measurement method . . . . .	34
3.4.2	Final method choice . . . . .	35
3.5	Blood oxygen saturation . . . . .	36
3.6	Final concept . . . . .	36
<b>4</b>	<b>Detailed Design</b>	<b>38</b>
4.1	Hardware . . . . .	38
4.1.1	Temperature sensor . . . . .	38
4.1.2	Pulse oximeter . . . . .	40
4.1.3	Control and communication hardware . . . . .	42
4.2	Software . . . . .	44
4.2.1	Sensor communication . . . . .	44
4.2.2	Core temperature . . . . .	45
4.2.3	PPG signal processing . . . . .	48
4.2.4	Beat detection . . . . .	49
4.2.5	SpO <sub>2</sub> calculation . . . . .	54
4.2.6	PC interface . . . . .	56
<b>5</b>	<b>Experimental trial</b>	<b>58</b>
5.1	Participant selection . . . . .	58
5.2	Benchmark validation . . . . .	59
5.3	Method . . . . .	60
<b>6</b>	<b>Results and Discussion</b>	<b>63</b>
6.1	Background . . . . .	63
6.2	Core temperature . . . . .	64
6.2.1	Group calibration . . . . .	64
6.2.2	Intra-participant calibration . . . . .	64
6.2.3	Discussion . . . . .	65
6.3	Heart rate . . . . .	67
6.3.1	Beat detection algorithm . . . . .	67

<i>CONTENTS</i>	<b>ix</b>
6.3.2 Beat period and average heart rate . . . . .	69
6.3.3 Discussion . . . . .	70
6.4 Respiratory rate . . . . .	71
6.5 Blood oxygen saturation . . . . .	73
6.6 Results summary . . . . .	75
<b>7 Conclusion</b>	<b>76</b>
7.1 Device development . . . . .	76
7.2 Experimental trial . . . . .	77
7.3 Data analysis and results . . . . .	77
7.3.1 Core temperature . . . . .	77
7.3.2 Heart rate . . . . .	77
7.3.3 Respiratory rate . . . . .	78
7.3.4 Blood oxygen saturation . . . . .	78
7.4 Suggestions for future work . . . . .	78
7.5 Conclusion . . . . .	79
<b>Appendices</b>	<b>80</b>
<b>A Calculations</b>	<b>81</b>
A.1 Battery life calculation . . . . .	81
A.2 Component selection . . . . .	82
<b>B Printed circuit boards</b>	<b>85</b>
B.1 Schematic of PCB . . . . .	85
B.2 PCB layouts . . . . .	87
<b>C Calibration</b>	<b>88</b>
C.1 Temperature calibration . . . . .	88
C.1.1 Group calibration . . . . .	88
C.1.2 Intra-participant calibration . . . . .	89
C.2 SpO <sub>2</sub> calibration . . . . .	89
<b>D Proof of ethical approval</b>	<b>91</b>
<b>E Detailed Results</b>	<b>95</b>
E.1 PhysioNet beat detection . . . . .	95
E.2 Core temperature . . . . .	96
E.3 Trial data beat detection . . . . .	97
E.4 Respiratory rate . . . . .	98
E.5 Blood oxygen saturation . . . . .	99
<b>List of References</b>	<b>100</b>

# List of Figures

2.1	Anatomical structures of the auricle . . . . .	5
2.2	Anatomy of the of the external ear . . . . .	5
2.3	Temperature ranges in healthy humans . . . . .	7
2.4	Planck's law . . . . .	12
2.5	Infrared thermometer fundamentals . . . . .	13
2.6	Cosinuss Degree . . . . .	13
2.7	Ear electrocardiography . . . . .	15
2.8	Two modes of PPG . . . . .	15
2.9	Photoplethysmography principles . . . . .	16
2.10	Ear photoplethysmography . . . . .	17
2.11	Comparison of photoplethysmograms to an electrocardiogram . . . . .	18
2.12	Cosinuss One . . . . .	18
2.13	Ear pulse wave measurement device . . . . .	19
2.14	Breathing through microphones . . . . .	20
2.15	Detecting respiration through ballistocardiography . . . . .	21
2.16	Absorption spectra of oxy- and deoxyhaemoglobin . . . . .	22
2.17	Bragi Dash . . . . .	25
3.1	ST60 Micro . . . . .	28
3.2	NJL5501R . . . . .	33
3.3	MAX30100 block diagram . . . . .	33
3.4	Ear-Monitor concept . . . . .	37
4.1	Telemedicine flow of information . . . . .	38
4.2	TMP006 PCB . . . . .	39
4.3	MAX30100 package diagram . . . . .	40
4.4	MAX30100 PCB . . . . .	41
4.5	Ear-Monitor hardware block diagram . . . . .	42
4.6	Ear probe . . . . .	43
4.7	Hardware of the Ear-Monitor . . . . .	43
4.8	Ear-Monitor software block diagram . . . . .	44
4.9	Reading 16-bit values . . . . .	45
4.10	TMP006 calibration curve from datasheet . . . . .	47
4.11	PPG signal processing . . . . .	48

*LIST OF FIGURES***xi**

4.12	AC extraction . . . . .	49
4.13	Low-pass filter . . . . .	50
4.14	PPG characteristics . . . . .	50
4.15	Slope summing function . . . . .	51
4.16	SSF with detected beats and threshold . . . . .	53
4.17	Peak detection example . . . . .	53
4.18	Heartbeat periods and chest expansion . . . . .	54
4.19	Current balancing . . . . .	56
4.20	Ear-Monitor user interface . . . . .	57
5.1	Benchmark devices . . . . .	59
5.2	Recording session . . . . .	60
5.3	Recording session set-up with participant . . . . .	62
6.1	Group calibration temperature correlation . . . . .	65
6.2	Intra-participant calibration temperature correlation . . . . .	65
6.3	Temperature errors . . . . .	66
6.4	Beat detection comparison . . . . .	68
6.5	Number of beats correlation . . . . .	69
6.6	Beat period correlation . . . . .	70
6.7	Heart rate correlation . . . . .	70
6.8	Number of breaths correlation . . . . .	72
6.9	SpO <sub>2</sub> correlation . . . . .	74
A.1	MAX30100 pulse diagram . . . . .	81
A.2	Switching circuit diagram . . . . .	84
B.1	Headband PCB schematic . . . . .	86
B.2	Headband PCB top layout . . . . .	87
B.3	Headband PCB bottom layout . . . . .	87
C.1	Temperature errors before and after calibration . . . . .	89

# List of Tables

2.1	Respiratory rate through neural networks . . . . .	21
2.2	SpO <sub>2</sub> accuracy . . . . .	24
3.1	Summary of considered methods . . . . .	26
3.2	Contact thermometer evaluation . . . . .	27
3.3	Non-contact thermometer evaluation . . . . .	28
3.4	Ear ECG evaluation . . . . .	30
3.5	Ear PPG evaluation . . . . .	31
3.6	Ear BCG evaluation . . . . .	31
3.7	Ear PCG evaluation . . . . .	32
3.8	Ear accelerometer evaluation . . . . .	34
3.9	Ear microphone evaluation . . . . .	35
3.10	Respiratory-related heart rate characteristics evaluation . . . . .	35
3.11	Ear SpO <sub>2</sub> evaluation . . . . .	36
4.1	T <sub>DIE</sub> example calculation . . . . .	46
4.2	T <sub>DIE</sub> example calculation . . . . .	47
5.1	Demographic summary of participants . . . . .	59
6.1	Mean errors of the respiratory rate measurements . . . . .	72
6.2	Summary of statistical results . . . . .	75
A.1	Current consumption per component . . . . .	82
A.2	Voltage specific current consumption per component . . . . .	83
A.3	Voltage regulators . . . . .	83
E.1	Results of the beat detection algorithm on the PhysioNet data . . . . .	95
E.2	Temperature results . . . . .	96
E.3	Results of the beat detection algorithm on the trial data . . . . .	97
E.4	Respiratory rate results . . . . .	98
E.5	SpO <sub>2</sub> results . . . . .	99

# Nomenclature

## Variables

$A$	Adsorption factor	[ ]
$B_\lambda$	Spectral radiance	[W·sr <sup>-1</sup> ·m <sup>-3</sup> ]
$c$	Speed of light	[m·s <sup>-1</sup> ]
$k$	Window size	[Samples]
$k_B$	Boltzman's constant	[J·K <sup>-1</sup> ]
$L$	Path length	[m]
$h$	Planck's constant	[kg·m <sup>2</sup> ·s <sup>-1</sup> ]
$I$	Light intensity	[cd]
$N$	Number of conversions	[Conversions]
$Q$	Thermal radiation	[W·m <sup>-2</sup> ]
$R$	SpO <sub>2</sub> modulation ratio	[–]
$T$	Temperature	[K]
$T_{\text{DIE}}$	Die temperature	[°C]
$T_{\text{OBJ}}$	Object temperature	[°C]
$T_{\text{REF}}$	Reference temperature	[°C]
$t$	Adaptive threshold	[–]
$V_{\text{SENSOR}}$	Sensor voltage	[mV]
$x_n$	Raw PPG value	[–]
$y_n$	Filtered AC PPG value	[–]
$z_n$	SSF output	[–]
$\alpha$	Scaling factor	[–]
$\epsilon$	Molar absorptivity	[L·mol <sup>-1</sup> ·m <sup>-1</sup> ]
$\varepsilon$	Emissivity	[–]
$\lambda$	Radiation wavelength	[m]
$\sigma$	Stefan-Boltzman constant	[W·m <sup>-2</sup> ·K <sup>-4</sup> ]
$\emptyset$	Diameter	[mm]
$\varphi$	Molar concentration	[mol·L <sup>-1</sup> ]

# Chapter 1

## Introduction

This thesis reports on a project undertaken in die biomedical field of wearable electronics. Great advances in the miniaturisation of electronics and wireless communication have challenged and transformed the norm of how we use electronics to listen to the language of our bodies.

### 1.1 Background

The project revolved around the continuous measurement of vital signs. These signs are objective parameters that give an indication of physical well-being and the state of essential physiological functions. For example, infections are indicated by a rise in core temperature (DerSarkissian, 2016), pneumonia can be detected by a shortness of breath (Mayo Clinic, 2017), an abnormal decrease in blood oxygen saturation during sleep can be a warning sign for sudden infant death syndrome (Thach, 2008) and a rise in heart rate can indicate physical stress (Karriem-Norwood, 2017). These signs can be detected electronically before traditionally observable symptoms appear. In many cases, the determining factor in the success of a treatment is whether the illness is detected early enough. Because of this, the importance and usefulness of a continuous, wearable health monitor should not be underestimated.

The primary objectives of the project were to design, develop and evaluate a proof of concept wearable device that can monitor vitals signs through the external ear canal. The device is to be worn in the ear like an earphone, with supporting electronics located in a headband. It records multi-parameter vital sign measurements and transmits collected data through a wireless connection to a supporting system for analyses and storage. This supporting system can be used by a physician, caretaker or the wearer, to monitor and track his/her health.

Henceforth, this device is referred to as the ‘Ear-Monitor’. This report discusses the project aim and objectives, relevant literature and the design, manufacturing and testing of the Ear-Monitor.

## 1.2 Aim and objectives

The aim of this project was to develop and test a proof of concept wearable device that can monitor vital signs through the external ear and transmit collected data wirelessly to a storage system. Vital signs include core temperature, heart rate, respiratory rate and blood oxygen saturation.

In order to achieve the aim of this project, the following three objectives had to be met:

- Develop a device to measure core temperature, heart rate, respiratory rate and blood oxygen saturation through the external ear of the wearer.
- Conduct a trial experiment to test the device on a sample of human participants.
- Use the collected data from the trial to evaluate the accuracy of the measurements made by the device.

## 1.3 Motivation

This project originated from a need found in medical practice, which requires a non-invasive and mobile vital sign monitoring method in non-clinical settings.

Access to accurate, long-term data can lead to improved diagnosis of health issues and a better understanding of how our bodies respond to drugs, exercise, emotions and our environment. Traditionally, vital sign monitoring is done with a stationary, dedicated device for each signal to be measured. Due to the numerous large and stationary pieces of equipment needed for traditional patient monitoring, it is apparent that it is not suitable for vital sign monitoring in everyday life.

The Ear-Monitor overcomes the limitations of cumbersome clinical vital sign monitoring, by proving that it is practical to measure the mentioned vital signs through the external ear canal. Future research can be done to miniaturise the electronics and allow the entire device to fit in a hearing aid type of package. The methods developed during this project will aid the development of a commercial version of the Ear-Monitor. A large group can benefit from a device like this and applications include the following:

- Monitoring the health of patients with chronic diseases.
- Studying the effect of prescription drugs or other treatments.
- Monitoring the health of people working under strenuous conditions, such as heavy machinery operators and soldiers.
- Monitoring neonate and infant health in nurseries and at home.



- Tracking the health and fitness of athletes.

The ear was chosen as monitoring location for various reasons. Firstly, the anatomy of the ear and the proximity of an ear-worn device to the tympanic membrane means that all the mentioned vital signs can theoretically be measured from this location. This eliminates the need for multiple devices or wires connecting sensors to different parts of the body. The absence of sensors on traditional locations, such as the chest or limbs, and the absence of connective wires mean that the ear-worn device is minimally obstructive for the wearer, especially by freeing up the hands and allowing free movement.

Secondly, the shape of the external ear is ideal for supporting a device without the need for straps or adhesives. Furthermore, the head remains relatively stationary in relation to the rest of the body. This reduces the risk of motion artefacts corrupting the signals of interest. An ear-worn device can be embedded in the already familiar shape of an earphone or hearing aid.

The final motivation for using the ear as location for the health monitor was its novelty. As will be apparent from the literature review in this report, there is opportunity for research to be done in the unsaturated field of ear-worn health monitors.

## 1.4 Document outline

The rest of this document will be structured as follows:

- Chapter 2: A literature study will review relevant sources regarding the anatomy of the ear, physiology of vital signs and work done by others in the field of ear vital sign monitoring.
- Chapter 3: The generation of a concept will be discussed, including the process of generating, evaluation and integrating different subsystem solutions.
- Chapter 4: The detailed design of the Ear-Monitor will be discussed, with separate attention given to hardware and software design.
- Chapter 5: The trial will be designed to test the Ear-Monitor. The methods and equipment used in the trial will be discussed in this chapter.
- Chapter 6: The results from the trial will be presented and discussed. Attention will be given to each vital sign individually.
- Chapter 7: The conclusion will summarise the project. Attention will be given to the objectives, to what extent they were achieved, the most important findings and suggestions for future work.

# Chapter 2

## Literature review

This chapter describes the technological and biological context within which the project was undertaken. An overview of the anatomy of the ear, which is relevant to this study, is given. Thereafter, background is given on the physiology of each of the four vital signs. Finally, the technology relevant to the measurement of each vital sign required of the Ear-Monitor is discussed in terms of theory and the work done by others.

### 2.1 Ear anatomy

The area that is available for the Ear-Monitor to record the vital sign measurements is the external ear. It includes the auricle, the ear canal with surrounding tissue and the lateral side of the tympanic membrane. Each part of the ear anatomy is discussed, especially with regards to its ability to emit information related to vital signs or to support the device in another way.

#### 2.1.1 Auricle

The auricle is the visible part of the ear. It forms a C-shaped funnel that protrudes from the skull. Its structure is predominantly formed by yellow elastic cartilage covered by skin. Its complex folded shape differs between individuals, but certain structures are present in all normal auricles and have been named. As can be observed in Figure 2.1, the concha is the indented part next to the ear canal. This area is an ideal location for a wearable device. The device can be held in place by the tragus and a probe can easily extend into the ear canal.

The external ear is supplied with blood from the auricular arteries. These arteries branch from the carotid artery, which supplies the rest of the brain with blood. Being made mostly of cartilage and located at an extremity of the body, the auricle is not a suitable location for taking temperature measurements, as its temperature is easily influenced by ambient conditions.

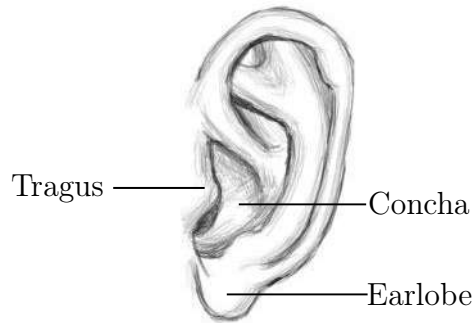


**Figure 2.1:** Anatomical structures of the auricle

The layer of skin covering the auricle contains blood vessels and therefore the earlobe is a popular location for traditional pulse oximetry measurements. This is a possible location for an ear-worn device to make a heart rate and peripheral blood oxygen saturation (SpO<sub>2</sub>) measurement (Poh *et al.*, 2010). The blood vessels of the earlobe are, however, susceptible to vasoconstriction due to cold or hypovolaemia (World Health Organization, 2011). This will reduce the blood perfusion of the subcutaneous tissue, making it harder to record accurate heart rate and SpO<sub>2</sub> measurements.

### 2.1.2 Ear canal

The external ear canal is the tube running from the floor of the auricle to the middle ear, ending blindly at the tympanic membrane. Figure 2.2 depicts the structure of the ear as seen from a coronal plane section.

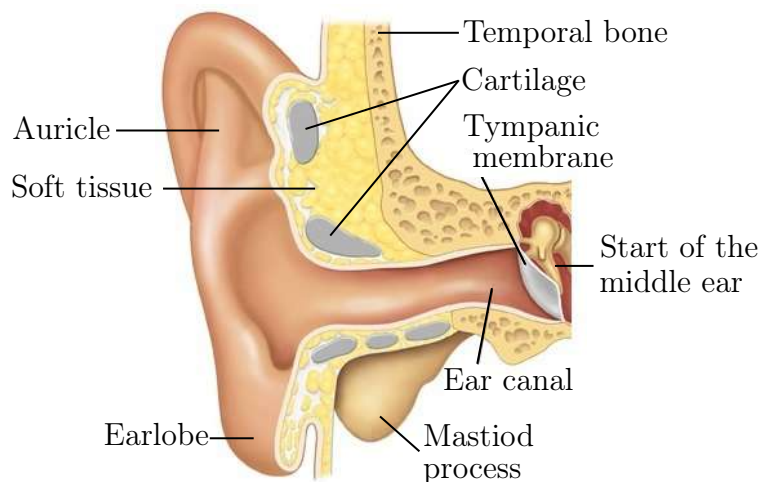


**Figure 2.2:** Anatomy of the of the external ear (Doctor online, 2016)

The auricle is visible and the shape and relative size of the canal can be observed. The ear canal in adults is approximately 25 mm long and have a diameter of 5 to 7 mm (Alvord and Farmer, 1997). The outer third of the

external ear canal is surrounded by cartilage and fibrous tissue (Encyclopædia Britannica, 2015). The inner two-thirds are surrounded by the temporal bone. Thin skin forms the lining of the canal and contains glands that secrete ear wax. Hairs are found in the outer part of the canal. The ear canal of infants starts out relatively straight, but obtains a definite S-shape as the head develops (Alvord and Farmer, 1997). This S-shape is important to keep in mind when placing a sensor to measure tympanic temperature. Ear canal size also varies between individuals. Therefore, an ear probe should be designed to fit in a variety of ear canal shapes and sizes.

The secluded nature of the ear canal means that it has a relatively constant temperature. Air trapped in the canal by a plug of high thermal resistance will reach thermal equilibrium close to the temperature of the canal wall and tympanic membrane. This is a better location for a core temperature measurement, but will still be influenced by the ambient temperature. The wall of the ear canal is well supplied with blood. Blood vessels just beneath the thin layer of skin make the ear canal a possible location for measuring heart rate and blood oxygen saturation.

### 2.1.3 Tympanic membrane

The tympanic membrane forms the medial boundary of the external ear canal. It is a smooth elliptical membrane with a thickness of approximately 0.074 mm (Alvord and Farmer, 1997). The membrane is slanted relative to the external ear canal.

As with the rest of the external ear, the tympanic membrane is supplied with blood from a branch of the carotid artery, therefore sharing its supply with the brain, including the hypothalamus, the thermoregulation centre of the body. It is the most medial part of the external ear, and is therefore the least susceptible to be influenced by ambient temperature. This is the reason why the tympanic membrane is one of the best locations to measure core body temperature. The location is conventionally used by physicians to measure core temperature, as it is quick and minimally invasive (Gasim *et al.*, 2013). Variations in body temperature can be sensed faster on the tympanic membrane than on other locations on the body. Contact with the membrane can cause discomfort and harm to the patient, therefore non-contact infrared thermometers are usually used.

## 2.2 Vital sign physiology

This section reviews the theory and research done on the physiological aspects of each vital sign that the Ear-Monitor is required to measure. The importance of each of the four vital signs is discussed, including the typical range of

measurements expected from healthy adults and the causes and implications of deviations from these measurements.

### 2.2.1 Core temperature

Thermoregulation is the process of the human body to keep its internal temperature within certain limits to create a favourable environment for chemical reactions to take place (Holland, 2016). The temperature control centre of the body is in the hypothalamus and it regulates temperature by maintaining a fine balance between heat production and heat loss. Normal human core temperature varies between 36.5 °C and 37.5 °C (Jones, 2010). Inability to maintain this balance may indicate problems in the well-being of a person. Elevated temperature (hyperthermia) due to a fever can indicate the presence of an infectious disease. Abnormally low temperature (hypothermia) can be caused by exposure to cold, metabolic disorders or infection. Both hyper- and hypothermia can be life-threatening. A core temperature measurement is often a key indication to start treatment or not. Therefore, temperature measurement is part of a full clinical examination.

The location where temperature is measured is a key factor, as temperature is not constant throughout the body. This is because heat production and heat loss are not constant throughout the body, which means body extremities are usually cooler than the core. Traditional locations for measuring temperature are the tympanic membrane, axilla, mouth, rectum, oesophagus, forehead and urinary bladder. The mean temperature of these areas varies as well. A systematic literature review done by Sund-Levander *et al.* (2002) combined the results of twenty studies to identify oral, rectal, tympanic and axillary temperature ranges in healthy humans. Figure 2.3 illustrates the results.

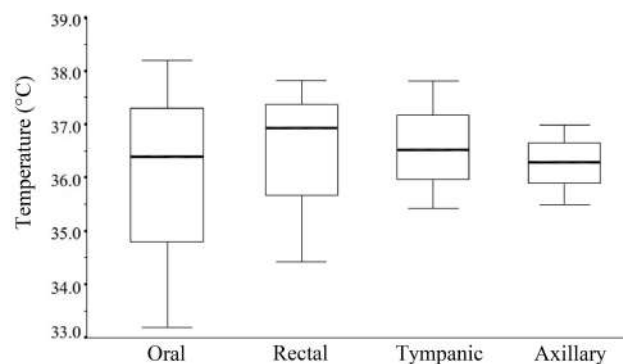


**Figure 2.3:** The results from 20 studies reviewed by Sund-Levander *et al.* (2002)

The location of the device in development is restricted to the ear, therefore the tympanic membrane is the preferred location for temperature measurements. The studies indicate that the tympanic membrane is a valid location to measure accurate core temperature.

### 2.2.2 Heart rate

The presence of a heartbeat is paramount to sustain the vital cardiac output, supplying blood to the whole body. Heart rate can be controlled or maintained through two different regulatory systems: the intrinsic conduction system and the nervous system. The intrinsic conduction system works through the rhythmic contraction and relaxation of the heart muscle tissue. The heart rhythm is regulated by the sinoatrial node. The nervous system can influence the heart rate through sympathetic and parasympathetic nerves running from the cardiovascular centre in the medulla oblongata to the heart. The heart rate is varied to control the blood flow and blood pressure in the body.

The heart is the source of a group of bio-signals. The firing of nodes and propagation of electrical charges through neurons and the conductive cardiac muscles emit electrical signals that can be detected through electrodes. The contraction of the ventricles forces blood into the arteries, causing a temporary increase in blood pressure. This pressure increase propagates through the arteries as a wave, causing a temporary local increase in blood volume. Pressure and volume changes can be detected. Blood turbulence and the opening and closing of heart valves cause the characteristic heart sound and chest movements, both indications of heart rate.

Heart rate is influenced by numerous physiological factors, including oxygen, carbon dioxide and hydrogen ion levels, blood pressure, stress and exercise. Pathological factors can include fever, sepsis, heart disease and anaemia. Tachycardia is an abnormally high resting heart rate, generally above 100 beats per minute (bpm), whereas bradycardia is a lower-than-normal resting heart rate, usually below 60 bpm (Laskowski, 2015). Although these two conditions are not necessarily danger signs, they may be indications of health problems and therefore heart rate measurement is part of any medical examination.

### 2.2.3 Respiratory rate

Respiration is the first step in the chain of events to transport oxygen to the cells of the body for metabolism to provide the body with energy. Respiration ventilates the lungs with air through inhalation and exhalation. The respiratory rate of a healthy adult at rest is usually between 12 and 20 breaths per minute (Charbek, 2015). This can vary drastically if the body is experiencing physical or emotional stress. An increase in respiratory rate can be caused by a fever, pulmonary dysfunction or any one of numerous medical conditions.

Respiratory rate monitoring is especially useful for diagnosing sleep apnoea. Symptoms include regular pauses in respiration or periods of shallow breathing (hypopnea) during sleep. This causes an oxygen deficiency in the body and lowers the quality of sleep. Short-term symptoms include excessive daytime sleepiness, morning headaches, impaired alertness and vision problems. If left

untreated, sleep apnoea can lead to high blood pressure, diabetes, depression, worsening of attention deficit hyperactivity disorder (ADHD), stroke, heart failure, irregular heartbeats and heart attacks (Blaht, 2016). Sufferers may be unaware of their condition and a sure-fire method of diagnosing it is by monitoring respiratory rate during sleep, traditionally done during an overnight sleep study.

### 2.2.4 Blood oxygen saturation

Haemoglobin is the oxygen transporter protein found in red blood cells. Blood is oxygenated in the lungs and then carries  $O_2$  to the rest of the body for aerobic respiration necessary to produce energy. The correct levels of oxygen in the blood are vital to the health of the individual.

Arterial oxygen saturation,  $SaO_2$ , refers to the concentration fraction of oxygenated haemoglobin to total concentration of haemoglobin in arterial blood. This fraction is calculated by Equation 2.1,

$$SaO_2 = \frac{C(HbO_2)}{C(HbO_2) + C(Hb)} \quad (2.1)$$

where  $C(HbO_2)$  is the concentration of deoxygenated haemoglobin (deoxy-haemoglobin) and  $C(Hb)$  is the concentration of oxygenated haemoglobin (oxy-haemoglobin).

Blood oxygen saturation of 95 to 100% is normal in healthy humans. Hypoxaemia is the condition when the saturation is below 90%. This can be an indication of circulatory or ventilatory problems, anaemia or sleep apnoea. Levels below 80% can impede organ function and can lead to organ failure and cardiac or respiratory arrest. The brain is extremely susceptible to damage when deprived of oxygen. Cerebral hypoxia is the insufficient supply of oxygen to the brain. This can cause brain damage and, in severe cases, brain death.

## 2.3 Vital signs measurement theory

This section accumulates a thorough understanding of the theory and current state of technology relevant to the measurement of each vital sign required of the Ear-Monitor. Attention is given to the different methods available to determine each vital sign. The section also refer to various articles and studies done by researchers in the same field of study. The aim was to gather all the relevant information to make an informed selection of the methods and sensors the Ear-Monitor will use to measure each vital sign.



### 2.3.1 Core temperature

Various methods are available for measuring core temperature. The mercury-filled thermometer was used by early physicians to study the thermoregulation of the human body and crudely identify fevers (Pearce, 2002). Since then, mercury has been replaced by coloured alcohol or another heat sensitive liquid due to toxicity of mercury. Another type of fluid-filled thermometer is the liquid crystal thermometer. It contains liquid crystals that change colour at different temperatures. The use of these two types of fluid-filled thermometers has decreased significantly due to the accuracy, speed and convenience of digital thermometers.

Digital thermometers are now the industry standard for measuring core temperature. Central to any digital thermometer lies a transducer that converts temperature to an electrical signal. Resistance temperature detectors (RTDs), thermocouples, thermistors and thermopiles are discussed. These can be divided into contact and non-contact thermometers.

#### 2.3.1.1 Contact thermometers

These thermometers function by means of measuring their own temperature, with the assumption that both their own and the object of interest's temperature are in thermal equilibrium. Therefore, they are usually placed in contact with the object. When using a contact thermometer in the ear, the sensor part of the thermometer can be placed in contact with the ear canal wall, the air inside the canal or the tympanic membrane itself. Several types of contact thermometers exist, including RTDs, thermocouples, thermopiles and thermistors.

#### Resistance Temperature Detector

RTDs use the temperature-resistance relationship for metals to measure temperature. Thin wire coils or films of platinum, copper or nickel are usually preferred, as these materials have stable and repeatable temperature-resistance relationships over a wide temperature range.

#### Thermocouple

Thermocouples make use of the thermo-electric effect to make a temperature measurement. It consists of two dissimilar conductors connected at the one end, known as the hot junction, while the other ends are known as the cold junction and are connected to a voltage meter via common conductors. A voltage is generated dependent on the temperature difference between the hot and cold junctions. Thermocouples do not respond to absolute temperature, therefore, their accuracy depends on how well the reference temperature can be defined. Thermocouples are very versatile and widely used in clinical applications, but the downside is that



their output signal is low and non-linear, therefore requiring a sensitive and stable voltage measuring device (Jones, 2010).

### **Thermopile**

Thermocouples can be connected in series and are then called thermopiles. This configuration sums the output voltages, resulting in temperature averaging. This method improves accuracy by reducing noise. Thermopiles can be used in contact and non-contact applications.

### **Thermistor**

A thermistor is a type of semiconductor whose resistance varies with changes in temperature. Thermistors differ from RTDs in that they are usually made of ceramics, have higher precision over a smaller temperature range and can have a negative relation to temperature. Thermistors are preferred above RTDs and thermocouples for use as biomedical sensors owing to their faster response time and higher sensitivity over a smaller range. The smaller range does not matter, as the temperature range of interest in bio-sensors is small and well-defined.

### **Contact Thermometer Application**

In the case of RTDs and thermistors, the measuring element is placed in position and a current is sent through the sensor. By measuring the voltage across the resistive element, it is possible to calculate the voltage and subsequently determine the temperature. In the case of a thermocouple, the hot junction can be placed in contact with the canal wall or tympanum. Typically, the hot junction is enclosed in a soft material to protect the canal and tympanum. The canal is sealed off and time is allowed for the area to equilibrate to tympanic temperature.

Placing a thermometer in contact with the tympanic membrane gives an accurate measurement, but can cause discomfort to the wearer. There is also a risk of harming the tympanic membrane. Sensors in contact with the ear canal wall or the air inside the canal run the risk of making errors by measuring the temperature of objects that are not in thermal equilibrium with the tympanic membrane. These limitations lead to the consideration of non-contact thermometers.

#### **2.3.1.2 Non-contact thermometers**

Thermopiles can be used to detect thermal radiation without being in contact with the object. All matter with temperatures above 0 K radiates electromagnetic radiation according to the Stefan-Boltzmann law. The thermal radiation,  $Q$ , per unit area is given by Equation 2.2,

$$Q = \varepsilon\sigma T^4 \quad (2.2)$$

where  $\varepsilon$  is the emissivity,  $\sigma$  the Stefan-Boltzman constant and  $T$  the temperature of the object of interest. The wavelength distribution varies according to the temperature of the object and is described by Planck's law, given by Equation 2.3,

$$B_{\lambda}(\lambda, T) = \frac{2hc^2}{\lambda^5} \frac{1}{e^{\frac{hc}{\lambda k_B T}} - 1} \quad (2.3)$$

where  $B_{\lambda}$  is the spectral radiance,  $\lambda$  the radiation wavelength,  $h$  Planck's constant,  $k_B$  Boltzman's constant,  $c$  the speed of light and  $T$  the temperature of the object of interest. By maximising  $B_{\lambda}$ , it is possible to find the dominant wavelength that is emitted at a certain temperature. Figure 2.4 depicts a plot made of spectral radiance versus wavelength at  $T = 37^{\circ}\text{C}$ , the core temperature of the human body. It is evident that the dominant wavelength is at  $9.35\ \mu\text{m}$ . This is in the infrared range, and therefore this type of thermal radiation thermometer is called an infrared thermometer.

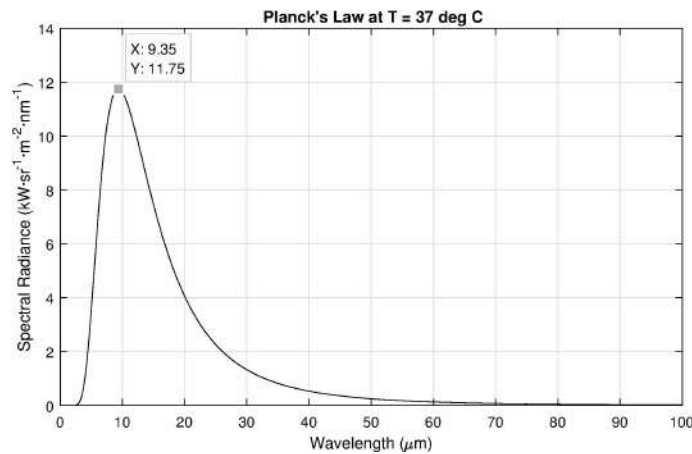


**Figure 2.4:** Dominant radiation wavelength at  $37^{\circ}\text{C}$  using Planck's law

In the case of measuring the temperature of the tympanic membrane, the temperature of the hot junction is determined by the radiation received from the tympanum minus the radiation radiated by the sensor itself.

When dealing with thermal radiation, an important aspect is emissivity. Emissivity is the ability of an object to radiate thermal energy. It is quantified as a ratio of thermal energy emitted by a surface relative to the thermal energy emitted by an ideal blackbody at the same temperature. A blackbody has an idealised surface that reflects no radiation, which means all energy radiated from the surface is due to the temperature of the surface. Therefore, a blackbody has an emissivity of 1 and has the maximum theoretical thermal radiation at a given temperature. The accuracy of an infrared sensor depends on the ability of the object to emit sufficient thermal radiation for the sensor to detect. Cross-referencing various emissivity tables, it was found that the

emissivity of human skin is 0.98, which means that it is an excellent emitter of thermal energy (Optotherm, 2017; Stumme *et al.*, 2003; ThermoWorks, 2017). The ear drum is covered with skin, making it an ideal target object for a non-contact thermometer.

An infrared thermometer generally consists of a thermopile attached to a blackbody and shielded by an infrared filter that also acts as a lens to focus infrared waves (Karaki and Polyziev, 2014). Silicone (Si) is typically used for the filter, for it is opaque to visible light, but transparent to infrared wavelengths. This set-up, depicted in Figure 2.5, allows for the non-contact temperature sensing of the tympanic membrane. Unlike heart and respiratory rates, core body temperature varies slowly. It takes minutes to vary significantly. Therefore, the sampling period of core temperature can be as long as 10 seconds.

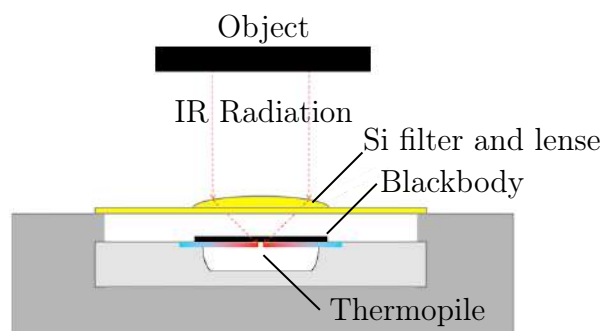


**Figure 2.5:** Fundamentals of a infrared thermometer (Karaki and Polyziev, 2014)

### 2.3.1.3 Commercial ear thermometers

Ear thermometers are widely used at home and in hospitals. Ear contact thermometers such as Novatemp<sup>®</sup> and Starboard<sup>®</sup> claim a  $\pm 0.2^{\circ}\text{C}$  accuracy (Novatemp, 2011; Starboard, 2016). Non-contact infrared ear thermometers usually have a similar-rated accuracy. None of these are, however, wearable devices.

The Degree<sup>®</sup>, shown in Figure 2.6, is a continuous in-ear thermometer for children, developed by Cosinuss, a company specialising in wearable sensors.



**Figure 2.6:** CAD model of the Degree<sup>®</sup> (Cosinuss, 2017b)

The bulk of the device is worn behind the ear, and a wire runs over the auricle to the ear canal, in which a probe is placed. The device takes its temperature measurements with a sensor placed in contact with the canal wall. The manufacturer claims an accuracy of  $\pm 0.1$  °C (Cosinuss, 2017b). It monitors temperature continuously and sends real-time data to a mobile phone.

Apart from the Degree<sup>®</sup>, there is not much literature on wearable ear thermometers. Two patents were found describing similar devices: US 6556852 B1 and US 20090221888 A1. The first proposes the use of an infrared sensor pointed at the tympanic membrane, and the latter does not specify the method of measuring. The trial executed as part of this project added to this insufficient body of knowledge.

## 2.3.2 Heart rate

There are various options available to monitor heart rate. Electronic monitoring methods include electrocardiography (ECG), photoplethysmography (PPG), ballistocardiography (BCG), phonocardiography (PCG) and Doppler flow meters.

### 2.3.2.1 Electrocardiography

ECG is a recording of the electrical activity of the heart over a period of time. Electrical activity arises from the depolarisation and re-polarisation of the heart muscle during the cardiac cycle. The most prominent electrical charge is the QRS-complex, which corresponds to the ventricular depolarisation and is visible on the electrocardiogram as a sharp peak in the millivolt range. ECG is the recommended way of monitoring heart rate in most intensive care units. A cardiologist will use a 12-lead electrocardiograph with 10 electrodes placed in a specific configuration on the chest. Various wearable devices use ECG to measure heart rate. Fitness monitors normally use a chest strap with electrodes to detect the electrical activity of the heart.

Studies have been done developing wearable ECG devices for clinical use. The latest in wearable ECG electrodes is the use of dry polymer-based materials (Wang *et al.*, 2010) or non-contact electrodes that can be placed on top of clothing (Lin *et al.*, 2013). This is an improvement on the standard conductive gels or adhesives and can be used repeatedly. Unfortunately, these electrodes still need to be placed on the chest.

An ear-located ECG monitor has been developed by Winokur *et al.* (2012). This device uses a single-lead setup with one electrode placed on the mastoid bone behind the ear and a reference electrode placed on the neck. This configuration relies on the conductive properties of human tissue to carry electrical charges from the heart to the ear. They were able to use the electrocardiogram in conjunction with PPG and BCG to determine various heart intervals and

track changes in mean arterial blood pressure. Figure 2.7 depicts the device of Winokur *et al.* (2012) and a plot of its electrocardiogram. No heart rate information was extracted.

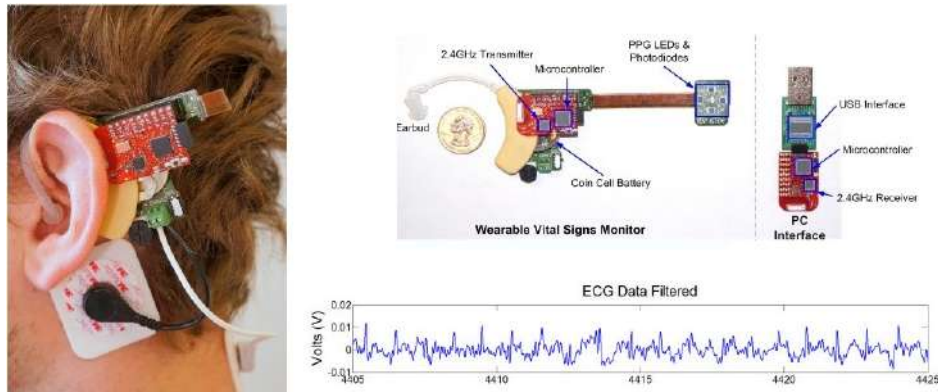


Figure 2.7: Ear-worn device developed by Winokur *et al.* (2012)

### 2.3.2.2 Photoplethysmography

PPG produces an optically obtained plethysmogram, which plots the volume of an organ over time. PPG is used to measure the change in the volume of blood vessels close to the skin surface. When the left ventricle contracts, a pressure pulse propagates through the arteries from the heart to the extremities of the body. This wave corresponds to the systolic blood pressure. Blood vessel walls contain elastic fibres that allow it to stretch. This means that the diameter of vessels increases when the blood pressure increases, causing arteries to stretch and contract with each cardiac cycle. PPG is used to determine heart rate by measuring this volumetric variation.

A photoplethysmograph can non-invasively determine peripheral arterial blood volume by shining light through the skin surface, into the dermis and subcutaneous tissue, and collecting the light transmitted or reflected. Light shined into the tissue can be reflected, absorbed or allowed to transmit through. This leads to the two modes of PPG operation depicted by Figure 2.8.

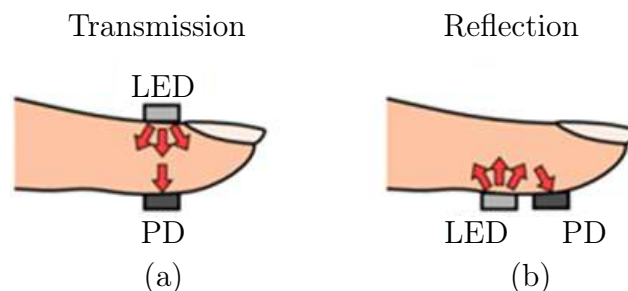
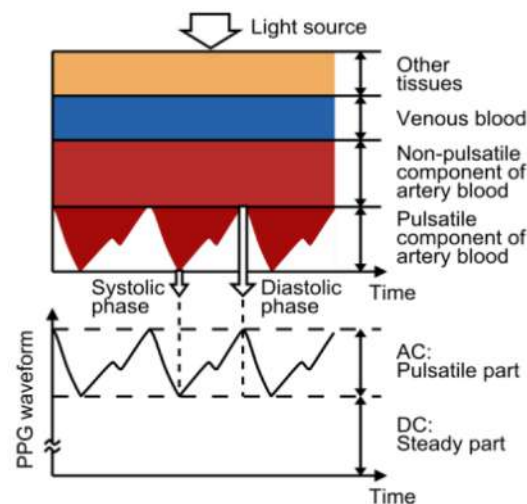


Figure 2.8: (a) Transmission mode PPG; (b) reflection mode PPG (Tamura *et al.*, 2014)

During transmission mode PPG, the emitter and detector face each other and are separated by tissue that transmits the light. Transmission mode PPG is limited to locations on the body where transmitted light can be detected, such as the finger, ear lobe, concha and tragus. These locations have limited blood perfusion, especially at low temperatures. During reflection mode PPG, the emitter and detector are placed on the same plane and both face towards the tissue. Light from the emitter is reflected by the tissue and captured by the detector. The emitter and detector need to be optically isolated so that light cannot pass from the one to the other without going through the tissue. Reflectance mode PPG can be used at more locations, but is more susceptible to motion artefacts (Tamura *et al.*, 2014).

According to Lambert's law, the amount of light absorbed is proportional to the length of the path that the light has to travel in the absorbing substance (Encyclopædia Britannica, 2009). Therefore, a change in blood vessel diameter increases the distance the light has to travel, causing a change in light absorption. This can be detected by measuring reflected or transmitted light. Variation in the light reflected or transmitted is synchronised with the heart rate. Shorter light wavelengths are mostly absorbed by the tissue, while longer wavelengths can penetrate deeper. Red and near infrared light are preferred for transmission PPG. Green light is becoming more popular for shallow reflectance PPG, due to larger light variations during the cardiac cycle and less noise than near infrared PPG (Tamura *et al.*, 2014).

The signal read by the photodetector of the pulse oximeter consists of an AC component superimposed on a DC signal, as is illustrated by Figure 2.9.



**Figure 2.9:** Basic operating principles of PPG (Tamura *et al.*, 2014)

The DC component is due to the constant transmission or reflection of light by the body's tissue: skin, fat, venous blood and the non-pulsating arterial blood. The AC component is the variation in transmitted or reflected light

due to the change in diameter of the arteries and therefore synchronised to the heart rate. The AC component is usually between 0.5 to 2% of the DC component (Tavakoli Dastjerdi, 2006). Figure 2.9 illustrates the way in which the heart rate is visible in a photoplethysmograph. It shows that the blood volume increases with each heartbeat, and that this causes more light to be absorbed, therefore less detected by the photodetector.

A literature review of previous studies in the field of ear PPG revealed six devices relevant to this study.

Shin *et al.* (2009) presented a wearable music headset with an integrated transmission PPG ear clip that attaches to the ear lobe. The device includes an accelerometer to aid in the removal of motion artefacts. Evaluation was done through a study comparing the heart rate from the device to that made with a conventional ECG recorder. This study revealed a heart rate error of 0.6%.

Poh *et al.* (2010) designed a wearable PPG with a magnetic earring sensor. The bulk of the device sits in front of the ear and is held in place by a band around the auricle, as can be seen in Figure 2.10. A reflective PPG sensor is held against the ear lobe by placing a magnet on the opposite side. The device also includes an accelerometer to make baseline measurements for motion artefact cancellation. A study was conducted to compare the PPG signals measured by the wearable device to chest ECG signals collected by an FDA-approved commercial system. While standing motionless, the study found a very high correlation between the ear PPG and the chest ECG with a mean bias of  $0.62 \pm 4.51\%$  with ECG reference measurements.

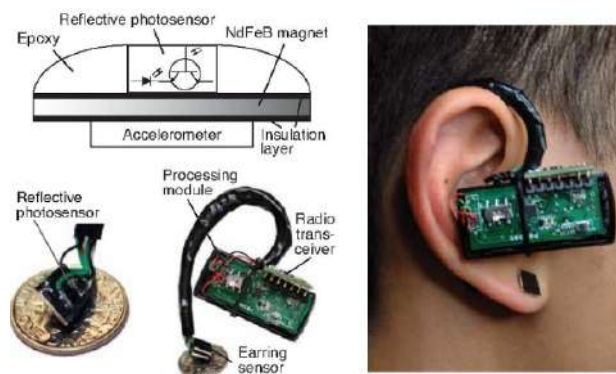


**Figure 2.10:** Wearable ear PPG device by Poh *et al.* (2010)

Da He *et al.* (2010) researched an ear-worn heart rate monitor containing a PPG sensor in reflectance mode. Red light is shined into the tissue behind the ear and collected by a photodiode chip with an integrated transimpedance amplifier. Signals were not digitalised on the device, but recorded and processed



in MATLAB. The collected signal was compared with a transition finger PPG and a chest ECG. Figure 2.11 illustrates this comparison.

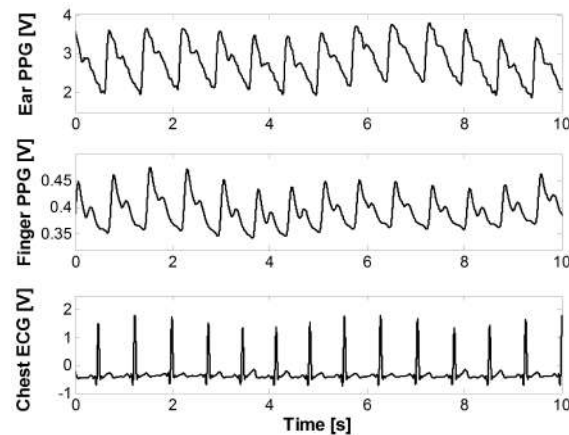


**Figure 2.11:** A comparison between behind-the-ear PPG, finger PPG and chest ECG (Da He *et al.*, 2010)

Winokur *et al.* (2012) developed a similar device that shines 660 nm and 940 nm light waves through tissue at the mastoid bone and collects the reflected light with four photodetectors. A PPG front end conditioned the signals and their device sent the raw heartbeat information to a PC through a radio connection. This is the same device that records ECG and is used to analyse heart intervals and mean blood pressure rather than heart rate.

Buske *et al.* (2009) proposed yet another location. They modified a pair of headphones to measure a transmission PPG from the concha. During the testing phase the device showed a mean heart rate accuracy of around 85% when compared to an ECG.

Finally, the Cosinuss One<sup>®</sup>, as depicted by Figure 2.12, is a commercial device that monitors heart rate through the ear canal. The earpiece presses against the ear canal wall and records a PPG in reflection mode. It targets athletes that want to monitor their bodies during exercise.



**Figure 2.12:** Cosinuss One<sup>®</sup> ear-worn heart rate device (Cosinuss, 2017a)



### 2.3.2.3 Ballistocardiography

BCG is the measurement of the mechanical effects of the beating heart on the body over time. Typically, accelerometers or pressure sensors are used to measure movement or forces on the surface of the body. BCG has been researched for use in ear heart rate extraction.

In a wearable device proposed by Da He *et al.* (2010), mechanical vibrations associated with heart rate are converted to electronic signals through capacitive sensing electrodes placed behind the ear. This method works through measuring the change in capacitance between the two electrodes as the distance between them changes due to heart rate vibrations.

A study by Winokur *et al.* (2012) proposed measuring the head-to-foot axis recoil due to the blood volume shift during cardiac ejection. This is done by placing a microelectromechanical systems (MEMS) accelerometer behind the auricle. Due to the movement-dependent method of operation, this technology is extremely susceptible to motion artefacts and it can only be used when the body is stationary.

A variation of this technology was discussed in an article by Park *et al.* (2015). They proposed using a scissor-shaped hinge mechanism in the ear canal that measures the change in the canal size due to the in-ear blood pulse waves. The mechanical movement is converted to an electrical signal through a piezoelectric film sensor. Figure 2.13 depicts two photos of this device.



**Figure 2.13:** Device to measure ear pulse waves due to the cardiac cycle (Park *et al.*, 2015)

### 2.3.2.4 Other heart rate methods

Electronic stethoscopes use a microphone to record heart sounds. A plot of the heart sounds is known as a phonocardiogram. The heart makes a distinct series of sounds during the cardiac cycle due to blood turbulence and the shutting of heart valves. The period of this sound series can be used to determine heart rate and it does not require skin contact.

A Doppler flow meter can be used to detect the alternating blood current component in near-surface arteries. This component is synchronised to the

heart rate frequency. The device uses ultrasound or electromagnetic waves to achieve the Doppler shift.

A study done at Stanford Medicine by Shcherbina *et al.* (2017) reviewed seven commercially available wearable (wristband) heart rate monitors. They found mean errors ranging from 2.5 to 8.8%.

### 2.3.3 Respiratory rate

Unlike the other vital signs, a subject cannot measure his or her own respiratory rate. As soon as a subject is consciously thinking about respiration, breathing usually slows. Measuring needs to happen while the subject's thoughts are otherwise occupied. Therefore, a continuous measuring method is preferred. Typically, a nasal mask or chest strap is used to measure respiration.

#### 2.3.3.1 Respiratory rate ear sensors

Ear-located devices that extract respiration information are rare, but some literature sources are available.

Goverdovsky *et al.* (2016) tested an ear probe with two embedded microphones. The microphones could detect the sound created by turbulence in the airways for breathing rates higher than 12 breaths per minute. Figure 2.14 shows plots of the normalised sound amplitude recorded at 16 and 28 breaths per minute. Variation during breathing can be seen in both recordings.

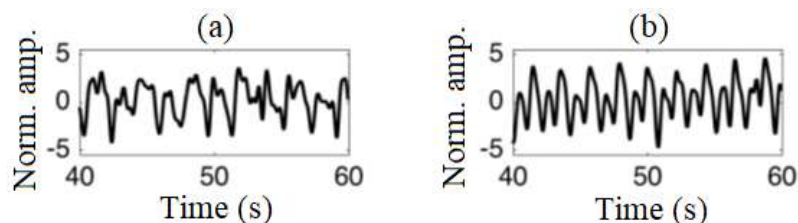


**Figure 2.14:** Breathing detected through microphones inside the ear canal at (a) 16 and (b) 28 breaths per minute (Goverdovsky *et al.*, 2016)

Da He *et al.* (2010) did extensive research on the ear as a location for vital sign monitoring. They extracted respiratory rate from baseline oscillations in a BCG signal recorded by capacitive electrodes placed behind the ear. Mechanical movement is converted to electrical signals by these electrodes. Therefore, the movement of the head due to respiration is seen on the ballistocardiogram as baseline oscillations, as illustrated by Figure 2.15.

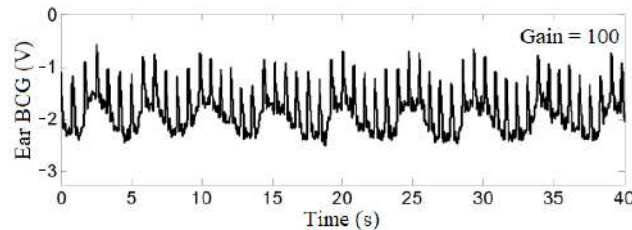


**Figure 2.15:** Baseline oscillations in BCG signal due to breathing (Da He *et al.*, 2010)

### 2.3.3.2 Respiratory-related heart rate characteristics

A different approach is to extract respiratory rate by analysing heart rate. A PPG signal contains three distinct respiratory-related characteristics: amplitude modulation (AM), respiratory-induced intensity variation (RIIV) and frequency modulation (Johansson, 2003).

AM is due to blood pressure changes during the respiratory cycle, called Pulsus Paradoxus. RIIV is changes in the volume of the dermis and subcutaneous capillary bed. It is visible as baseline variation in the PPG signal. Frequency modulation of the heart rate that is synchronised to the respiration rate is called respiratory sinus arrhythmia (RSA).

RSA can also be detected in ECG, but differs from the fluctuations seen in chest ECG due to electrodes movement relative to the heart and changes in chest impedance during the respiratory cycle (Moody *et al.*, 1986). These fluctuations cannot be detected in the ear. RSA is observed as baseline oscillation in heart rate in synchrony with respiratory rate. The heart rate increases during inspiration and decreases during expiration (Yasuma and Hayano, 2004). According to a study done by Stratton *et al.* (2003), the variation in heart rate due to RSA is higher in younger test subjects, with a 74% increase in children versus a 52% increase in adults.

Research has been done to develop algorithms to utilise these characteristics to extract respiratory rate from PPG signals. Clifton *et al.* (2007) used wavelet analysis and achieved a respiratory rate accurate to within one breath per minute and Leonard *et al.* (2006) documented a respiratory rate error of 7.9%. Johansson (2003) developed two neural network algorithms that use the different respiratory-related characteristics of PPG signals to detect breaths. Table 2.1 shows the results of the best algorithm.

**Table 2.1:** Results of the respiratory rate extraction through neural networks (Johansson, 2003)

Respiratory-related characteristics	False positive (%)	False negative (%)
RSA	3.7	6.9
AM	5.2	4.7
RIIV	5.2	5.9

### 2.3.4 Blood oxygen saturation

Oxygen saturation can be measured by means of an arterial blood gas test, resulting in an arterial oxygen saturation reading. This requires drawing a blood sample for testing and therefore was not relevant to this study. An alternative method is pulse oximetry. This method estimates peripheral oxygen saturation,  $SpO_2$ , through the spectrophotometric analysis of PPG signals captured at two different wavelengths. This is a clinically accepted estimation of arterial oxygen saturation (Aoyagi, 2003).

#### 2.3.4.1 Pulse oximetry theory

Blood oxygen saturation estimation through pulse oximetry relies on the different adsorption spectra of oxyhaemoglobin and deoxyhaemoglobin. Figure 2.16 shows the absorption spectra of oxy- and deoxyhaemoglobin. It can be noted that deoxyhaemoglobin has a significantly higher absorption of red light, while oxyhaemoglobin has a slightly higher absorption of infrared light.

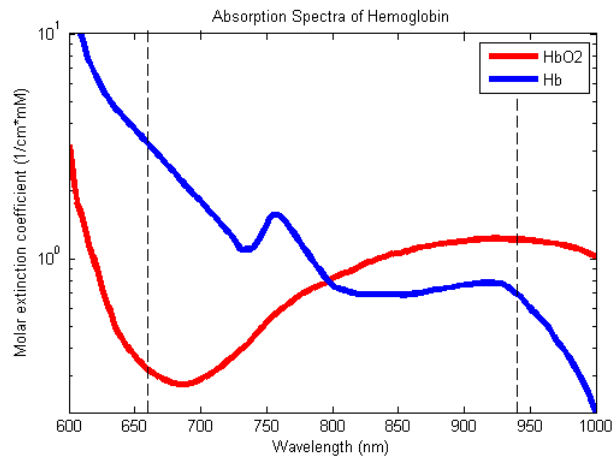


**Figure 2.16:** Absorption spectra of oxy- and deoxyhaemoglobin (Curtin, 2012)

According to the Beer-Lambert law, the amount of light absorbed by a dissolved substance is proportional to its concentration (Encyclopædia Britannica, 2009). Therefore, oxygenated blood (with a higher concentration of oxyhaemoglobin) absorbs more infrared light and reflect more red light, whereas deoxygenated blood (with a higher concentration of deoxyhaemoglobin) absorbs more red light and reflect more infrared light. This explains why oxygenated blood appears bright red, while deoxygenated blood is a darker shade of red.

Red and infrared light are shined into the peripheral tissue and the light reflected or transmitted is measured for both wavelengths. Literature and commercial devices usually use wavelengths of 660 nm (red) and 940 nm (near

infrared) (Bagha and Shaw, 2011; Bheema lingaiah *et al.*, 2013; Chan and Underwood, 2005; Duun *et al.*, 2007; Tytler and Seeley, 1986). The ratio of reflected or transmitted light is unique to a certain level of blood oxygen saturation and is used to estimate blood oxygen saturation.

The Beer-Lambert law describes the absorption of a specific wavelength of light by a substance in a homogeneous solution (Bagha and Shaw, 2011). It is used to calculate light intensity, as shown by Equation 2.4, or it can be manipulated to give what is called the unscattered absorption factor, as shown in Equation 2.5 (Kennedy, 2015).

$$I = I_o e^{-\epsilon_\lambda \varphi L} \quad (2.4)$$

$$A = \epsilon \varphi L = \ln \left( \frac{I_o}{I} \right) \quad (2.5)$$

In equations 2.4 and 2.5,  $I$  is the intensity of light passing through the solution,  $I_o$  is the intensity of the light entering the solution,  $\epsilon$  is the wavelength-dependent molar absorptivity,  $\varphi$  is the concentration of the substance,  $L$  is the path length the light needs to travel through the substance and  $A$  is the dimensionless adsorption factor.

Equation 2.5 can be used to calculate the concentration of oxyhaemoglobin in the blood of the peripheral tissue, provided that the absorptivity and path length of all materials inside the tissue is known. This is not practical, as the thickness and absorptivity of skin and subcutaneous tissue vary between individuals. Furthermore, this equation is also not valid when taking into account the reflection of light, which is fundamental when the application requires reflection mode pulse oximetry.

To solve this problem, a modulated relationship, seen in Equation 2.6, is used that compensates for the different DC absorption between patients (Bagha and Shaw, 2011; Bheema lingaiah *et al.*, 2013; Duun *et al.*, 2007; König *et al.*, 1998; Nitzan *et al.*, 2014; Oak and Aroul, 2015),

$$R = \frac{\left( \frac{AC}{DC} \right)_{\text{red}}}{\left( \frac{AC}{DC} \right)_{\text{IR}}} \quad (2.6)$$

where  $R$  is the SpO<sub>2</sub> modulation ratio. This ensures that the O<sub>2</sub> saturation of only the arterial blood is calculated. The ratio is checked against an empirical determined curve. The standard formula for this curve is found in literature as % SpO<sub>2</sub> = 110 – 25 $R$  (Oak and Aroul, 2015), but it can vary from device to device.

As mentioned, O<sub>2</sub> can be calculated using reflected or transmitted light. Light that is not absorbed or scattered by tissue can be either reflected, or transmitted. Therefore, both reflected and transmitted light are proportional

to the amount of light absorbed. Transmittance mode pulse oximeters are more common, but their use is restricted to parts of the body that allow light to pass through, such as a fingertip or earlobe.

Pulse oximetry is clinically accepted and currently the most accurate way to monitor O<sub>2</sub> saturation non-invasively (Aoyagi, 2003; Chan *et al.*, 2013; DeMeulenaere, 2007; Lee *et al.*, 2016). This being said, note should be taken of the limitations of this method. Pulse oximeters measure O<sub>2</sub> saturation indirectly by analysing differences in light absorption, rather than directly measuring the oxygen concentration of blood, as is done during a blood gas test. This allows ease of use and non-invasive measurement abilities, but sacrifices some accuracy. Various studies have been conducted to quantify the accuracy of the pulse oximeter. Table 2.2 summarises some of these studies.

**Table 2.2:** SpO<sub>2</sub> accuracy

Accuracy	Source
±2%	Fahy <i>et al.</i> (2011)
±4%	DeMeulenaere (2007)
±2.1%	Louw <i>et al.</i> (2001)
±3%	Sinex (1999)

The results differ in their exact quantities, but there is no doubt about an uncertainty factor of at least ±2% that should be kept in mind when taking measurements with a pulse oximeter.

#### 2.3.4.2 Work done by others

Standard locations for pulse oximetry include the fingertip, earlobe, ankle and forehead. A study comparing fingertip and earlobe pulse oximetry to an arterial blood gas test found that finger pulse oximetry differed by a mean of -0,71% and earlobe pulse oximetry differed by a mean of +4.2% (Olive *et al.*, 2016). Literature and commercial wearable pulse oximeters typically utilise a finger clip to measure SpO<sub>2</sub> (Huang *et al.*, 2014; Khalifa *et al.*, 2014; Pujary *et al.*, 2003; Watthanawisuth *et al.*, 2010). This location is not ideal for continuous monitoring and is especially susceptible to motion artefacts. Although the fingertip location was not of interest to this study, the literature was still reviewed, as similar principles can be applied to in-ear pulse oximetry.

Earlobe pulse oximetry is usually done through a sensor that clips to the ear lobe, and is attached to a stationary device. Wearable in-ear pulse oximetry is still novel and not well covered in literature. There are some patents filed for wearable in-ear SpO<sub>2</sub> devices (US 20050177034 A1, US 4086915 A, US 3412729 A and US 6556852 B1). The Bragi Dash (Bragi, 2017), shown in Figure 2.17,

is one of the first commercial devices to claim this ability. However, little academic material is available.



**Figure 2.17:** Bragi Dash

A study done by Aziz *et al.* (2006) tested a wireless earlobe-mounted pulse oximeter on a group of subjects. Subjects were tested while sitting, walking and running. During the sitting and walking phases, they recorded SpO<sub>2</sub> measurements of above 95%, which was ‘as expected’ according to them. However, during the running phase, they could not obtain any accurate measurements.

## 2.4 Conclusion

This chapter revealed the literature context in which the Ear-Monitor project is undertaken. From the ear anatomy section, it is concluded that the external ear has good potential as the location for a vital signs monitor. Firstly, the wall of the ear canal is well perfused with blood and a pulse can be detected through various methods. Secondly, the external ear shares its blood supply with that of the hypothalamus, which causes the tympanic membrane to have a good representation of the core body temperature. Finally, the ear canal and auricle shape is ideal to hold an ear probe containing various sensors in place to make continuous vital sign measurements.

An understanding is obtained about the physiology of the four relevant vital signs. A thorough knowledge of the origin and effects of a vital sign, lead to the understanding of the different ways in which it can be measured. The expected range of measurements of each vital sign aids in the selection of the appropriate sensors to make the required measurements.

Various articles and commercial products relevant to this study are reviewed and reveal the limitations of the current state of the field. Firstly, few academic material on wearable ear temperature and SpO<sub>2</sub> monitors are available. And secondly, none of the reviewed devices measure all four of the vital signs set out in the objectives of this project. The Ear-Monitor project sets out to address these limitations.

# Chapter 3

## Concept selection

This chapter builds on the knowledge gained in the literature review and explains the logic applied to select the methods and sensors to realise each vital sign monitoring requirement of the Ear-Monitor. Selections were made by analysing the advantages and disadvantages of each option and combining these with sound engineering judgement.

### 3.1 Engineering specifications

The two main criteria when selecting sensors were the size and the quality of the measured signal. Ideally, all measurements should be made by sensors inside the ear canal. Sensors should produce a clear signal that is invulnerable to artefacts. Table 3.1 summarises the options considered for the various requirements of the Ear-Monitor. ‘Respiratory-related heart rate characteristics’ is abbreviated as RRHRC.

**Table 3.1:** Summary of considered methods

Temperature	Heart rate	Respiratory rate	SpO <sub>2</sub>
<ul style="list-style-type: none"> <li>• Contact thermometers</li> </ul>	<ul style="list-style-type: none"> <li>• ECG</li> <li>• PPG</li> </ul>	<ul style="list-style-type: none"> <li>• Accelerometer</li> <li>• Microphone</li> <li>• RRHRC</li> </ul>	<ul style="list-style-type: none"> <li>• Pulse oximetry</li> </ul>
<ul style="list-style-type: none"> <li>• Non-contact thermometers</li> </ul>	<ul style="list-style-type: none"> <li>• BCG</li> <li>• PCG</li> </ul>		

### 3.2 Core temperature

The Ear-Monitor measures core temperature from the inside of the ear canal. The main criteria are sensor size and measurement accuracy. The method and sensor selections are discussed separately.



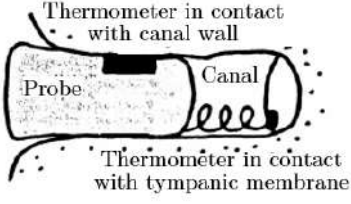
### 3.2.1 Measurement method

Two temperature measurement methods were considered, namely contact and non-contact thermometers.

#### 3.2.1.1 Contact thermometers

A contact RTD, thermocouple or thermistor is placed in contact with the canal wall, canal air or tympanic membrane. Table 3.2 summarises the evaluation.

**Table 3.2:** Contact thermometer evaluation

 <p>Thermometer in contact with canal wall</p> <p>Probe</p> <p>Canal</p> <p>Thermometer in contact with tympanic membrane</p>	<p><b>Advantages</b></p> <ul style="list-style-type: none"> <li>• It is available in small sizes, ideal for the size restrictions of the ear canal.</li> <li>• It renders good accuracy.</li> <li>• Converting transducer voltage to temperature is simpler than with non-contact thermometers.</li> </ul>
<p>Sensor size: 0.5×2.3 mm Measurement accuracy: 0.15 °C</p>	<p><b>Disadvantages</b></p> <ul style="list-style-type: none"> <li>• Canal wall and canal air temperature measurements can easily be influenced by ambient temperature conditions.</li> <li>• Tympanic membrane contact can cause discomfort and harm to the wearer.</li> <li>• More time is needed to take measurements, as the sensor needs to be in thermal equilibrium with the object.</li> </ul>

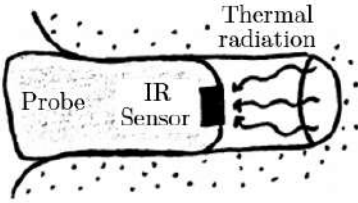
#### 3.2.1.2 Non-contact thermometers

A non-contact, infrared sensor is placed inside the ear canal and pointed at the tympanic membrane. Table 3.3, on the next page, summarises the evaluation.

#### 3.2.1.3 Final method choice

A non-contact, infrared sensor was selected for the Ear-Monitor. User safety, without significant performance compromise, gives it superiority over contact thermometers for this application. The lower accuracy is justified by the fact that the tympanic membrane is a better representation of core body temperature.

**Table 3.3:** Non-contact thermometer evaluation

	<p><b>Advantages</b></p> <ul style="list-style-type: none"> <li>• The sensor can measure the temperature of the tympanic membrane directly, which is the best representation of core temperature in the ear.</li> <li>• Temperature conversion compensates for different ambient temperature conditions.</li> <li>• No contact with the tympanic membrane significantly lowers the injury risk to the user.</li> </ul>
<p>Sensor size: 1.6 to 4 mm Ø Measurement accuracy: 0.2 to 0.5 °C</p>	<p><b>Disadvantages</b></p> <ul style="list-style-type: none"> <li>• Non-contact temperature sensors are typically bigger than contact thermometers, adding to the size limitation challenge.</li> <li>• If the tympanic membrane does not fill a considerable fraction of the sensor's field of view (FOV), erroneous measurements can occur.</li> </ul>

### 3.2.2 Sensor selection

To realise non-contact temperature measurement, two infrared sensors were considered: the ST60 Micro from Dexter Research Center and the TMP006 from Texas Instruments.

#### 3.2.2.1 ST60 Micro

The ST60 Micro, depicted in Figure 3.1, is a one-channel, 80-junction, completely analogue temperature sensing device.

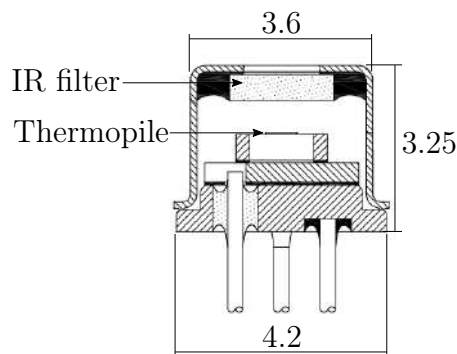


**Figure 3.1:** ST60 Micro diagram with dimensions in mm (Dexter Research Centre, 2004)

It is enclosed in a Micro-TO package, which is 4.09 mm in diameter. The manufacturer emphasises the ST60 Micro's versatility and proposes its use in tympanic ear thermometers. A die-temperature ( $T_{\text{DIE}}$ ) thermistor is available for ambient temperature compensation. Four wires are used to supply the sensor with power and to read transduced voltages.

### 3.2.2.2 TMP006

The TMP006 is a fully integrated infrared sensor measuring only  $1.6 \times 1.6 \times 0.8$  mm, ideally suited for a narrow ear canal. Thermophile voltage and sensor temperature are made digitally available through hardware registers. These two values are used to calculate the object temperature. Registers are accessed by a microcontroller unit (MCU) through I<sup>2</sup>C communication. Values are digitalised by a 16-bit on-chip analogue-to-digital converter (ADC), eliminating the need for supporting analogue filters and amplifiers. The user guide of the TMP006 suggests that it can be used to calculate the surface temperature of target objects with emissivity values greater than 0.7, and preferably greater than 0.9. The literature study revealed that the emissivity of the eardrum is 0.98, placing it well within the required range.

### 3.2.2.3 Final sensor choice

The simple shape of the ST60 Micro makes it easy to mount, but the diameter of the package may not fit in smaller ear canals and leaves little room for the other sensors. Therefore, the ST60 Micro was eliminated.

The smaller package size and on-chip ADC justified the selection of the TMP006 for use in the Ear-Monitor. The TMP006 needs no separate analogue filter and amplifier. Furthermore, the manufacturer supplies detailed calibration documentation, allowing for more accurate and time-effective calibration.

## 3.3 Heart rate

The Ear-Monitor extracts heart rate from in or around the ear canal. The main criteria are sensor size, unobtrusiveness and the susceptibility of the signal to noise. The method and sensor selection are discussed separately.

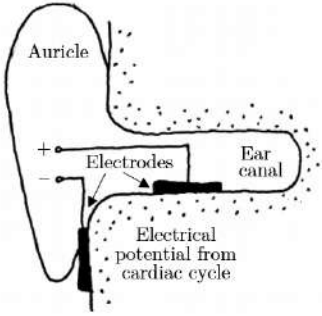
### 3.3.1 Measurement method

The following four methods from literature were considered to measure heart rate: ear ECG, ear PPG, ear BCG and ear PCG. Each option is evaluated separately.

### 3.3.1.1 Ear ECG

As shown by Winokur *et al.* (2012), an electrocardiogram can be detected behind the ear. One electrode is placed behind the ear on the mastoid bone and the other on the back of the neck. A differential amplifier and ADC are used to acquire the signal. Table 3.4 summarises the evaluation.

**Table 3.4:** Ear ECG evaluation

	<p><b>Advantages</b></p> <ul style="list-style-type: none"> <li>• ECG is the standard method used by cardiologists to measure heart rate.</li> <li>• Other cardiac information can be extracted from the ECG signal e.g. heart rhythm, heart damage and the state of the conductive heart tissue.</li> <li>• There is no pulse transit time delay.</li> </ul>
<p>Sensor size: 10 mm <math>\emptyset</math> electrodes  Unobtrusiveness: Poor – electrode needed behind ear and on neck  Signal robustness: Noisy (Winokur <i>et al.</i>, 2012)</p>	<p><b>Disadvantages</b></p> <ul style="list-style-type: none"> <li>• The sensor cannot be fitted entirely inside the ear canal.</li> <li>• Two electrodes are needed.</li> <li>• Separate signal acquisition electronics are needed.</li> </ul>

### 3.3.1.2 Ear PPG

A light-emitting diode (LED) and photodiode are used to detect variation in subcutaneous tissue blood volume due to the beating heart. Literature identifies three possible locations: inside the ear canal, the earlobe and the concha. With unobtrusiveness in mind, focus was placed on the ear canal method and reflective mode PPG. Table 3.5, on the next page, summarises the evaluation.

### 3.3.1.3 Ear BCG

A pressure-sensitive sensor or accelerometer is placed inside the ear canal to detect the mechanical effects of the pulsating heart. Table 3.6, on the next page, summarises the evaluation.

### 3.3.1.4 Ear PCG

A microphone is placed inside the ear canal and identifies heartbeats by analysing the sound produced by the cardiac cycle. Table 3.7, on the page after the next, summarises the evaluation.

Table 3.5: Ear PPG evaluation

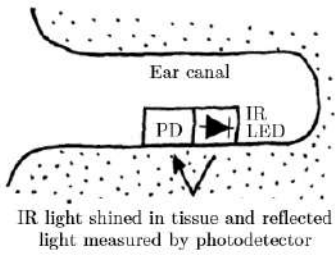
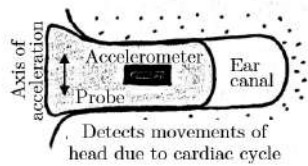
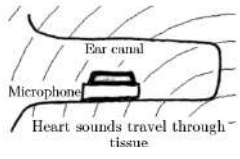
 <p>The diagram shows a cross-section of an ear canal. Inside, there is a small rectangular sensor unit containing a Photodiode (PD) and an Infrared Light Emitting Diode (IR LED). An arrow points from the IR LED towards the ear canal wall, and another arrow points from the ear canal wall back to the PD. Below the diagram, the text reads: "IR light shined in tissue and reflected light measured by photodetector".</p>	<p><b>Advantages</b></p> <ul style="list-style-type: none"> <li>• A substantial pressure pulse can be detected in and around the ear.</li> <li>• Pulse oximetry, a type of PPG, is a tried and tested way of measuring heart rate and SpO<sub>2</sub>.</li> <li>• Respiratory-related characteristics such as AM, RIIV and RSA are found in PPG signals and can be used to determine respiratory rate.</li> </ul>
<p>Sensor size: Smallest – 1.9×2.6×0.8 mm  Unobtrusiveness: Good – fits inside ear canal  Signal noise: Low – clear pressure wave visible  (Da He <i>et al.</i>, 2010)</p>	<p><b>Disadvantages</b></p> <ul style="list-style-type: none"> <li>• PPG is susceptible to motion artefacts and variation in blood perfusion.</li> <li>• Few PPG sensor packages are available to fit inside the ear canal.</li> <li>• Using separate LEDs and photodetectors increase the complexity and size for the proof of concept Ear-Monitor.</li> </ul>

Table 3.6: Ear BCG evaluation

 <p>The diagram shows a cross-section of an ear canal. Inside, there is a small rectangular sensor unit containing an Accelerometer and a Probe. A vertical double-headed arrow to the left of the sensor is labeled "Axis of acceleration". Below the diagram, the text reads: "Detects movements of head due to cardiac cycle".</p>	<p><b>Advantages</b></p> <ul style="list-style-type: none"> <li>• Pressure sensors can be made small enough for the limited space in the ear canal.</li> <li>• The accelerometer can also be used to measure respiratory rate.</li> </ul>
<p>Sensor size: Smallest – 3×3×1 mm (ST Electronics, 2016a)  Unobtrusiveness: A part of the sensor protrudes from the ear; can be made smaller  Signal noise: High (Da He <i>et al.</i>, 2010; Winokur <i>et al.</i>, 2012)</p>	<p><b>Disadvantages</b></p> <ul style="list-style-type: none"> <li>• The signal detected by Da He <i>et al.</i> (2010) and Winokur <i>et al.</i> (2012) appears noisy and detecting beats are troublesome.</li> <li>• This method is influenced by motion artefacts to such an extent that it is unusable for most forms of practical use.</li> </ul>

**Table 3.7:** Ear PCG evaluation

	<p><b>Advantages</b></p> <ul style="list-style-type: none"> <li>• It can be used to detect breathing as well, as shown by Goverdovsky <i>et al.</i> (2016).</li> </ul>
<p>Sensor size: <math>4 \times 3 \times 1</math> mm (ST Electronics, 2016b)  Unobtrusiveness: Can fit inside the ear canal  Signal noise: High</p>	<p><b>Disadvantages</b></p> <ul style="list-style-type: none"> <li>• Sounds from other sources such as movement and speaking corrupt the signal.</li> </ul>

### 3.3.1.5 Final method choice

Ear PPG was selected as the Ear-Monitor's method of measuring heart rate. PPG produces a clear signal that will allow for accurate beat detection. This method can also be incorporated into the SpO<sub>2</sub> measurement sensor, eliminating the need for two different sensors. The entire sensor fits inside the ear canal, making it unobtrusive. This method is also less susceptible to noise than ear BCG or a phonocardiogram.

## 3.3.2 Sensor selection

Reflection mode ear canal PPG was selected to measure heart rate. Three PPG sensors options were considered, namely separate LEDs and photodetector, the NJL5501R by JRC and the MAX30100 by Maxim Integrated.

### 3.3.2.1 Separate LEDs and photodetector

Surface-mount technology (SMT) LEDs are used with one or more photodetectors. The components are mounted on a thin printed circuit board (PCB) and placed in the ear probe. The LEDs and photodetectors can be placed in various precise configurations and a wider choice of individual transducers can be used. Additional analogue electronics are needed to drive the LEDs, conditioning the detector signal output and compensating for ambient lighting. A commercial integrated analogue front-end (AFE) chip such as Texas Instruments' AFE4400 is used to perform this task.

### 3.3.2.2 NJL5501R

The NJL5501R is an SMT photo-emitter and detector contained in one  $1.9 \times 2.6 \times 0.8$  mm package, as shown in Figure 3.2. Red and infrared LEDs make it suitable for reflective pulse oximetry and heartbeat detection. Its small size allows it to fit in the ear canal while leaving adequate space for other sensors. It requires

all the same supporting electronics such as using the separate LEDs and a photodetector method.

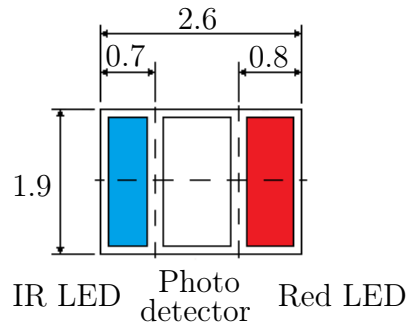


**Figure 3.2:** NJL5501R diagram from the datasheet (JRC, 2013)

### 3.3.2.3 MAX30100

The MAX30100 is a single-chip pulse oximeter and heart rate detector. It has red and infrared LEDs, a photodetector, a 16-bit ADC and digital filters all in one  $5.6 \times 2.8 \times 1.2$  mm, 14-Pin package. The LEDs and photodetector are in the same plane, which means it operates in reflective mode. Like the TMP006, it uses the I<sup>2</sup>C protocol to communicate with an MCU. Configuration registers allow the designer to specify sample rate, LED currents and LED pulse width. Figure 3.3 shows a block diagram of the internal systems of the MAX30100.

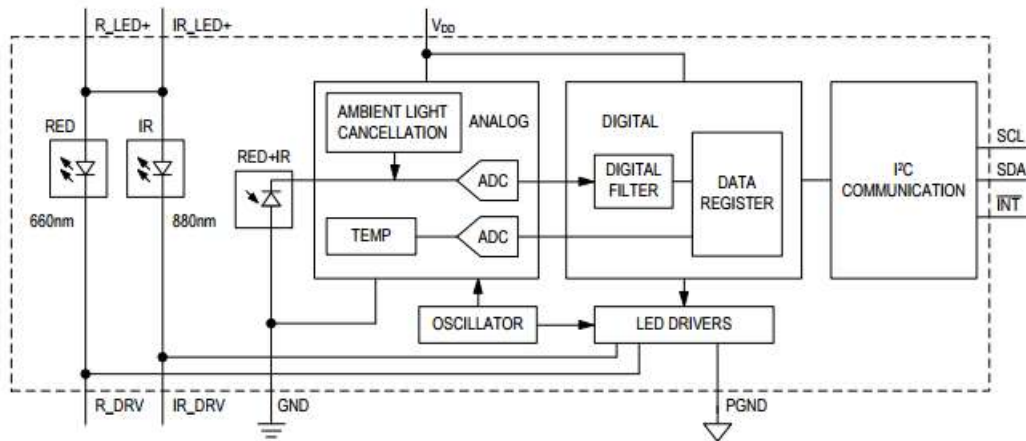


**Figure 3.3:** MAX30100 block diagram from the datasheet (MAX30100, 2014)

The MAX30100 uses a 3.3 V supply and programmable current sources to drive the LEDs, while digital operations are done at 1.8 V. It draws between 6 and 12 mA while recording red and infrared PPGs. It has a digital 50 and 60 Hz notch filter to reject powerline interference. LED current can be varied individually from 0 to 50 mA and the alternating LED pulse widths can be

varied from 0.2 to 1.6 ms. A sample rate can be selected between 5 and 1 000 samples per second.

### 3.3.2.4 Final sensor choice

The MAX30100 was selected for use in the Ear-Monitor. It has optimised optics to guide outgoing and incoming light. It has integrated ambient light cancellation. Its entire AFE is integrated, which means that no additional electronics are needed, apart from the I<sup>2</sup>C lines and power regulators. This gives it a big advantage over the more complex, separate LEDs and photodetector method. Its small size and reflective mode of operation allow it to be placed inside the ear canal. Data recorded by the MAX30100 can be used to calculate heart rate and SpO<sub>2</sub> as well.

## 3.4 Respiratory rate

The Ear-Monitor measures respiratory rate from inside the ear canal. The main criteria are sensor size and susceptibility to noise corruption.

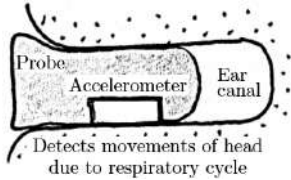
### 3.4.1 Measurement method

The following three respiratory rate measurement methods from literature were considered: accelerometer, microphone and respiratory related heart rate characteristics. Each option is evaluated separately.

#### 3.4.1.1 Accelerometer

A small MEMS accelerometer is placed inside the ear canal and measures the movement of the head caused by breathing. Table 3.8 summarises the evaluation.

**Table 3.8:** Ear accelerometer evaluation

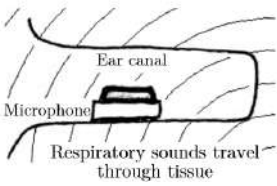
	<p><b>Advantages</b></p> <ul style="list-style-type: none"> <li>• The accelerometer can serve the dual purpose of measuring breathing and heart rate, thereby saving space.</li> </ul>
<p>Sensor size: 3×3×1 mm (ST Electronics, 2016a) Noise: Very high</p>	<p><b>Disadvantages</b></p> <ul style="list-style-type: none"> <li>• This method is extremely vulnerable to noise from other movements.</li> </ul>



### 3.4.1.2 Microphone

A microphone is placed inside the ear canal and records the sound of air moving through the respiratory tracts, allowing the respiratory rate to be determined. Table 3.9 summarises the evaluation.

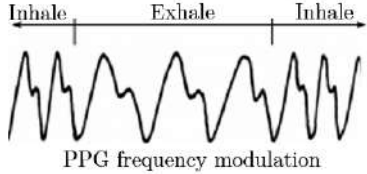
**Table 3.9:** Ear microphone evaluation

	<p><b>Advantages</b></p> <ul style="list-style-type: none"> <li>• The microphone can serve the dual purpose of measuring breathing and heart rate, thereby saving space.</li> </ul>
<p>Sensor size: <math>4 \times 3 \times 1</math> mm (ST Electronics, 2016b) Noise: Very high</p>	<p><b>Disadvantages</b></p> <ul style="list-style-type: none"> <li>• This method is extremely vulnerable to noise from other sounds, such as talking or ambient noise.</li> </ul>

### 3.4.1.3 Respiratory-related heart rate characteristics

Variations in heart rate are used to determine respiratory rate. These include AM, RIIV and RSA. Table 3.10 summarises the evaluation.

**Table 3.10:** Respiratory-related heart rate characteristics evaluation

	<p><b>Advantages</b></p> <ul style="list-style-type: none"> <li>• No dedicated sensor is needed.</li> <li>• It is less susceptible to noise than the accelerometer or microphone method.</li> </ul>
<p>Sensor size: No sensor needed Noise susceptibility: Low</p>	<p><b>Disadvantages</b></p> <ul style="list-style-type: none"> <li>• Only steady and relatively slow respiratory rates can be detected.</li> </ul>

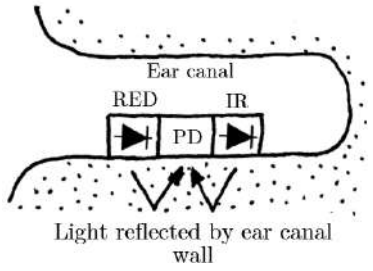
## 3.4.2 Final method choice

Respiration measurement through analysing respiratory-related heart rate characteristics, of which heart rate frequency modulation through RSA was found to be the most detectable, was selected for use in the Ear-Monitor. This method saves space by not requiring a dedicated sensor. It is also the least susceptible to noise from other sources. No sensor selection is needed for this vital sign, as all the work is done by the MCU.

### 3.5 Blood oxygen saturation

Pulse oximetry is the only practical way for the Ear-Monitor to measure blood oxygen saturation. The MAX30100 selected for measuring heart rate is equipped for this task. A red and infrared LED as well as a photodetector are available for the joint function of measuring heart rate and SpO<sub>2</sub>. Table 3.11 summarises the evaluation.

**Table 3.11:** Ear SpO<sub>2</sub> evaluation

	<p><b>Advantages</b></p> <ul style="list-style-type: none"> <li>• The pulse oximeter can serve the dual purpose of measuring SpO<sub>2</sub> and heart rate.</li> <li>• The sensor is small enough to fit inside the ear canal</li> </ul>
<p>Sensor size: 5.6×2.8×1.2 mm</p>	<p><b>Disadvantages</b></p> <ul style="list-style-type: none"> <li>• Pulse oximetry has an inherent margin of error larger than that of a blood gas test.</li> <li>• It is susceptible to motion artefacts and errors due to low blood perfusion.</li> </ul>

### 3.6 Final concept

The final concept was obtained by combining the methods and sensors selected in this chapter, which are summarised as follows:

- Core body temperature is measured by the TMP006 infrared sensor, located at the tip of the Ear-Monitor's ear probe and pointed at the tympanic membrane.
- Heart rate is measured by the MAX30100 reflective pulse oximeter placed on the side of the ear probe and facing the canal wall. The PPG signal is used to calculate heart rate.
- Respiratory rate is calculated by analysing RSA, which is the frequency modulating respiratory-related heart rate characteristic.
- SpO<sub>2</sub> is also measured by the MAX30100. The red and infrared PPGs obtained from the ear canal wall are used for this calculation.

In addition, a MCU, battery and wireless transceiver were selected for the Ear-Monitor. The Arduino Pro Mini MCU has the necessary input/output

(I/O) pins for serial communication with the sensors and wireless module. It is also easy to program, making it ideal for the proof of concept version of the Ear-Monitor. Lithium polymer (LiPo) batteries are currently the best choice when regarding capacity, compactness, rechargeability and price. It was therefore selected to supply power to the Ear-Monitor. Bluetooth is the typically used standard for transmitting data over short distances and is supported by most modern smart devices. The HC-05 Bluetooth modem was selected and allows the Ear-Monitor to send data to a supporting device through a wireless connection. Figure 3.4 shows a diagram of the Ear-Monitor concept with a more detailed drawing of the ear probe with the selected sensors.

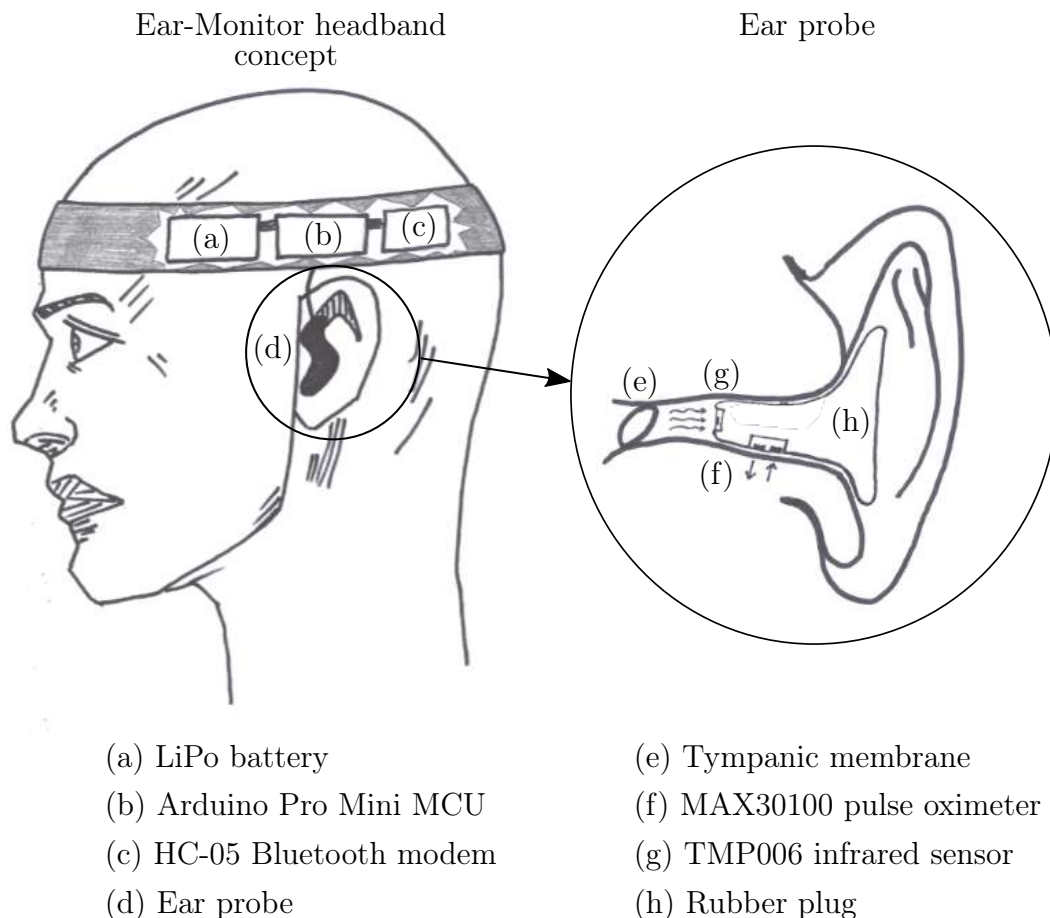


**Figure 3.4:** Ear-Monitor concept with components labelled

# Chapter 4

## Detailed Design

This chapter documents the detailed design of the subsystems of the Ear-Monitor. The hardware and software facets are discussed separately.

### 4.1 Hardware

A typical telemedicine configuration was used for the Ear-Monitor and its supporting system. It is similar to the configuration used by Wang *et al.* (2010) and Prawiro *et al.* (2016) for their respective wearable health monitors. The ear probe is the signal acquisition module of the Ear-Monitor and contains the sensors. An MCU is used to control the flow of data within the Ear-Monitor. Data is sent by means of a wireless transceiver to a device running supporting software, where data is stored for later access. Figure 4.1 illustrates the flow of information through the hardware set-up.



**Figure 4.1:** Flow of information in a typical telemedicine set-up

The detailed design of each of the key parts of hardware of the Ear-Monitor is documented in the following section.

#### 4.1.1 Temperature sensor

The non-contact infrared TMP006 was selected to measure tympanic membrane temperature in the Ear-Monitor. Four wires are connected for power and serial communication lines. The package has eight solder balls for surface

mounting on a PCB. A big challenge was to mount this micro-component. Various methods were tested:

- A PCB was designed and manufactured, but mounting the TMP006 on this PCB proved to be problematic. Because of its miniature size, an SMT component placement system and a reflow solder oven are required for mounting, but this was not available at the time.
- The device footprint and wire connection pads were etched into copper clad flexible circuit board sheets. Solder paste and a heat gun were used to mount the TMP006. Etching the flexible circuit board worked well, but mounting the TMP006 proved to be unreliable, as connections were sometimes not made properly or the component was damaged.
- Pre-mounted boards were acquired and the excess material was cut away to allow wires to be soldered to the exposed tracks.

This last method proved to be the best solution for the proof of concept version of the Ear-Monitor. It was necessitated by the lack of advanced facilities to mount micro SMT components. The flexible circuit board method will be preferable when an SMT component placement system is available. Figure 4.2 shows the procured, pre-mounted boards and the cut-out component with the four connections. 3.3V and ground (GND) are connected to a power regulator and the two serial communication wires are connected to the serial communication I/O pins of the MCU.

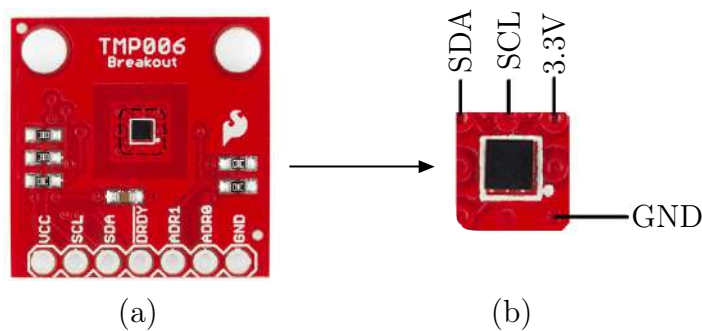


**Figure 4.2:** (a) TMP006 pre-mounted board; (b) the cut-out sensor segment with four connections labelled

According to the user guide of the TMP006, the sensor captures radiation from almost its entire 180° FOV, but the most of the received signal comes from sources that are parallel to, and precisely in front of the sensor. The final target object temperature is an integration of all the radiation signals captured across the FOV of the sensor.

The user guide also states that the smaller the object is, the closer it should be placed to the sensor to prevent other objects from entering the FOV. The TMP006 is placed at the tip of the ear probe within 5 mm of the tympanic membrane. This position removes the risk of contact with the membrane, while still ensuring that thermal radiation from the canal is detected. Energy from the ear canal itself is inevitably detected by the sensor, but the majority of the radiation comes from the membrane and it is assumed that the wall near the membrane is in thermal equilibrium with the membrane within an acceptable margin.

Energy radiated or conducted between the PCB and the sensor can cause temperature calculation errors. To prevent this, the sensor and PCB should be kept at the same temperature. The ear probe set-up of the Ear-Monitor is favourable for this task, as the PCB is very small and contains no other heat-generating components. Also, the target object (tympanic membrane) stays at a constant temperature, so the sensor experiences no heat fluctuations. It is, however, necessary to allow time for the sensor and PCB to reach thermal equilibrium once placed inside the ear canal, before accurate measurements can be taken. This is not a problem, as the device was designed to be worn continuously for long periods.

### 4.1.2 Pulse oximeter

The MAX30100 pulse oximeter was selected to record red and infrared photoplethysmographs from inside the ear canal. These are used for determining heart rate and  $SpO_2$ . The MAX30100 is controlled through five connection wires, connected to seven of the fourteen pins of the package. Figure 4.3 shows a diagram of the MAX30100 package and the required connections for operation. 3.3 V, 1.8 V and GND are connected to a power regulator and the two serial communication lines are connected to the serial communication I/O pins of the MCU.

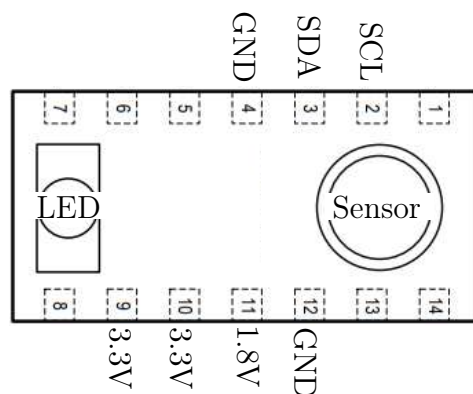


**Figure 4.3:** MAX30100 package diagram with required connections for operation (MAX30100, 2014)

As with the TMP006, the mounting of the extremely small MAX30100 was a great challenge. The first attempt was to design and manufacture a PCB on the typically used, 1.6 mm thick, FR4 PCB material. This PCB proved to be too thick and its inflexibility caused additional problems in ensuring firm contact with the ear canal wall. The solution was to etch the footprint, tracks and pads into flexible circuit board material. The etching process involved the following:

- Design the layout on EAGLE PCB open-source software.
- Print the mirrored layout on toner transfer paper.
- Prepare the copper clad material by cleaning it with rubbing alcohol.
- Transfer the ink from the toner transfer paper to the copper clad material by applying heat and pressure.
- Submerge the copper clad material with ink layout in ferric chloride ( $\text{FeCl}_3$ ).
- Remove the remaining ink with acetone to reveal the copper tracks.

The ferric chloride dissolves all the copper that is exposed, leaving copper tracks that were covered by the ink during etching. The flexible copper clad material is  $60\ \mu\text{m}$  thick, which is ideal for the size limitations inside the ear canal. Figure 4.4 shows the layout designed and resulting etched flexible circuit board. The flexible nature of the circuit board allows it to be folded in half to form a two-sided circuit board, saving space and placing all the connection pads on the same end. It also allows for uniform and firm contact between the MAX30100 and the ear canal wall. Wires for power and communication were soldered to the five connection pads.

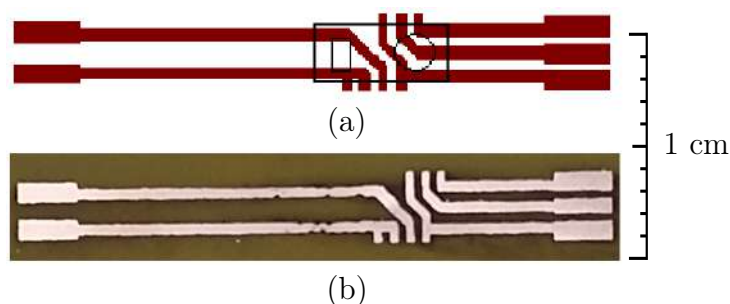


**Figure 4.4:** (a) Layout as designed on EAGLE PCB with the outline of the MAX30100 shown in black; (b) the finished flexible PCB with copper tracks

### 4.1.3 Control and communication hardware

The remaining electronic components consist of the Arduino MCU, HC-05 Bluetooth modem and battery. A PCB was designed to integrate all the different hardware subsystems. Additional electronics include the power regulators, I<sup>2</sup>C pull-up resistors and a charging circuit for the LiPo battery. An on-off switch and power-on indicator LED were also added.

10 k $\Omega$  pull-up resistors on the SDA and SCL lines are recommended for standard I<sup>2</sup>C communication and were therefore included in the design. A 7.4 V, 2000 mAh rechargeable LiPo battery was selected to supply power to the Ear-Monitor. The Ear-Monitor can be operated for 25.9 hours on a charge (calculations in Appendix A). The Arduino has its own power regulation circuitry on board and can be connected directly to the battery. Two low drop-out voltage regulators were selected to supply 1.8 V and 3.3 V to the sensors and Bluetooth modem. A charging circuit was added to allow the battery to be charged without physically disconnecting it from the device. Decoupling capacitors were added to all power supply lines. Figure 4.5 depicts a block diagram of the hardware of the Ear-Monitor. The diagram is split between the PCB components worn on the head and the components in the ear probe.

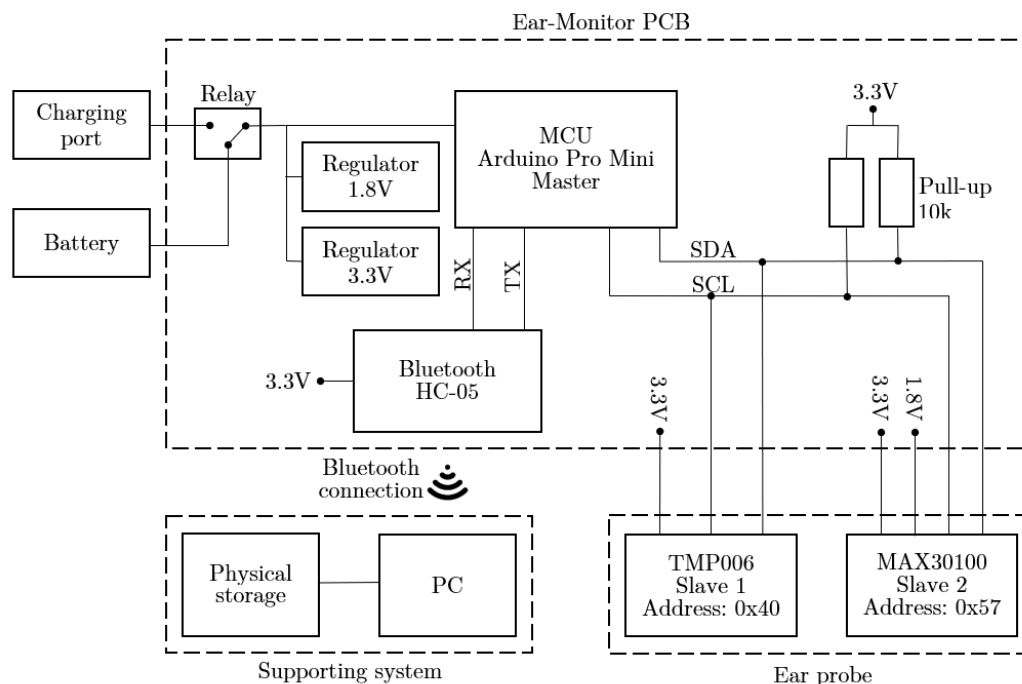


**Figure 4.5:** Block diagram of the Ear-Monitor's hardware components

A schematic diagram and PCB layout are included in Appendix B. Calculations to select certain components are included in Appendix A. The MCU, battery, Bluetooth modem and PCB are worn in a headband around the head in this proof of concept version of the Ear-Monitor. Only the TMP006 and



MAX30100 are located at their correct positions in the ear canal, and held in place by the ear probe. The ear probe is connected by a wire to the electronics in the headband. Data is sent from the headband to the PC through the wireless connection. It is well within the abilities of the current state of technology to reduce the size of all the electronics to a hearing aid, or even an ear probe size device. Such miniaturisation was, however, not within the scope of this project.

An ear probe is designed to hold the MAX30100 and TMP006 in the correct positions in the ear canal and restricts their movement to minimise artefacts. Sugru<sup>®</sup> is the brand name for a mouldable silicone elastomer that is ideal for this application. According to the product documentation, it is non-toxic and does not cause skin irritation. The mouldable putty is pressed into the ear and assumes its shape, but does not conform completely. Therefore, it allows the probe to fit in different ear shapes. When cured, it has a sturdy, but flexible structure. Slots and holes are cut into the moulded probe to hold the sensors and wires. Figure 4.6 is a photo of the completed ear probe and Figure 4.7 depicts the entire hardware set-up of the Ear-Monitor.



Figure 4.6: Ear probe with TMP006 visible

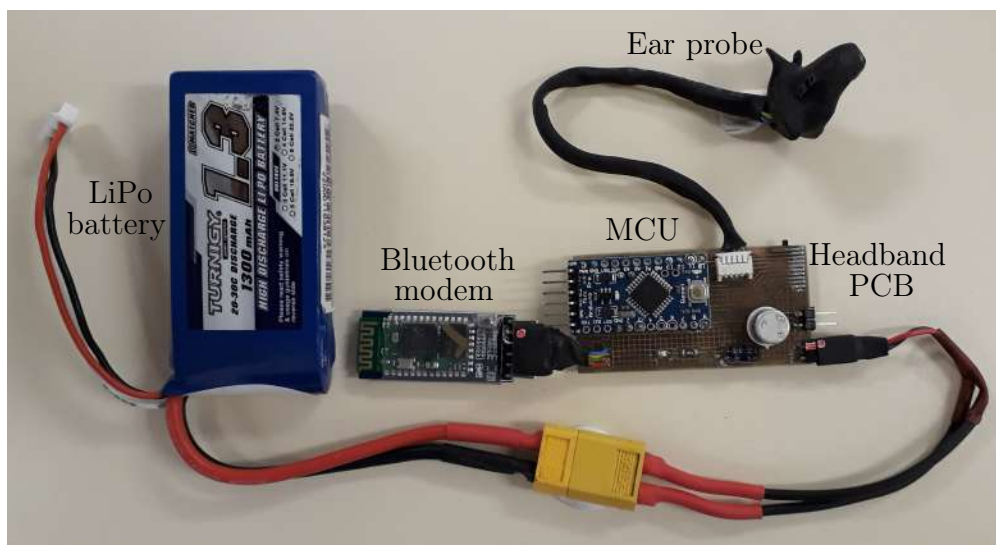
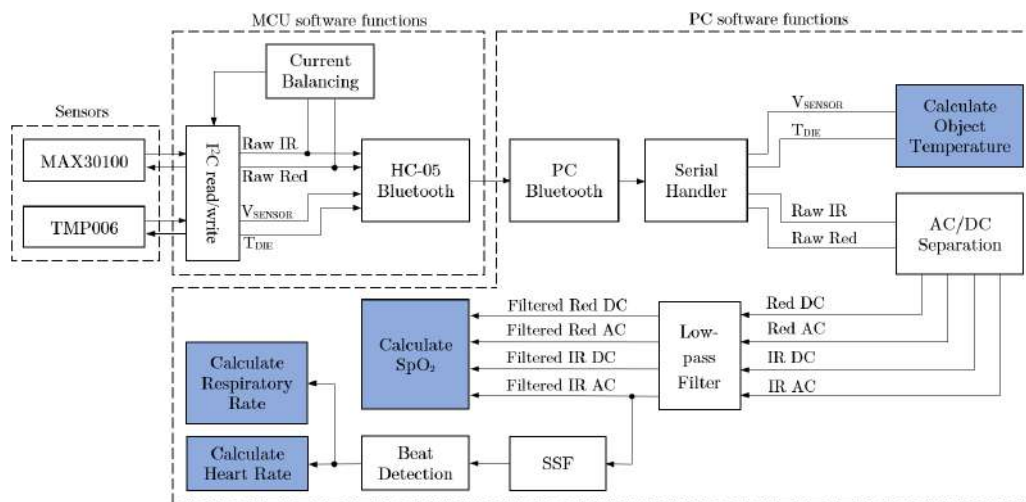


Figure 4.7: Hardware of the Ear-Monitor

## 4.2 Software

Software was written for the MCU and for the PC receiving and storing the data. MCU software is based on C++ and developed using the Arduino IDE. MCU software handles sensor communication, timing, selected processing functions and the transmission of collected data via the Bluetooth modem. The PC software is based on Java and developed using the Processing IDE. The PC software listens on the Bluetooth serial port, processes received data, displays the data via a user interface and stores the received data on the local hard drive.

Figure 4.8 describes the flow of data through the various software functions. The final calculated vital signs are shown in blue. The diagram is split between the MCU functions and PC functions. MCU and PC software are connected through the Bluetooth connection. The main functions are discussed in this section.



**Figure 4.8:** Block diagram of the flow of information through the various software functions; final calculated vital signs are shown in blue

### 4.2.1 Sensor communication

Software was written for the MCU to communicate with the sensors and Bluetooth module. The MAX30100 and TMP006 have different default addresses and can share one I<sup>2</sup>C bus for communication with the MCU. I<sup>2</sup>C communication happens one byte at a time with no parity and most significant bit (MSB) first. The eighth bit of the address indicates a read or write request. Figure 4.9 explains how the software reads 16-bit values from the TMP006 registers. Values from the MAX30100 are read in a similar way. Communication with sensors consists of two steps: configuration and reading data.

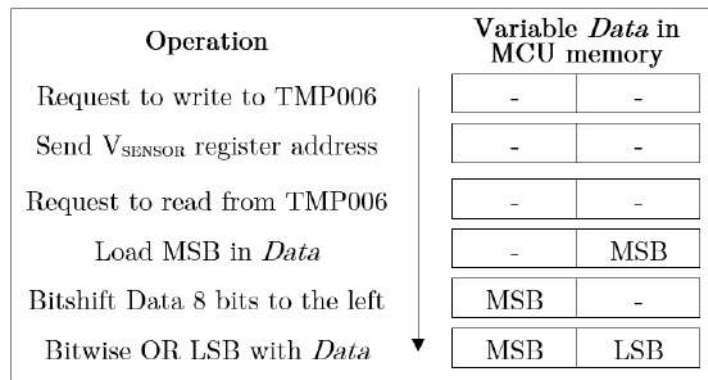


**Figure 4.9:** Diagram of how the software reads 16-bit values from the TMP006 registers

#### 4.2.1.1 Sensor configuration

Upon power-on, both sensors start with their default configurations. The MCU was programmed to reconfigure both sensors on start-up. This is done by writing values to the various configuration registers. The MAX30100 was set to SpO<sub>2</sub> mode with 1600  $\mu$ s LED pulse width, 50 Hz sampling rate and 50 mA current supply to both LEDs. The TMP006 was set to use the average of 16 conversions per output, meaning it will sample at 0.25 Hz. This was done, because the application does not demand a high sampling rate and increasing the number of samples per output will reduce noise ( $\pm 0.125$  °C). These configurations are done every time the Ear-Monitor is powered on.

#### 4.2.1.2 Reading sensors data

After configuration is done, the MCU enters a continuous loop of sensor data reading. An important feature of the MAX30100 is its 64-byte deep first-in, first-out (FIFO) register which is used to store the output values. Each output set consists of a 16-bit red and 16-bit infrared value, which means that there are four bytes per output and therefore 16 sets of output values can be held in the FIFO at any time. The MCU reads four bytes at a time from the FIFO to obtain the latest red and infrared values. The TMP006 has two separate registers for die temperature and sensor voltage. These registers are read through Arduino's Wire library. The MAX30100 outputs at 50 Hz and the TMP006 at 0.25 Hz. A timing loop was created to ensure that the values are read from the sensors in time.

### 4.2.2 Core temperature

After start-up configuration, two values,  $V_{\text{SENSOR}}$  and  $T_{\text{DIE}}$ , are read from the TMP006 through the I<sup>2</sup>C connection every four seconds.

$T_{DIE}$  is measured by an on-chip precision thermistor and digitalised to a 14-bit value in binary two's complement, signed integer format with one LSB equal to  $0.03125^\circ\text{C}$ . After two bytes have been read from the TMP006's  $T_{DIE}$  register (as shown in Figure 4.9), it is bitshifted twice to the right to get the 14-bit value and then divided by 32 to get the temperature in  $^\circ\text{C}$ . Table 4.1 shows an example calculation to obtain  $T_{DIE}$ . This conversion is done on the MCU and the value in  $^\circ\text{C}$  is transmitted over the Bluetooth connection.

**Table 4.1:**  $T_{DIE}$  example calculation

Digital output	Right shifted twice	Decimal	$\div 32$
0000 1100 1000 0000	0000 0011 0010 0000	800	$25^\circ\text{C}$

$V_{SENSOR}$  is the output of the thermopile and ranges from  $-5.12$  to  $5.12$  mV. The 16-bit ADC converts this analogue value to a digital value with an LSB equal to  $\frac{5.12 - (-5.12)}{2^{16}} = 156.25$  nV. Conversion to voltage is done prior to sending the voltage value over the Bluetooth connection.

$T_{DIE}$  and  $V_{SENSOR}$  are received by the PC software, where they are used to calculate  $T_{OBJ}$ . One sensor voltage and die temperature conversion cycle takes 250 ms, and the device gives the designer an option to choose the number of conversions ( $N$ ) per output sample. The average of the  $N$  samples is loaded into the output register every  $N \times 250$  ms. In this design  $N$  is chosen to be 16 and the time per register output equals four seconds.

#### 4.2.2.1 Calculating $T_{OBJ}$

$T_{DIE}$  and  $V_{SENSOR}$  are used to calculate  $T_{OBJ}$ . The datasheet of the TMP006 suggests using the relationship:

$$T_{OBJ} = \sqrt[4]{T_{DIE}^4 - \frac{f(V_{SENSOR})}{S}} \quad (4.1)$$

where  $f(V_{SENSOR})$  is a function that compensates for heat flow in the form of convection and conduction. The function is described in two stages by:

$$V_{OS} = B0 + B1(T_{DIE} - T_{REF}) + B2(T_{DIE} - T_{REF})^2 \quad (4.2)$$

and

$$f(V_{SENSOR}) = (V_{SENSOR} - V_{OS}) + C(V_{SENSOR} - V_{OS})^2 \quad (4.3)$$

where  $V_{OS}$  is a compensating offset voltage,  $T_{REF}$  is a reference temperature equal to  $25^\circ\text{C}$  and  $B0$ ,  $B1$ ,  $B2$  and  $C$  are calibration parameters.  $S$  takes into account the object emissivity ( $\epsilon$ ), Stefan-Boltzman constant ( $\sigma$ ) and the non-ideal absorption of the sensor itself. It is described by:

$$S = S0(1 + A1(T_{DIE} - T_{REF}) + A2(T_{DIE} - T_{REF})^2) \quad (4.4)$$

where  $S0 = \varepsilon\sigma$ ,  $T_{REF} = 25^\circ\text{C}$  and  $A1$  and  $A2$  are parameters experimentally derived through calibration.

The TMP007 is the same sensor as the TMP006, but with a built-in mathematics engine. The recommended calibration parameters from the TMP007's data sheet are shown in Table 4.2. These parameters can also be seen as the default calibration parameters for the TMP006 and are selected as a starting point for the calibration process.

**Table 4.2:**  $T_{DIE}$  example calculation

S0	C	A1	A2	B0	B1	B2
4.43e-14	0	9.99e-4	-6.02e-6	-3.09e-5	-8.72e-8	1.30e-8

The TMP006 in the Ear-Monitor operates in a relatively narrow temperature range. Plotting the  $T_{OBJ}$  equation over the range  $T_{OBJ} = 35$  to  $40^\circ\text{C}$ ,  $T_{DIE} = 35$  to  $39^\circ\text{C}$  and  $V_{SENSOR} = -46.88$  to  $23.44\ \mu\text{V}$  with recommended calibration parameters (Table 4.2) reveals a surface resembling a flat plane. This plot can be seen in Figure 4.10.

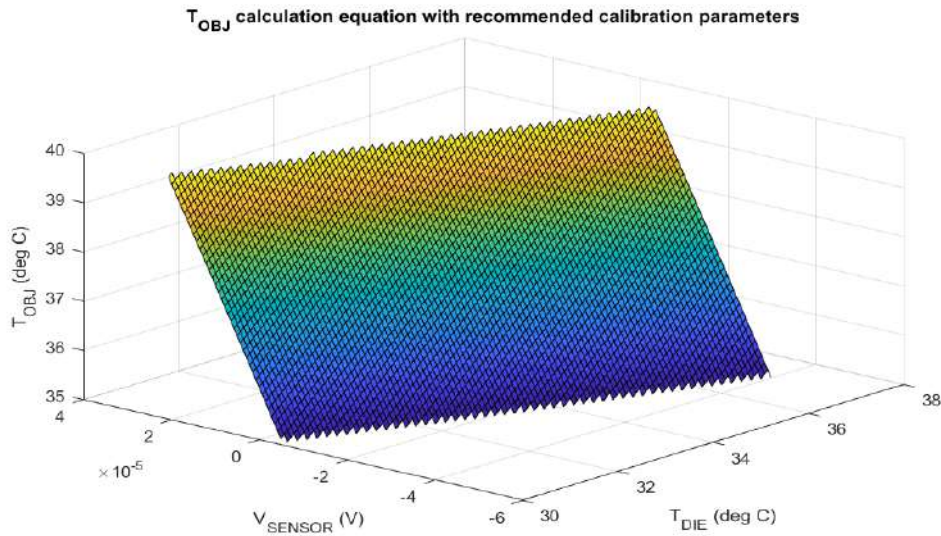


**Figure 4.10:** Plot of the  $T_{OBJ}$  equation with recommended calibration parameters over the operating temperature range of the Ear-Monitor

This linear characteristic of the TMP006 in the operating temperature range of the Ear-Monitor is used to simplify the  $T_{OBJ}$  calculation method, as described in equations 4.1 to 4.4. These bulky recommended equations are replaced by a first-degree polynomial formula for a flat plane, as described by:

$$T_{OBJ} = P0 + P1 \cdot T_{DIE} + P2 \cdot V_{SENSOR} \quad (4.5)$$

where  $P0$ ,  $P1$  and  $P2$  are parameters to be determined by a calibration process that follows the trial stage. The temperature calibration procedure is included in Appendix C. The the resulting formula for  $T_{OBJ}$  can be see in Equation 4.6.

$$T_{OBJ} = 22.85 + 0.04803T_{DIE} - 13440V_{SENSOR} \quad (4.6)$$

### 4.2.3 PPG signal processing

The PPG signal is crucial to the calculation of heart rate, respiratory rate and  $SpO_2$ . This signal is captured by the MAX30100 pulse oximeter. The MAX30100 has on-chip digital filters for 50 and 60 Hz interference and low-frequency ambient noise. Despite on-chip filtering, signal drift and high-frequency noise still contaminate the signal. This causes the detection of false heartbeat peaks and noisy  $SpO_2$  calculations. An AC and DC extraction algorithm and low-pass filter were designed to prime the signal for further processing. Figure 4.11 shows how the signal samples for the MAX30100 are processed.  $x_n$  is the PPG signal measured by the MAX30100 in the ear canal and  $y_n$  is the processed signal.

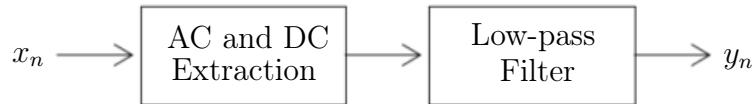


**Figure 4.11:** The raw PPG signal,  $x_n$ , is sent through AC and DC extraction and filtering functions

#### 4.2.3.1 AC and DC separation

An algorithm was implemented to digitally separate the AC and DC components of the red and infrared signals. Signal separation needs to be done in real time and with the minimal computational overhead, because it is executed on the MCU. The following infinite impulse response (IIR) filter is used for AC extraction (Koblenski, 2015):

$$w_n = x_n + \alpha \cdot w_{(n-1)} \quad (4.7)$$

$$y_n = w_n - w_{(n-1)} \quad (4.8)$$

where  $x_n$  is the raw ADC value from the MAX30100,  $w_n$  is an intermediate value and  $y_n$  is the filter output. This filter has a narrow stop band at the DC frequency when the scale factor,  $\alpha$ , is close to 1. Scale factor  $\alpha = 0.7$  was chosen, as it gives the best DC rejection while maintaining an acceptable response time. The DC component of the signal is used during LED bias adjustment and  $SpO_2$  calculations. To get the DC value, the AC value is subtracted from the raw signal. Alternative AC extraction methods tested were high-pass finite impulse response (FIR) filtering and moving average subtraction. These



methods were rejected, because a high-pass FIR filter is too computationally intensive and moving average subtraction will also attenuate frequencies close to DC. Figure 4.12 shows the PPG signal before and after the AC extraction function.

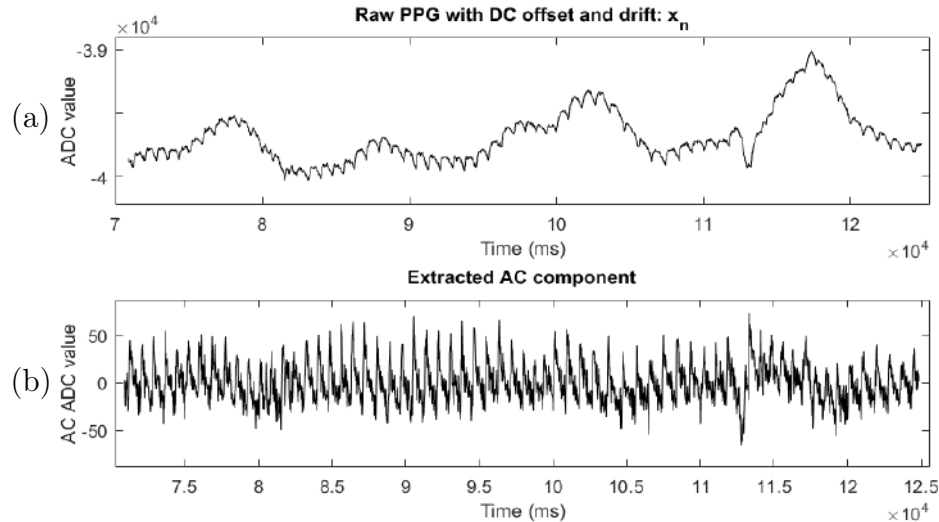


**Figure 4.12:** (a) The raw infrared signal contaminated by DC offset and drift; (b) the extracted AC component of the signal

#### 4.2.3.2 Low-pass filter

The separated AC and DC components of the red and infrared signals are passed through a third-order IIR Butterworth filter. The coefficients were calculated with MATLAB for a cut-off frequency of 3 Hz. Equation 4.9 is the transfer function  $H(z)$  of the filter.

$$H(z) = \frac{0.0048 + 0.0143z^{-1} + 0.0143z^{-2} + 0.0048z^{-3}}{1.0000 - 2.2501z^{-1} + 1.7564z^{-2} - 0.4683z^{-3}} \quad (4.9)$$

Figure 4.13, on the next page, shows the effect of the low-pass filter on the AC signal as extracted in the AC and DC separation function.

#### 4.2.4 Beat detection

Heartbeats appear as peaks on the inverted PPG signal. The infrared PPG is chosen for beat detection, as infrared light absorption by oxyhaemoglobin is higher than that of red light. Therefore, infrared pulse peaks are more prominent and better suited for the detection of heartbeats. A software algorithm was developed to detect these peaks in order to calculate average heart rate, breathing rate and  $SpO_2$ . The algorithm takes as input the filtered infrared PPG signal ( $y_n$ ) and outputs a timeseries of the heartbeats. Figure 4.14 shows a plot of a PPG signal with characteristic features labelled.

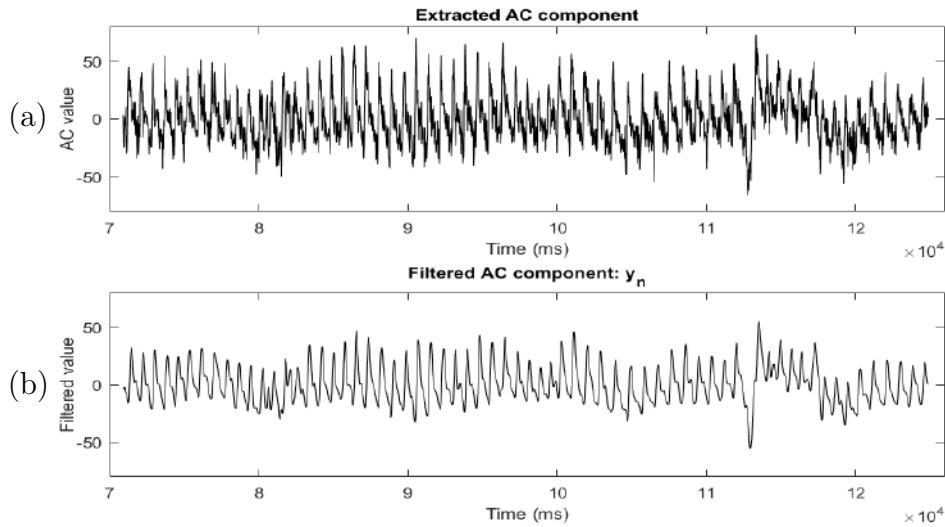


**Figure 4.13:** (a) The AC component of the infrared signal before filtering; (b) the signal after filtering

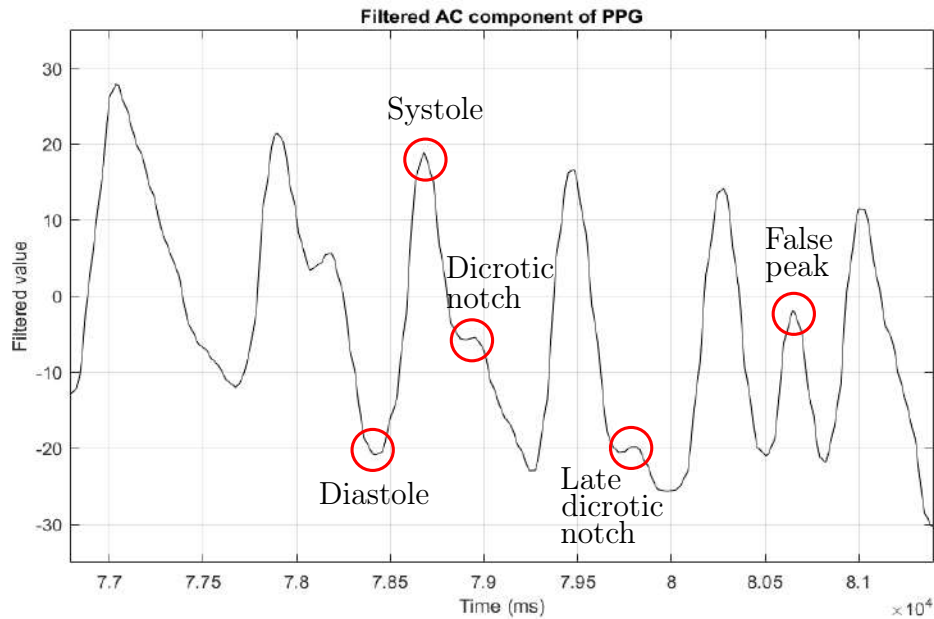


**Figure 4.14:** Filtered AC component of PPG with important features labelled

This signal extract shows the challenges of the peak detection algorithm. The amplitude of the peaks varies significantly and local maxima, which can trigger false positives, are present. The intermediate peak in the descending part of the peak is the dicrotic notch, due to the aortic valve closing. Only true systolic peaks should be registered as a heartbeat. The beat detection algorithm needs to be robust, computationally inexpensive and should not require any user-specific modifications.

These obstacles were overcome by a two-stage peak detection algorithm



developed specifically for the PPG of the Ear-Monitor. The algorithm builds on the work done by Park *et al.* (2015), Zong *et al.* (2003) and Elgendi *et al.* (2013).

#### 4.2.4.1 Stage 1

Stage 1 is a morphological conversion in the form of a slope summing function (SSF). This method was also used by Zong *et al.* (2003), Park *et al.* (2015) and Elgendi *et al.* (2013). The SSF is defined piecewise according to its derivative,  $\Delta y_n$ , as shown by Equation 4.10. The aim of the SSF is to enhance the rising section of the pulse peak while suppressing the falling section.

$$z_n = \sum_{i=n-k}^n \Delta y_i, \quad \text{where} \quad \Delta y_i = \begin{cases} \Delta y_i, & \text{if } \Delta y_i < 0 \\ 0, & \text{if } \Delta y_i \geq 0 \end{cases} \quad (4.10)$$

The  $n^{\text{th}}$  SSF output value,  $z_n$ , equals the sum of the previous  $k$  filtered PPG slopes as defined by the conditions in Equation 4.10. Zong *et al.* (2003) suggested choosing  $k$  as the typical duration of the pulse up-slope, so a moving sum window of  $k = 10$  was selected. Figure 4.15 shows the AC component of the PPG signal and the output of the SSF.

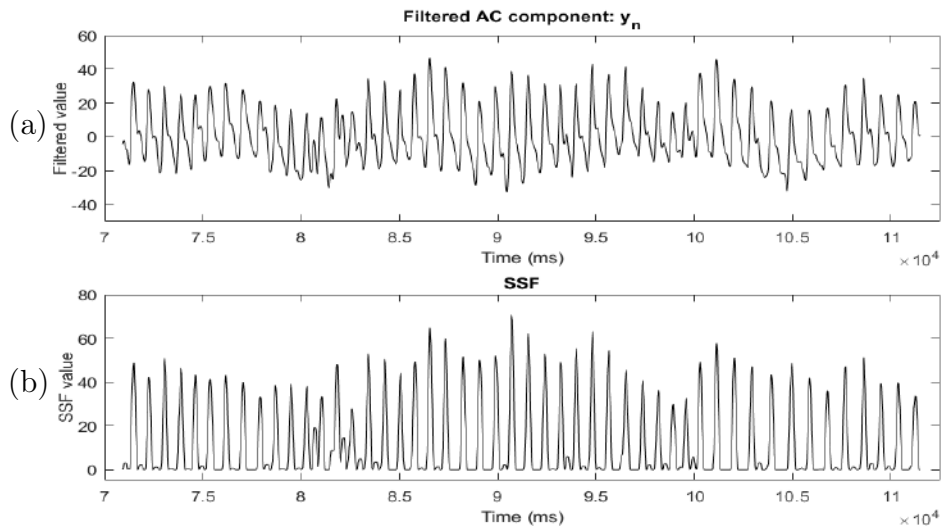


**Figure 4.15:** (a) The AC filtered component of the infrared signal; (b) the signal after passing through the SSF

#### 4.2.4.2 Stage 2

Stage 2 of the beat detection function is a set of decision making rules to determine whether a peak is present. Some of the rules were adapted from Park *et al.* (2015). Their algorithm was applied to in-ear pulse waves, which are closer to a ballistocardiogram than a photoplethysmogram. Therefore, the

decision rules in this function were chosen specifically for the Ear-Monitor and determined through experimentation.

**Rule 1: Adaptive threshold**

The adaptive threshold applied to this algorithm is related to the mean of the previous three detected SSF peak heights by Equation 4.11.

$$t = \alpha \frac{\sum_{k=0}^2 z_{n-k}}{3}, \quad (4.11)$$

where  $\alpha$  is an experimentally determined scaling factor equal to 0.5 and  $z$  is the output of the SSF. If the SSF signal amplitude rises above the threshold, a potential peak is awaited. Zong *et al.* (2003) used a threshold equal to 60% of the previous SSF peak amplitude, but this method proved to miss heartbeats if subsequent SSF maxima vary more than the threshold percentage. This problem was mitigated by basing the threshold on the previous three-peak average.

**Rule 2: Local maximum point**

Following the crossing of the threshold, the algorithm monitors the SSF output for a local maximum. This occurs at  $z_{n-1}$  when:  $z_{n-2} < z_{n-1} \geq z_n$ , where  $z$  is the output of the SSF.

**Rule 3: Waiting period**

If a local maximum is detected, the time elapsed since the previous successfully detected beat is tested. If the time is less than a dynamic waiting period, the local maximum is rejected. The waiting period is set to be 70% of the mean of the previous 10 beat periods.

Only if all three rules apply to an SSF value will it be registered as a peak. The time difference between the newly detected peak and the previous one is the heartbeat period. Another element to the beat detection algorithm is the threshold reset. If no local maximal is detected above the threshold for longer than two times the mean of the previous 10 beat periods, the threshold is reset to 1. This is in case the amplitude of the SSF peaks drops below the threshold and no beats are registered to update the threshold to a lower value. Figure 4.16 shows the example signal's SSF with detected beats. This example illustrates how the algorithm can successfully detect peaks of varying amplitude using the threshold method and how the time delay prevents the triggering of false peaks.

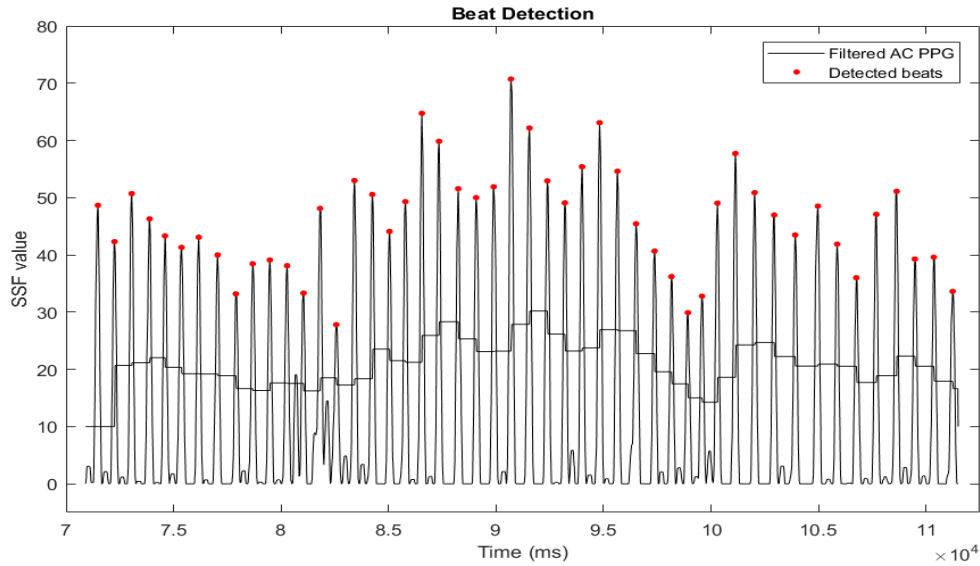


Figure 4.16: SSF with detected beats and threshold

Figure 4.17 illustrates how the SSF and beat detection algorithm can extract beats, even in noisy signals. It depicts an especially irregular AC component of the Ear-Monitor PPG signal (blue), the corresponding SSF (orange) and the adaptive threshold (gray). Detected peaks are marked in red. It can be seen how the SSF emphasises the rising slopes of the PPG signal, even when the amplitudes and baseline of the PPG varies significantly. The adaptive threshold prevents the detection of false peaks at (a) and (b) and the waiting period prevents the detection of false peaks at (c) and (d).

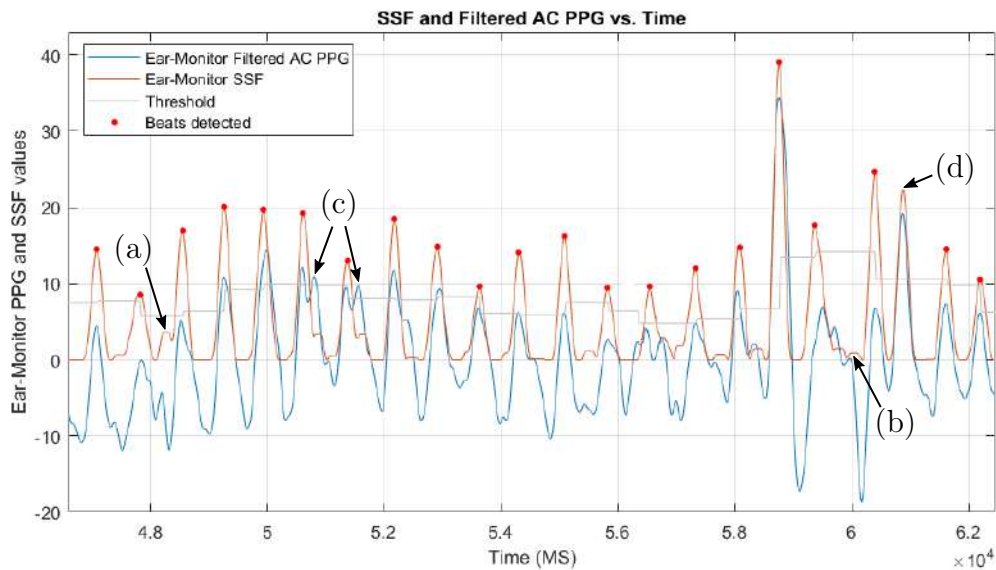


Figure 4.17: Peak detection example

#### 4.2.4.3 Heart and respiratory rate calculations

The Ear-Monitor uses a moving average of the previous 10 heartbeat periods to calculate heart rate in beats per minute. This calculation is executed every time a heartbeat is detected and is done by the PC software.

Respiration rate is determined by monitoring RSA, the frequency modulating respiratory-related heart rate characteristic. During inhalation, the heart rate increases and during exhalation, it decreases. RSA is not easily observed in a PPG plot, but becomes visible when plotting the heartbeat periods. Figure 4.18 shows plots of the heartbeat period and of the chest expansion due to the respiratory cycle. The synchronisation to the heart period variation and the respiratory rate is clearly visible, with each chest expansion maximum corresponding with a heartbeat period minimum.

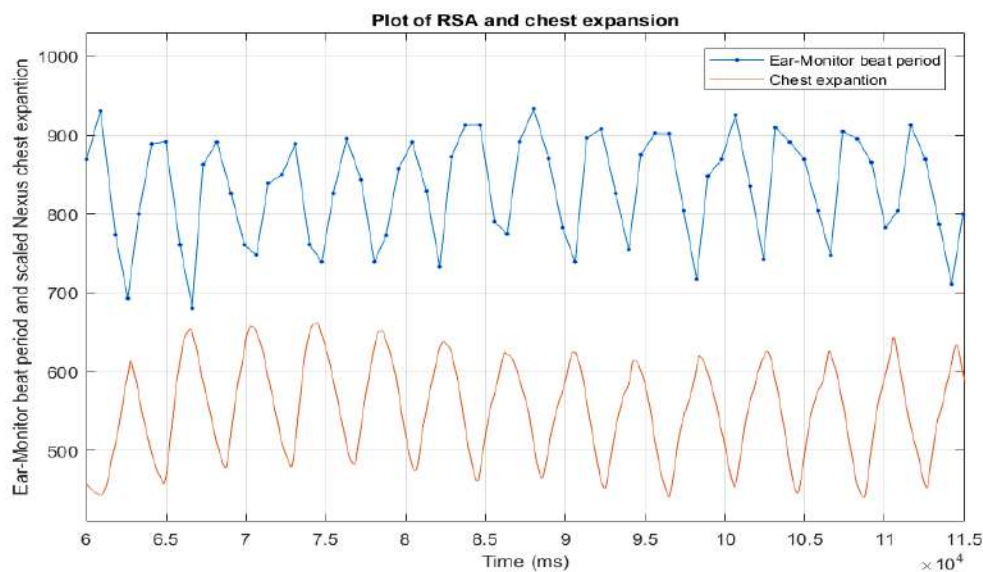


Figure 4.18: Plots of heartbeat periods and chest expansion

To remove noise and reduce false positives, a two-period moving average of the beat period signal is taken. An inhalation is registered each time a local maximum is detected on this filtered signal. The number of inhalations detected in a minute is used to calculate the respiratory rate in breaths per minute. The heartbeat periods can be seen as samples, and therefore the heart rate as the sample rate. This means that, according to the Nyquist theorem, the highest theoretical respiration rate that can be measured by the Ear-Monitor will equal half the heart rate.

#### 4.2.5 SpO<sub>2</sub> calculation

The MAX30100 outputs digital values representing the intensity of red and infrared light reflected by the tissue. Due to the different absorption spectra

of oxygenated and deoxygenated blood, these values are used to determine the fraction of peripheral blood oxygen saturation. MCU software was written to control the sensor and PC software was written to calculate the SpO<sub>2</sub>.

#### 4.2.5.1 Current balancing

The ratio of ratios method, discussed in the literature review and shown in Equation 4.12, was used to calculate SpO<sub>2</sub>.

$$R = \frac{\left(\frac{AC}{DC}\right)_{\text{red}}}{\left(\frac{AC}{DC}\right)_{\text{IR}}} \quad (4.12)$$

The motivation behind using this method was that it compensates for differences in DC reflection between individuals. For this to work, the difference between the red and infrared DC values used in the equation needs to be as small as possible. The currents to the red and infrared LEDs of the MAX30100 are set to 50 mA upon start-up configuration. To compensate for the fact that infrared light is reflected differently by the tissue than red light, a dynamic current balancing function was written.

The MAX30100 has a programmable register that allows for the individual current adjustment of red and infrared LED drivers. A negative feedback control system was implemented on the MCU to adjust the individual LED currents in order to lower the difference in reflection. A lower current equals a lower light intensity and subsequently, less reflection. The function checks the difference in infrared and red DC levels every second and adjusts the current to the LEDs until the difference is within an acceptable margin. Figure 4.19 shows a plot of this process. The difference in reflection starts out at 15 000, with both LED currents equal to 50 mA, and after five adjustments the difference is lowered to 1 000, with the red LED current unchanged and the infrared LED equal to 33.9 mA. As can be seen from Figure 4.19, the current adjustments happen in a stepwise fashion, with each step about 2 700. Therefore, to avoid oscillations, the margin was set to 2 000.

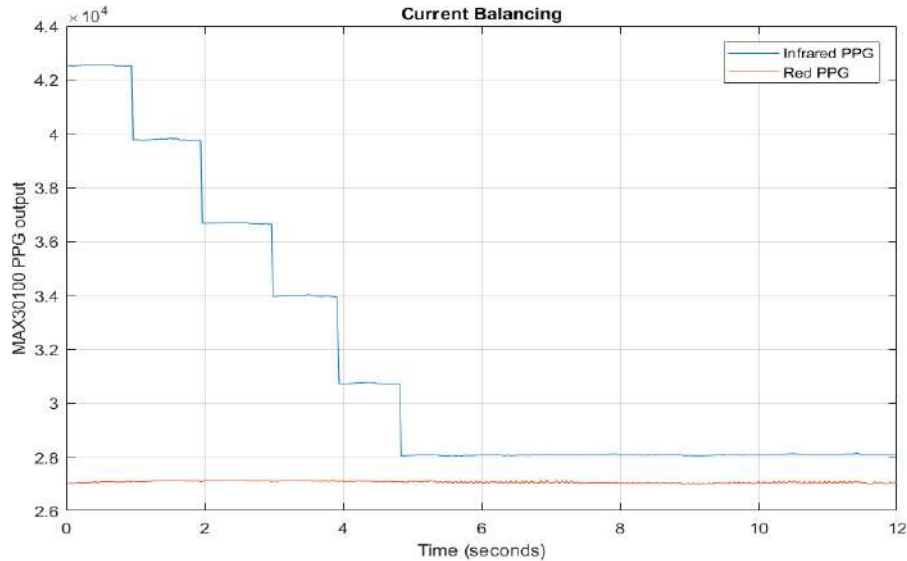


**Figure 4.19:** The current balancing function lowering the difference in detected light between red and infrared LED by adjusting the current to the infrared LED.

#### 4.2.5.2 Moving average SpO<sub>2</sub>

SpO<sub>2</sub> calculation was done by the PC interface software. The filtered AC and DC components of the infrared and red PPG signals, as calculated in the PPG signal processing section, were used in the ratio of ratios method.  $R$  was calculated using the mean of the absolute AC and DC values of the previous 12 heartbeats. These values are updated each time new PPG data becomes available.

The relationship between  $R$  and SpO<sub>2</sub> is unique for different devices and measurement locations. A calibration process, outlined in Appendix C, is conducted to find the relation for the Ear-Monitor and Equation 4.13 shows the resulting formula.  $R$  and SpO<sub>2</sub> are calculated on every heartbeat using the moving data window of the previous 12 heartbeats.

$$SpO_2 = 106.32 - 15 \cdot R \quad (4.13)$$

#### 4.2.6 PC interface

A graphical user interface was written in Processing to display the measurements on the computer screen and allows the user to set alarms and save the data. The interface receives variables from the various functions discussed. It displays these variables along with a series of real-time graphs and has the option to save the measured Ear-Monitor data in a .csv file for later reference or analysis. Figure 4.20 shows a screen shot of the user interface with (a) the SSF with detected beats, (b) the AC components of the red and infrared PPGs,

(c) respiration illustrated by plotting the heartbeat period, (d) temperature, (e) data written to .csv files and (f) alarm conditions.

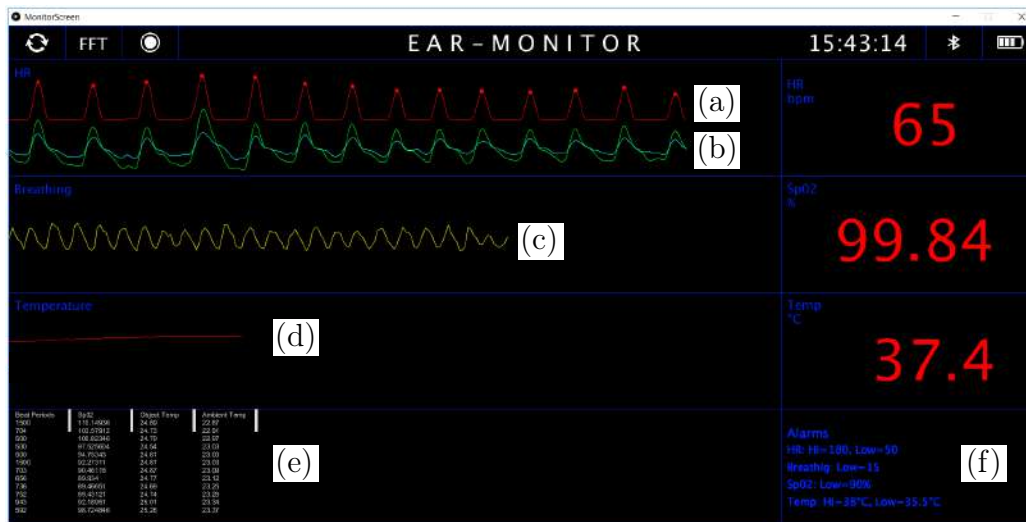


Figure 4.20: Ear-Monitor user interface

# Chapter 5

## Experimental trial

A trial was conducted during which the Ear-Monitor was tested on a sample of 16 healthy, adult volunteers. The trial's goal was twofold: firstly, to calibrate the temperature and SpO<sub>2</sub> algorithms and secondly, to evaluate the accuracy of the Ear-Monitor's measurements. This chapter describes the trial environment and the methods used to collect data for calibration and evaluation. Ethical approval was obtained for this trial from the Health Research Ethics Committee of Stellenbosch University, under the reference number M16/09/038 (proof of approval included in Appendix D).

### 5.1 Participant selection

Participants for the study were invited via a recruitment e-mail sent to students and staff at the Faculty of Engineering, University of Stellenbosch. Inclusion criteria were physical health, age ranges from 18 to 60 years and volunteers of any gender or race. Exclusion criteria were small ear canal size, ear abnormalities or injuries and general health issues. If the ear canal of the individual is smaller than 5 mm diameter, the probe of the Ear-Monitor will not fit. This also applies to ear abnormalities or injuries that prevent the use of an ear probe, for example an abnormal sharp bend in the ear canal or an inflamed or infected ear canal due to, among others, otitis externa (swimmer's ear). Individuals with self-diagnosed illness which would cause a risk if they participated, were also excluded. Potential participants were screened through a pre-test physical examination to determine whether they met all the criteria. Table 5.1 displays a demographic summary of the participants who were selected for the trial.



**Table 5.1:** Demographic summary of participants

Group	n	Average age
Male	13	24.5 $\pm$ 0.7
Female	3	23.3 $\pm$ 0.3
Total	16	24.3 $\pm$ 0.6

## 5.2 Benchmark validation

Evaluation was done for all four vital signs measured by the Ear-Monitor, namely core temperature, heart rate, respiratory rate and SpO<sub>2</sub>. The evaluation entailed comparing the vital sign measurements made by the Ear-Monitor to measurements made, in the same conditions, by industry-standard medical devices. The latter are referred to as benchmark devices. The measurements made by benchmark devices are referred to as benchmark measurements. In this trial, a device that conforms to the CE requirements qualified as a benchmark device. The CE mark is evidence that the benchmark device complies with the ISO 13485 standard for medical devices, which requires industry-standard accuracy.

Three benchmark devices, shown in Figure 5.1, were selected to provide the various benchmark measurements. A concise technical overview is given of each.

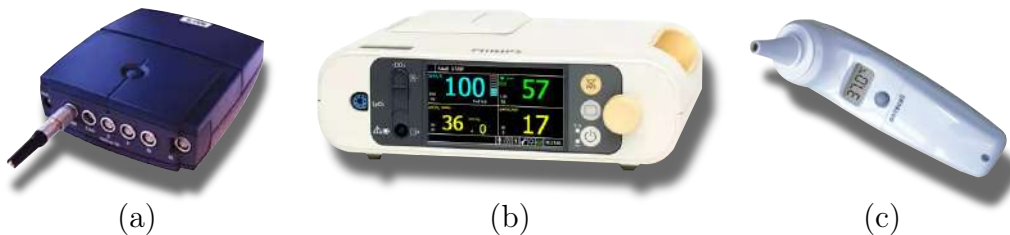


**Figure 5.1:** Benchmark devices: (a) Nexus-10; (b) SureSigns VM1; (c) ET-100A

The Nexus-10 physiological monitoring platform was selected to provide the benchmark heart rate and respiratory rate measurements. According to the manufacturer, the Nexus-10 is a data acquisition device with a 24-bit analogue to digital converter and an accuracy of  $\pm 2\%$ . It has a blood volume sensor, which measures a PPG signal from the fingertip at a sampling rate of 128 Hz. This PPG signal is used to provide the benchmark heart rate measurement. It also has an elastic chest strap to measure respiratory rate. The movement of the chest during the respiratory cycle is converted to a voltage signal and digitalised at a sampling rate of 32 Hz. This signal is used to provide the benchmark respiratory rate measurement. It uses a Bluetooth connection to send data to a computer. The BioTrace+ software package is used to display the recorded data in-real time, as well as store the data for post processing.

The SureSigns VM1 patient monitor from Philips was selected to provide benchmark SpO<sub>2</sub> measurements. The SureSigns VM1 uses a pulse oximeter attached to the fingertip to measure SpO<sub>2</sub>. Data is logged on the device's screen and updated at 1 Hz and stored on a computer for post processing. The device is recommended for use by healthcare professionals, emphasising its accuracy and reliability.

The ET-100A infrared ear thermometer was selected to provide the benchmark tympanic ear temperature measurements. The ET-100A complies with the EN12470-5:2003 standard for clinical thermometers, therefore satisfies an accuracy of  $\pm 0.2^{\circ}\text{C}$  over the range of 35.5 to 42°C. Its measurements are displayed on the device screen and data is entered and stored on a computer for post processing.

### 5.3 Method

Data was recorded from a single participant in a session. A recording session involved collecting four benchmark and four Ear-Monitor vital sign measurements simultaneously from one participant. Each recording session lasted for two minutes and was conducted twice per participant to ensure repeatability. Figure 5.2 shows a diagram of how all the devices were connected to the participants and which measurements were made by each device.

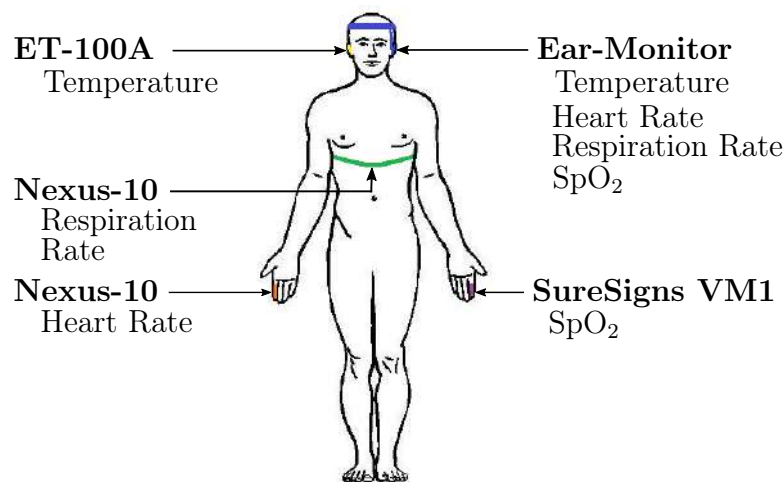


**Figure 5.2:** Diagram showing how devices were connected to the participants during the recording sessions

A recording session is summarised as follows:

- The trial environment was set up before the participant arrived. Equipment was disinfected and connected to the computer, ready for data capturing.
- The participant arrived and was briefed on the procedure and signed an informed consent form. The participant was also asked to clean his/her right ear with surgical spirits.
- The participant was seated stationary in front of a table containing all the equipment. Sensors were placed on the participant, as shown in Figure 5.2. Three tympanic temperature benchmark measurements were taken from the participant with the ET-100A.
- The recording session started. The participant sat still the entire time and breathed normally for the first 60 seconds, after which the participant was asked to breath at 15 breaths per minute by following a breathing metronome for another 60 seconds.
- After 60 seconds of controlled breathing (120 seconds of recording time in total), the recording session was concluded. Three more temperature benchmark measurements were taken with the ET-100A.
- Data from the Ear-Monitor and benchmark devices were stored on a computer in .csv format for post processing and analysis.

The breathing exercise was included due to the uncertainty whether the RSA would be detectable during normal breathing. During prototyping, it was more visible in beeper forced breathing. Therefore, if it is not detectable in normal breathing, the controlled breathing data can still be analysed to produce some results.

Figure 5.3 shows an image of one of the participants during a data recording session. The labelled equipment is (a) the computer with the Ear-Monitor user interface, (b) the Ear-Monitor on the participant with the red light of the MAX30100 visible through the tragus, (c) the SureSigns VM1, (d) its SpO<sub>2</sub> finger clip, (e) the Nexus-10, (f) its blood volume sensor finger clip and (g) its chest strap for measuring respiration. The ET-100A tympanic thermometer is labelled (h).

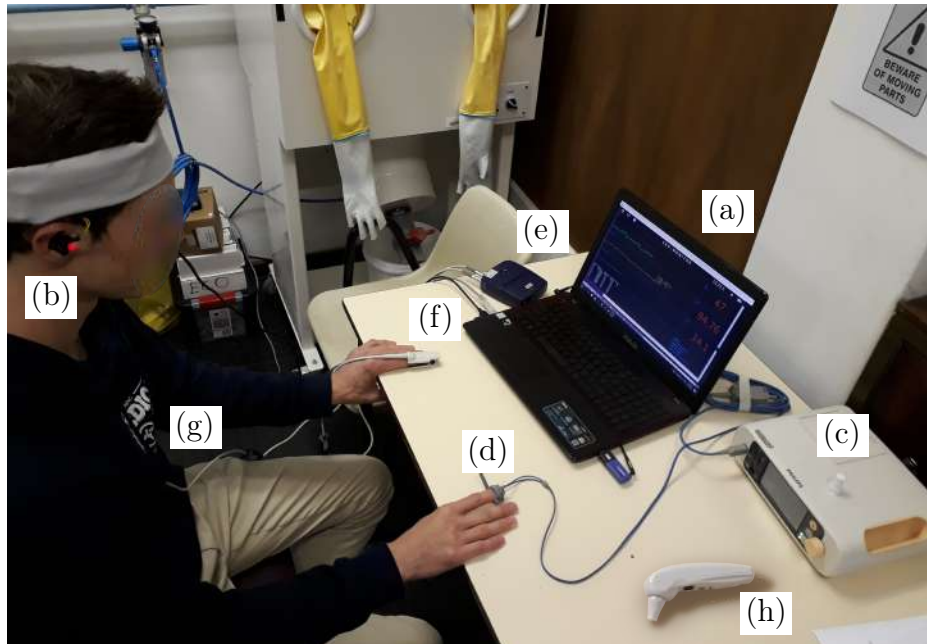


**Figure 5.3:** Recording session set-up with participant

# Chapter 6

## Results and Discussion

This chapter documents the results from the trial conducted on the Ear-Monitor. The aim is to quantify the level of comparability between the measurements of the Ear-Monitor and those of the benchmark devices. Through this, an understanding of the accuracy of the Ear-Monitor will be obtained. Each participant was acting as his/her own control in this type of comparative analysis. Results are discussed one vital sign at a time.

### 6.1 Background

Correlation between each vital sign and its benchmark is visualised through an interclass correlation (ICC) plot. On each ICC plot, the  $x = y$  line is plotted in black and a blue line is fitted to the data using the least squares method. Some of the terms used to evaluate correlation are defined as follows:

- **Correlation coefficient ( $r$ ):** This quantifies the strength of the linear dependence between the values in the two datasets.  $r$  varies from -1 to 1. A correlation coefficient close to 1 indicates a high level of positive correlation between the Ear-Monitor and benchmark datasets and is a favourable result.
- **p-value ( $p$ ):** The p-value is the probability of the data leading to an incorrect rejection of the null hypothesis, which is that there is no correlation between the Ear-Monitor and benchmark datasets. p-Values smaller than 0.05 indicate strong evidence against the null hypothesis, while p-values larger than 0.05 indicate weak evidence against the null hypothesis.  $p = 0$  indicates a p-value smaller than 0.00005, meaning that the correlation can be accepted with confidence.
- **ICC agreement ( $ICC_a$ ):** This value ranges from 0 to 1 and the following, often quoted interpretation is suggested by Cicchetti (1994):
  - 0 to 0.40: Poor

- 0.40 to 0.59: Fair
- 0.60 to 0.74: Good
- 0.75 to 1.00: Excellent
- **ICC consistency ( $ICC_c$ ):** This quantifies the consistency of conclusions made by different observers. It ranges from 0 to 1, where values closer to 1 indicate higher consistency.
- **95% confidence intervals:** These intervals are given for the  $ICC_a$  and  $ICC_c$  values. If the interval should contain zero, then the ICC is not significant.

## 6.2 Core temperature

The Ear-Monitor uses the TMP006 infrared sensor to measure the temperature of the tympanic membrane. The ET-100A tympanic thermometer is used as the benchmark device. During each recording session, 15 Ear-Monitor and three ET-100A data points were collected. It was assumed that the core temperature of the participant stayed constant during the duration of the recording session. Therefore, the averages for the ET-100A and Ear-Monitor measurements were compared. This is a valid assumption, as the standard deviations within recording sessions were found to be below  $0.08^\circ\text{C}$ . Datasets recorded from participants 1 and 5 were removed due to faulty recording sessions.

Results from the two calibration approaches are documented separately and then compared in the discussion. Detailed results are tabulated in Appendix E. All participants were healthy and benchmark temperatures ranged from  $36.33$  to  $38.55^\circ\text{C}$ .

### 6.2.1 Group calibration

Equation 4.6 was used by the Ear-Monitor to calculate the tympanic temperature of the participants. Figure 6.1, on the next page, depicts an ICC plot of the Ear-Monitor versus ET 100-A data points for the 28 recording sessions. The mean error was  $0.02 \pm 0.51^\circ\text{C}$ .

### 6.2.2 Intra-participant calibration

This method used data from the first recording session to calibrate the Ear-Monitor, and the data from the second session to evaluate the calibration. Figure 6.2, on the next page, depicts an ICC plot of the Ear-Monitor versus ET 100-A data points for the 14 recording sessions used for evaluation. The recording sessions used for calibration were not plotted, as they all lay on the  $x = y$  line. The mean error was  $-0.02 \pm 0.29^\circ\text{C}$ .

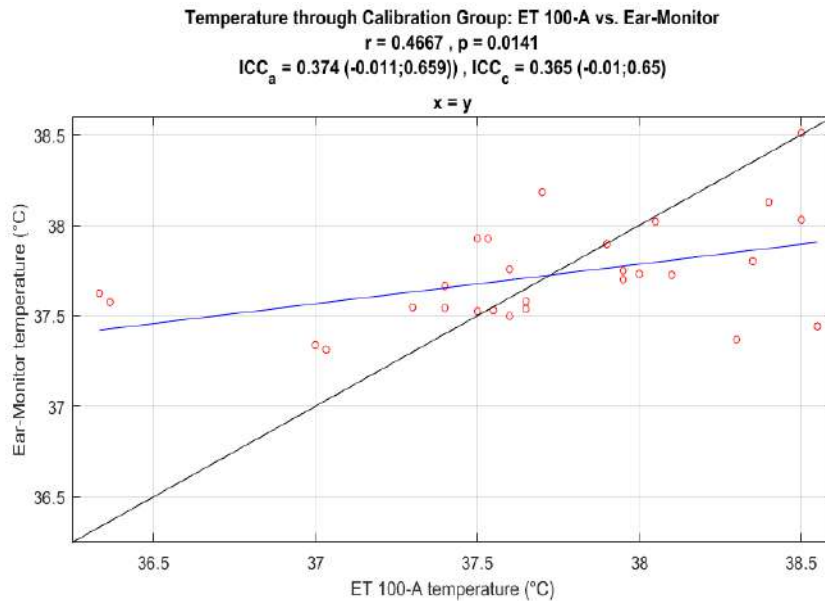


**Figure 6.1:** Temperature through the group calibration method: ET 100-A vs. Ear-Monitor

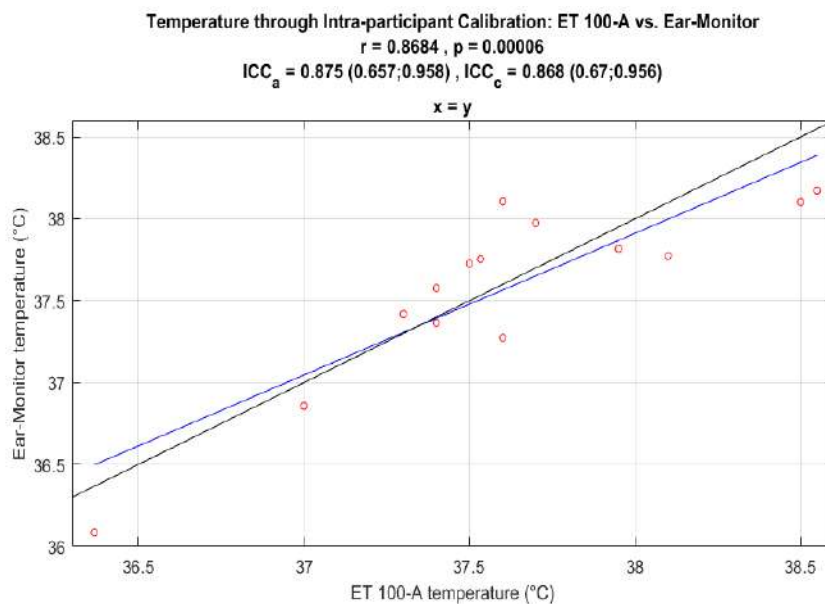


**Figure 6.2:** Temperature through the intra-participant calibration method: ET 100-A vs. Ear-Monitor

### 6.2.3 Discussion

The measurements inside a recording session were very similar. In the most dispersed recording session, 95% of the measurements were within  $\pm 0.16$  °C of the mean. This demonstrates the high precision of the TMP006, making it a

suitable choice for an infrared sensor. This level of precision is owing to the thermal consistency inside the ear canal. Air flow is negligible and the position of objects in the sensor's FOV stays constant.

The two different calibration methods can be compared through a box and whisker plot of their respective errors, as depicted in Figure 6.3. The superiority of the intra-participant calibration method can be observed in the smaller first and fourth quartiles. This indicates a significant reduction in large errors.

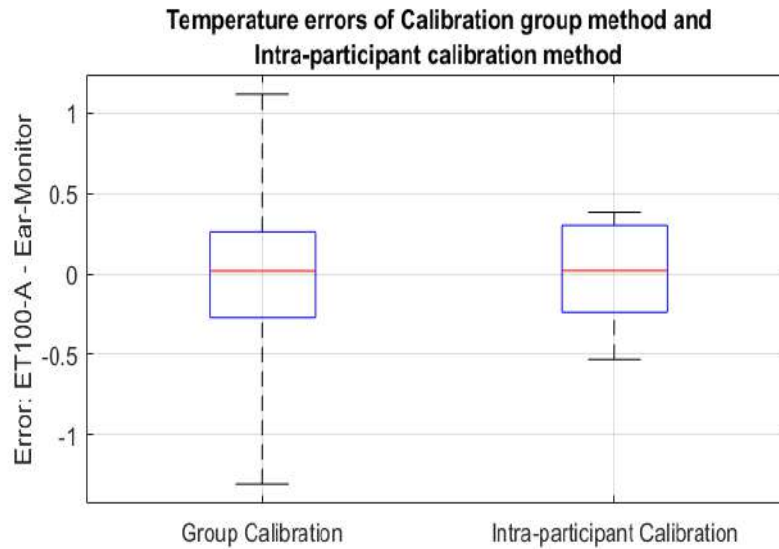


**Figure 6.3:** Temperature errors of the group calibration and intra-participant calibration methods

The 95% confidence intervals for  $ICC_a$  and  $ICC_c$  for the group calibration method included zero, which means that the correlation was not significant. In contrast, the ICC intervals for the intra-participant calibration method were well above zero, indicating a good correlation. Furthermore, the p-value was far below 0.05, indicating a very small probability of zero correlation. The data unanimously indicated that the intra-participant calibration method is superior to the group calibration method with regard to accuracy and correlation.

Although the intra-participant calibration method produced the best results, it should be kept in mind that this method requires a calibration sequence when it is used for the first time on an individual. The merit in the group calibration method lies in the fact that calibration is done only once: during manufacturing. With better probe design, the TMP006 can be located more consistently between different individuals and the group calibration method can become more accurate. However, currently the intra-participant calibration method is the best option.



As mentioned in the literature review, there are not many published results of wearable ear temperature monitors with which to compare the Ear-Monitor. There are, however, commercial devices available for comparison. The Novatemp<sup>®</sup> and Starboard<sup>®</sup> both claim an accuracy of  $\pm 0.2^\circ\text{C}$  (Novatemp, 2011; Starboard, 2016) and the Cosinuss Degree<sup>®</sup>, an accuracy of  $\pm 0.1^\circ\text{C}$  (Cosinuss, 2017b). The Ear-Monitor with intra-participant calibration displays a similar result, with an accuracy of  $-0.02 \pm 0.29^\circ\text{C}$ .

## 6.3 Heart rate

The Ear-Monitor uses an infrared PPG obtained by the MAX30100 in the ear canal to detect heartbeats via a beat detection algorithm. The average period between 10 successive beats is used to calculate the heart rate. The beat detection algorithm is at the core of the heart rate functionality of the Ear-Monitor, and therefore it was evaluated independently. This was followed by a comparative analysis between the individual beat periods and 10-beat moving average heart rates of the Ear-Monitor and Nexus-10 physiological monitor.

### 6.3.1 Beat detection algorithm

The beat detection algorithm used by the Ear-Monitor was first tested on open-source data from PhysioNet.org, and then on the data collected during the trial. The results of these two tests are discussed separately.

#### 6.3.1.1 PhysioNet data test

The beat detection algorithm was tested on PPG data from the open-source MIMIC database on PhysioNet.org (Goldberger *et al.*, 2000). This data was recorded from patients in intensive care units and was made available for developing and testing intelligent monitoring systems. PPG data was recorded with clinical finger pulse oximeters. Random ten-minute segments from 14 different patients were used to test the algorithm. Each set of data also included an ECG signal, which was used to identify the benchmark beats. The detailed results for this test is tabulated in Appendix E.

Of the 12 001 beats in all of the PhysioNet test datasets, 13 (0.11%) false positives and 91 (0.76%) false negatives were detected. Even though the beat detection algorithm was designed and tuned using PPG signals collected from the ear canal wall, it could accurately detect beats from finger pulse oximeters. This result demonstrates the robustness of the algorithm. Most false detections occurred where signals were corrupted by noise.

### 6.3.1.2 Trial data test

Subsequently, the algorithm was tested using the data collected during the trial. The number of beats detected for each participant by the Ear-Monitor was compared to the number of benchmark beats. The supporting software for the Nexus-10, BioTrace+, has a peak detection algorithm, but it was found that it misses some peaks. To ensure accurate benchmark peak detection, the photoplethysmogram from the Nexus-10 was inspected manually and peaks were marked by a human annotator. Figure 6.4 depicts plots of (a) the Ear-Monitor SSF with detected beats and (b) the Nexus-10 PPG signal with annotated beats. Beats are marked with red dots. In this example, 100% of the peaks were detected by the Ear-Monitor.

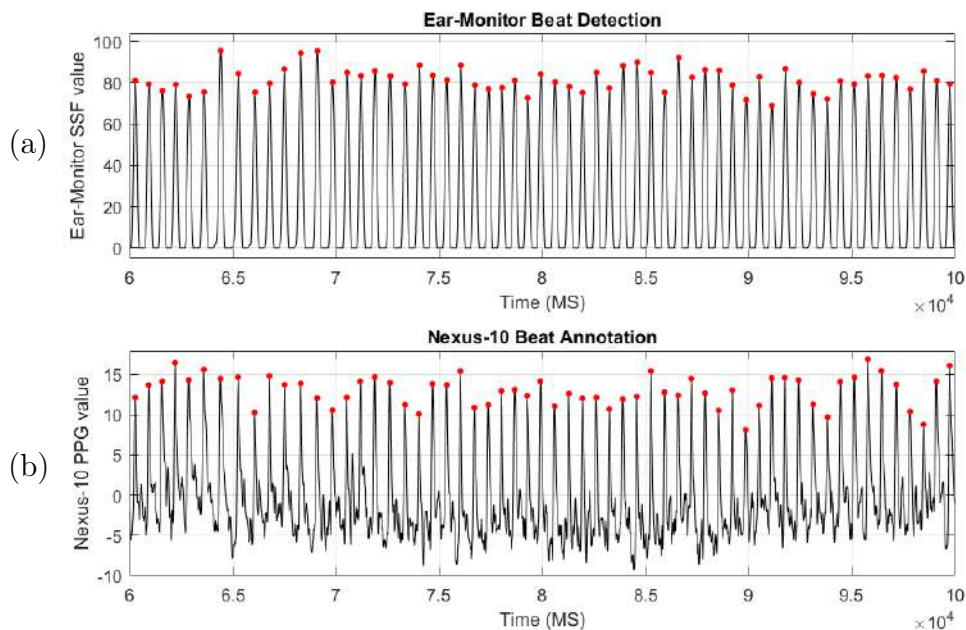


**Figure 6.4:** (a) The Ear-Monitor SSF with detected beats; (b) the Nexus-10 PPG signal with annotated beats

Appendix E tabulates the detailed results of the beat detection evaluation. Of the 4713 beats in the participant trial data, 10 (0.21%) false positives and 58 (1.23%) false negatives were detected. The mean error of the sample group was  $-1.53 \pm 2.88$  beats. It should also be noted 51 of the false negatives (87.9%) were from the data collected from only three of the participants: 5, 9 and 13. Figure 6.5 depicts an ICC plot of the number of annotated Nexus-10 beats versus the number of detected Ear-Monitor beats. A total of 32 sets of data points were compared. The number of benchmark beats ranged from 116 to 188.

This test demonstrates that the Ear-Monitor performed well in its task of detecting beats. The number of false negatives detected for the trial data

was higher than for the PhysioNet data. This can be ascribed to the fact that the PPG signal from three of the participants was of a notably lower quality. Although the adaptive threshold method detected the majority of the peaks, the amplitude of the SSF signal peaks varied prominently and very low amplitudes were missed by the algorithm. This can be caused by low blood perfusion in the ear canal or poor contact between the MAX30100 and the canal wall.

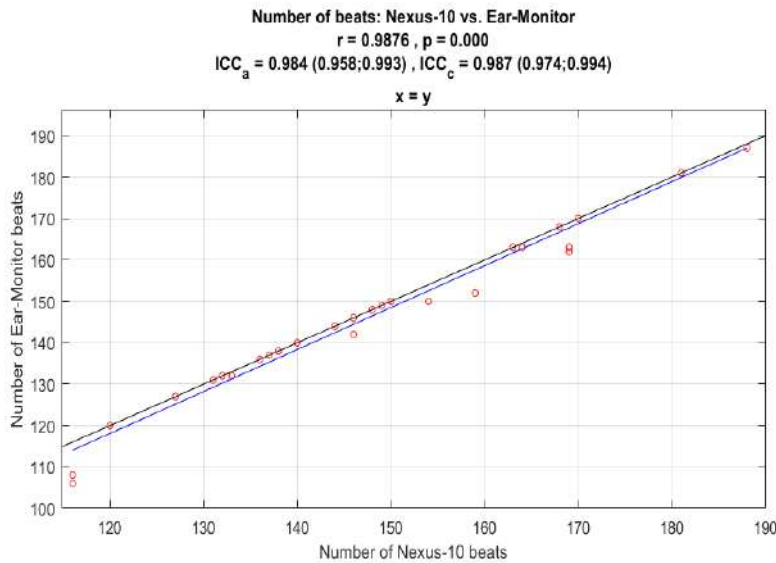


**Figure 6.5:** Number of beats: Nexus-10 vs. Ear-Monitor

### 6.3.2 Beat period and average heart rate

The accuracy of the heartbeat period was tested to determine whether beats were detected at the right position in time. Periods between subsequent beats detected by the Ear-Monitor were compared to periods between beats annotated on the Nexus-10 PPG signal. Figure 6.6, on the next page, depicts an ICC plot of Nexus-10 versus Ear-Monitor periods. A total of 4569 periods from 16 participants were compared. Benchmark periods ranged from 575 to 1198 ms. The mean error of the sample group was  $0.08 \pm 50.71$  ms.

The 10-beat average heart rate was calculated from the Ear-Monitor and Nexus-10 data and compared in the same way as with the beat periods. Figure 6.7, on the next page, depicts an ICC plot of Nexus-10 versus Ear-Monitor heart rates. A total of 4258 heart rate calculations were compared from 16 participants with benchmark heart rates varying from 54.2 to 100.0 bpm. The mean error of the sample group was  $0.03 \pm 0.72$  bpm.

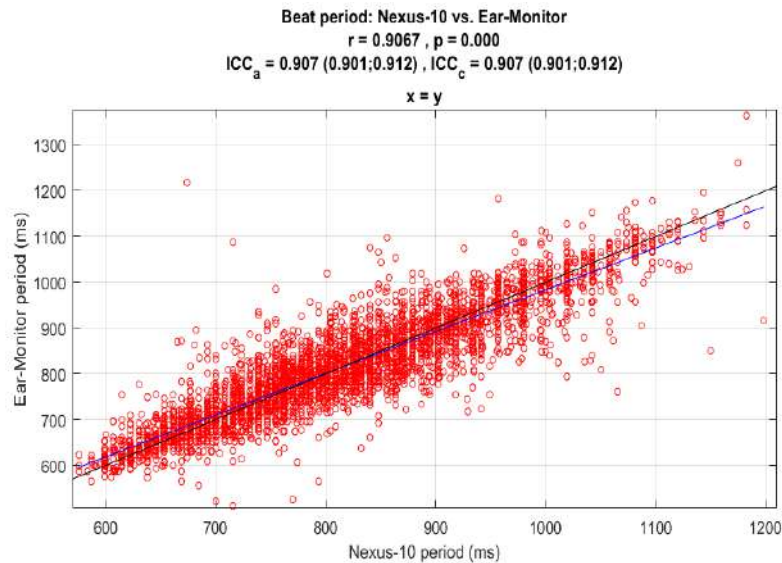


**Figure 6.6:** Beat period: Nexus-10 vs. Ear-Monitor

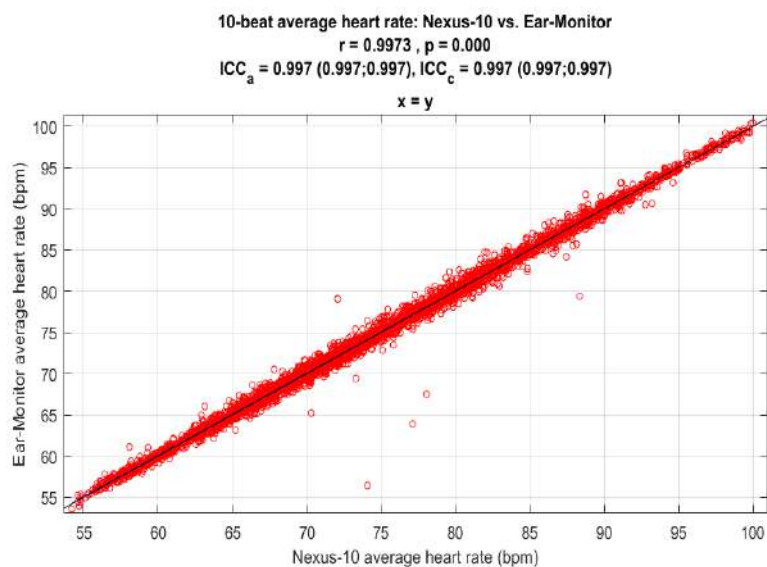


**Figure 6.7:** 10-beat average heart rate: Nexus-10 vs. Ear-Monitor

### 6.3.3 Discussion

The beat detection algorithm was evaluated based on PhysioNet data and data collected from participants during the trial. The algorithm performed better on the PhysioNet data than on the trial data. This can be due to the fact that three of the participants contributed to 87.9% of the false negatives detected in the trial data. These were all participants with smaller external ears, which could partly be ascribed to the fact that two of them are female. This highlights the effect the fit of the ear probe in the ear has on the accuracy

of the beat detection algorithm. A bad fit causes non-ideal contact between the MAX30100 and the canal wall, as well as reducing subcutaneous blood perfusion. This is a patient-specific inaccuracy and can be overcome by a more customised ear probe.

Even with these three individuals, the beat detection algorithm performed exceptionally good. On average,  $1.53 \pm 2.88$  beats were missed per two-minute recording session. The correlation of the number of beats detected between the Ear-Monitor and the benchmark device was high, with a correlation coefficient of 0.99 and a p-value of zero. The  $ICC_a$  and  $ICC_c$  were both excellent within a 95% confidence interval.

The beat period ICC plot in Figure 6.6 depicts a clear correlation. The large number of data points reveals the normal distribution of the data. The correlation coefficient, p-value,  $ICC_a$  and  $ICC_c$ , all indicated an excellent correlation. The Ear-Monitor can measure the period between heartbeats with a mean error of  $0.08 \pm 50.71$  ms. This notably high accuracy was improved even further by calculating the 10-beat average heart rate. The ICC plot of the average heart rate in Figure 6.7 illustrates an exceptional correlation between the Ear-Monitor and benchmark measurements. The Ear-Monitor can measure the heart rate of participants with a mean error of  $0.03 \pm 0.72$  bpm relating to a 1.04% error at 72 bpm. This compares favourably to the commercial wrist-worn heart rate monitors reviewed by Shcherbina *et al.* (2017).

## 6.4 Respiratory rate

The Ear-Monitor uses RSA to extract a respiratory rate. The chest strap connected to the Nexus-10 physiological monitoring platform was used to measure the benchmark respiration rate. Benchmark breaths from the Nexus-10 were manually annotated. The recording session consisted of one minute of normal breathing followed by one minute of regulated breathing at 15 breaths per minute. Appendix E tabulates the detailed results of the breaths detected for the 16 participants. Benchmark respiratory rates of the participants varied from 7 to 28 breaths per minute. The mean error was  $0.02 \pm 3.91$  breaths per minute.

It should be noted, however, that the majority of the inaccuracies can be traced to the recording sessions of participants 5, 9 and 13. Upon closer inspection, the following explanation can be given. Participant 5 and 13 both had a large number of false positives, the highest and third-highest average heart rates and very low heartbeat period variation due to RSA. Participant 9 had an unusually high resting respiratory rate (more than double that of the average of the rest of the participants), bordering on the maximum measurable rate according to the Nyquist theorem, which is equal to half the heart rate. This caused 51% of breaths to be missed during normal breathing. As ex-

pected, when the respiratory rate was lowered during the controlled breathing exercise, the breath detection accuracy returned to the group average. These three participants were regarded as outliers and were isolated from the rest in order to reveal the trends present in the bulk of the recording sessions.

The mean errors in respiratory rate between the benchmark Nexus-10 and the Ear-Monitor are tabulated in Table 6.1. Standard deviations are included and all values are in breaths per minute. When removing the outliers, the mean error of the normal and controlled breathing groups were closer to one another and the standard deviation of the errors were reduced by more than half.

**Table 6.1:** Mean errors of the respiratory rate measurements

Group	Outliers removed	Outliers included
Normal breathing	$-0.62 \pm 1.68$	$0.44 \pm 4.92$
Breathing exercise	$-0.50 \pm 1.10$	$-0.41 \pm 2.45$
All	$-0.56 \pm 1.41$	$0.02 \pm 3.91$

Figure 6.8 depicts an ICC plot of the Nexus-10 benchmark breaths versus the Ear-Monitor detected breaths. Triangles mark the number of breaths after one minute of normal breathing and circles mark the total number of breaths in the recording session, which includes the breathing exercise.

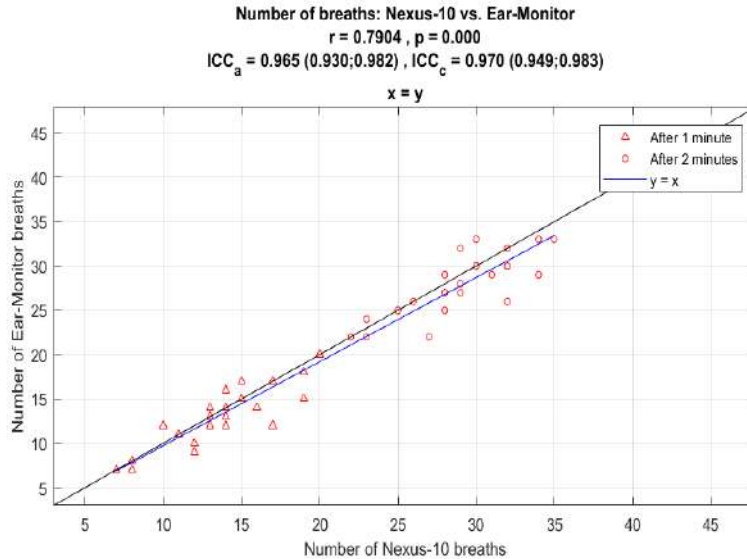


**Figure 6.8:** Number of breaths detected: Nexus-10 vs. Ear-Monitor (excluding outliers)

## Discussion

The breathing exercise was included in the trial, due to the uncertainty that the RSA will be visible during normal breathing. In general, participants



started breathing deeper during the breathing exercise. This resulted in a more accurate detection of breaths.

During normal breathing, the standard deviation for the data from the breathing exercise was lower, however, the Ear-Monitor still measured normal respiratory rate better than expected. According to the trial data (excluding the outliers), the Ear-Monitor correlates with the benchmark device with a coefficient of 0.76 and a p-value of zero.  $ICC_a$  and  $ICC_c$  indicated exceptional correlation agreement and consistency within the 95% confidence interval. The Ear-Monitor was able to calculate the respiratory rate of a participant breathing normally to within a mean accuracy of -0.62 breaths per minute with a standard deviation of 1.68 breaths per minute (11.45% standard deviation at 15 breaths per minute). This is slightly worse than, but comparable to, the one breath per minute accuracy from Clifton *et al.* (2007) and the 7.6% accuracy from Leonard *et al.* (2006). This can be ascribed to the fact that they used the more advanced approach of neural networks for detecting breaths from the RSA.

It can be seen that, on average, the Ear-Monitor detects a respiratory rate that is slightly lower ( $-0.56 \pm 1.40$  breaths per minute) than the actual rate. This means that the algorithm misses some breaths. This can be due to intermittent shallower and shorter breaths that do not cause a big enough variation in the heartbeat period.

The outliers were removed to emphasise the normal results, but they were not random and provided valuable insight into the limitations of using RSA to measure respiratory rate. It can be stated that elevated heart rates (higher than 80 bpm in this trial), reduce the magnitude of RSA and cause the detection of false breaths. Also, if the breathing rate approaches half the heart rate (Nyquist frequency), the sampling frequency is too low and more than half of the breaths are missed by the detection algorithm. These results can be summarised by saying that respiratory rate measurement through RSA is most accurate at a combination of low heart and respiratory rates.

## 6.5 Blood oxygen saturation

The Ear-Monitor uses the MAX30100 pulse oximeter to measure the blood oxygen saturation of the tissue in the wall of the ear canal. One  $SpO_2$  calculation is done every time the Ear-Monitor detects a heartbeat. The SureSigns VM1 from Philips was used to provide the benchmark  $SpO_2$  measurement. The SureSigns VM1 samples at 1 Hz, resulting in 120 samples per recording session. As with temperature, the  $SpO_2$  of a participant was assumed to stay constant over the duration of the two-minute recording session. Therefore, the averages of the SureSigns VM1 measurements and Ear-Monitor measurements were compared for each recording session.

All trial participants were in good health and benchmark  $\text{SpO}_2$  levels ranged between 96.38 and 100%. The measurements from the Ear-Monitor varied between 96.27 and 100%. Appendix E tabulates the detailed results. The mean error between the SureSigns VM1 and Ear-Monitor measurements was  $-0.22 \pm 1.50\%$ . Although this accuracy is good, when plotting the Ear-Monitor and SureSigns VM1 measurements, no significant correlation was observed. This ICC plot can be seen in Figure 6.9.

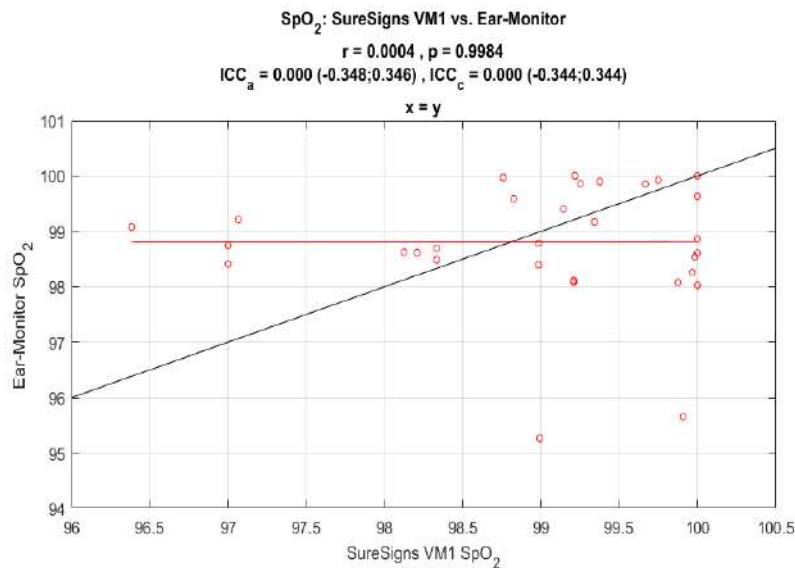


**Figure 6.9:**  $\text{SpO}_2$ : SureSigns VM1 vs. Ear-Monitor

## Discussion

By analysing the trial data, it was calculated that the Ear-Monitor can measure  $\text{SpO}_2$  in healthy individuals, with a mean error of  $-0.22 \pm 1.50\%$ .

However, because of the insignificant correlation, it could not be proven that this accuracy will continue if individuals with lower  $\text{SpO}_2$  levels are monitored. An attempt was made to induce hypoxia during pilot testing by holding the breath. However, this did not cause a detectable change in  $\text{SpO}_2$  measurements by the Ear-Monitor or SureSigns VM1. Clarity about the  $\text{SpO}_2$  performance of the Ear-Monitor can be obtained by testing it on hypoxic patients, but testing on unhealthy individuals was not within the scope of this project.

The  $\text{SpO}_2$  calculation method relies on the difference in the detected red and infrared light. According to the relationship found in literature, the magnitude of the infrared PPG should be higher than that of the red PPG (Oak and Aroul, 2015; Strogonovs, 2017). This can be observed in all the data recorded by the Ear-Monitor. If the  $\text{SpO}_2$  of the wearer decreases, the difference between the infrared and red PPGs should decrease as well, resulting in a higher  $\text{SpO}_2$  modulation ratio ( $R$ ) and, according to Equation 2.6, a lower



calculated SpO<sub>2</sub> value. This could not be observed in the trial data. The most probable reason is that the relationship was obscured by the inherent margin of error in pulse oximeters. The SpO<sub>2</sub> benchmark of the group was too constant, which means that there was not a big enough variation in SpO<sub>2</sub> among the individuals to be detected by the Ear-Monitor.

The lack of correlation within the testing range of values does not prove that the Ear-Monitor fails to measure SpO<sub>2</sub> accurately. Within the trial group, SpO<sub>2</sub> measurements all indicated that the participants were above the 95% mark required for healthy adults. This is the same result as that found by Aziz *et al.* (2006).

## 6.6 Results summary

The statistical analysis values for the trial data are summarised in Table 6.2.

**Table 6.2:** Summary of statistical results

Vital sign	Mean error	Correlation coefficient	p-value	ICC <sub>a</sub>	ICC <sub>c</sub>
Temperature group calibration	0.02 ±0.51	0.47	0.01	0.37 (-0.01;0.66)	0.37 (-0.01;0.65)
Temperature intra-participant calibration	-0.02 ±0.29	0.87	0	0.88 (0.66;0.96)	0.87 (0.67;0.96)
Heart rate	0.03 ±0.72	0.99	0	0.99 (0.99;0.99)	0.99 (0.99;0.99)
Respiratory rate	-0.56 ±1.41	0.79	0	0.97 (0.93;0.98)	0.97 (0.95;0.98)
SpO <sub>2</sub>	-0.22 ±1.50	0	0.99	0 (-0.35;0.35)	0 (-0.34;0.34)

# Chapter 7

## Conclusion

This thesis report on the development and evaluation of the Ear-Monitor, a wireless device that monitors multiple vital signs through the external ear. Vital signs include core temperature, heart rate, respiratory rate and blood oxygen saturation ( $\text{SpO}_2$ ). The motivation for this project was the need for a wearable device that can continuously and unobtrusively monitor the health of the wearer, while not constraining movement. Three objectives were set to guide the project towards reaching its aim:

- Develop a device to measure core temperature, heart rate, respiratory rate and blood oxygen saturation through the external ear of the wearer.
- Conduct a trial experiment to test the device on a sample of human participants.
- Use the collected data from the trial to evaluate the accuracy of the measurements made by the device.

This section aims to clarify to what extent these objectives were achieved. Attention is also given to the findings regarding the measurement of each vital sign and suggestions for future work.

### 7.1 Device development

The Ear-Monitor uses the TMP006 infrared sensor to measure tympanic temperature. The MAX10300 pulse oximeter is used, along with a beat detection algorithm, to calculate heart rate and  $\text{SpO}_2$ . Respiratory rate is measured through analysing RSA, the frequency modulation respiratory-related heart rate characteristic. The MCU, battery and Bluetooth modem are located in a headband around the wearer's head. A PCB was designed and manufactured to integrate all the electronic components in the headband. Sensors are located on a silicone ear probe that is connected to the headband and placed in the

external ear of the wearer. Collected data is sent through the wireless Bluetooth connection to a computer. Software was developed for the computer to analyse the data, calculate the vital sign values, display the information through a graphical user interface and store the data for later use.

## 7.2 Experimental trial

A trial was designed and conducted to test the Ear-Monitor on a sample of human participants. Each vital sign measured by the Ear-Monitor was compared to measurements made by selected benchmark devices. Sixteen participants were recruited for the trial. Data was collected from each participant in two two-minute recording sessions.

## 7.3 Data analysis and results

The data captured by the Ear-Monitor and various benchmark devices were compared one vital sign at a time. The Ear-Monitor was evaluated in terms of accuracy and correlation with the benchmark measurements. The findings of each of the vital signs are discussed in this section.

### 7.3.1 Core temperature

The TMP006 proves to be a precise sensor, making 15 consecutive measurements within a recording session with a mean standard deviation of 0.08 °C. Two calibration approaches were tested. Group calibration produced a statistically weak correlation with the benchmark ET-100A ( $r = 0.47$ ,  $ICC_a = 0.37$ ,  $ICC_c = 0.37$ ). Changing the calibration approach to intra-participant calibration improved the correlation considerably ( $p = 0$ ,  $r = 0.87$ ,  $ICC_a = 0.88$ ,  $ICC_c = 0.87$ ). These results indicate that the Ear-Monitor is capable of measuring consistent and accurate temperature, assuming that it is calibrated to the ear of the individual. This is due to the variation in ear canal shape and size between individuals. This leads to the conclusion that, in order to improve core temperature measurements further, an ear probe is needed that can place the TMP006 in the same position relative to the tympanic membrane between individuals, regardless of differences in external ear shape and size.

### 7.3.2 Heart rate

The Ear-Monitor can detect heartbeats in the data captured by the MAX10300 by means of a beat detection algorithm. Beats were detected from the trial data with a mean error of  $-1.53 \pm 2.89$  per two-minute recording sessions. When comparing beat period length between the Ear-Monitor and the Nexus-10, a statistical significant correlation was found ( $p = 0$ ,  $r = 0.91$ ,  $ICC_a = 0.91$ ,

$ICC_c = 0.91$ ). The 10-beat average heart rate was calculated from the beat period and the results showed that the Ear-Monitor can measure heart rate with a mean error of  $0.03 \pm 0.72$  bpm. Excellent correlation was found between the average heart rate of the Ear-Monitor and the Nexus-10 ( $p = 0, r = 0.99, ICC_a = 0.99, ICC_c = 0.99$ ). This led to the conclusion that the Ear-Monitor succeeds aptly in the task of measuring the heart rate of the wearer.

### 7.3.3 Respiratory rate

RSA is used by the Ear-Monitor to calculate the respiratory rate of the wearer. The results from the trial data led to a mean accuracy of  $0.02 \pm 3.91$  breaths per minute. It was observed that most of the inaccuracy originated from the recording sessions of three of the participants. Upon closer inspection, it was noted that these participants had either a high heart rate or high respiratory rate. Two deductions were made from this finding. Firstly, the effects of RSA are attenuated by a high heart rate, and secondly, a respiratory rate approaching half the heart rate causes many false negatives due to the Nyquist sampling limit. This led to the conclusion that respiratory rate measurement through RSA is most effective at low heart and respiratory rates. Removing the three outlier participants gave the Ear-Monitor an accuracy of  $-0.56$  breaths per minute with a greatly reduced standard deviation of  $1.41$  breaths per minute.

### 7.3.4 Blood oxygen saturation

The MAX30100 is used to collect the data used to calculate  $SpO_2$ . A modulation ratio between the red and infrared AC and DC components of the PPG signals collected from the ear canal wall is used. The mean error between the Ear-Monitor and SureSigns VM1 benchmark device was  $-0.22 \pm 1.50\%$ . This is a good accuracy within the testing range. The Ear-Monitor also indicated that all participants were healthy, with an  $SpO_2$  of above 95%, which is correct. However, the ICC analysis revealed no statistically significant correlation. Therefore, no predictions could be made about the accuracy of measurements made by the Ear-Monitor when the wearer has an  $SpO_2$  of lower than 96%. The lack of correlation can be ascribed to the inherent variability in pulse oximeter measurements.

## 7.4 Suggestions for future work

The Ear-Monitor achieved all of its objectives. However, there exists an opportunity for improvements and additions in future versions of this device.

Firstly, research can be done on an ear probe that better conforms to different ear shapes. It should place the infrared sensor in the same position relative to the tympanic membrane, regardless of the ear canal shape of the

wearer. Analysis of the trial data suggested that this will greatly improve the accuracy of the core temperature measurements. Furthermore, the probe should ensure uniform contact between the MAX30100 and the canal wall, even for smaller ear canal shapes. The results indicated that this will improve the accuracy of the beat detection algorithm. Considerations for the probe should include material, shape and different sizes.

Secondly, a more extensive trial can be done to test the Ear-Monitor. More participants should be tested, including hypoxic patients, to test the SpO<sub>2</sub> capabilities of the Ear-Monitor more thoroughly. The benchmark measurements from the SureSigns VM1 should be replaced or supplemented by a blood gas test for more accurate benchmarking.

Finally, the vital signs measurement capabilities can be extended to include the monitoring of electrical brain activity and research can be done into monitoring blood pressure through the ear canal. Diagnostic algorithms can be added to the supporting system on the computer and alarms can be triggered when health warning signs are detected.

## 7.5 Conclusion

Overall, the Ear-Monitor project was a success. The functional device and supporting software proved that it is possible for a wearable device to collect vital signs from the external ear and transmit data over a wireless connection to a nearby computer. Core temperature, heart rate, and respiratory rate are measured with sufficient accuracy, while SpO<sub>2</sub> is accurately measured on average, however, no significant correlation was found with the benchmark measurements, and further testing is needed. Novel methods are tested for heart beat detection and respiration measurement through the ear, and both deliver promising results. The Ear-Monitor project adds valuable academic information to the body of knowledge concerning wearable vital sign monitoring through the external ear, and lays the groundwork towards a commercial medical device.

# Appendices

# Appendix A

## Calculations

### A.1 Battery life calculation

#### Indicator LED current

A current is selected for the LED according to its data sheet. The resistance needed to realise this current is calculated.

Design current: 10 mA

Supply voltage: 3.3 V

Forward voltage drop: 2.1 V

Design resistance:  $\frac{3.3-2.1}{0.01} = 120 \Omega$

#### MAX30100 current

The current used by the MAX30100 is calculated. The supply current used for logic operations is 0.6 mA. The current supplied to the LEDs is controlled through the current balancing software function. The maximum current, when both LED are supplied with 50 mA, is calculated. The actual current used, will be lower when the current balancing function adjusts the currents. The two LEDs of MAX30100 are set to flash at 50 Hz with a pulse width of 1.6 ms. The pulse wave is depicted in Figure A.1.

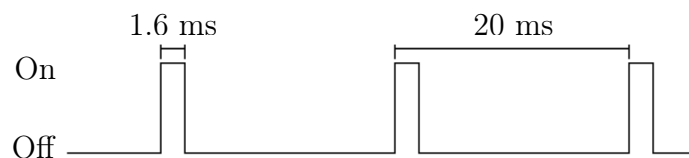


**Figure A.1:** Pulse diagram of one of the LEDs in the MAX30100

Digital logic current: 0.6 mA

LED supply current: 50 mA

Duty cycle:  $\frac{1.6}{20} \times 2 = 0.16$

Adjusted current:  $0.16 \times 50 = 8 \text{ mA}$

Total current:  $8 + 0.6 = 8.6 \text{ mA}$

### Total current

The theoretical current is calculated using the data sheet and calculated currents of the various major components. This is compared to the actual measured current used by the Ear-Monitor while operating. Table A.1 tabulates the theoretical current draw of the various components.

**Table A.1:** Current consumption per component

Component	Current (mA)
Arduino	10
HC-05	40
TMP006	10
MAX30100	8.6
On/Off LED	10
<b>Total</b>	<b>78.6</b>

The measured current is found to be 77.3 mA. A slight variation between the measured current and theoretical current is expected due to variations between actual values and values listed on the data sheets of the components and due to the effects of the current balancing function.

### Battery life

The predicted battery life can be calculated using the measured current

Predicted battery life:  $\frac{2000 \text{ mAh}}{77.3 \text{ mA}} = 25.87 \text{ h}$ .

## A.2 Component selection

This section describes the process followed to select the major electrical components. These components include the voltage regulators and the relay for the switching circuit.

### Voltage regulators

Voltage regulators are selected to regulate the supply voltage from the battery to 3.3 V and 1.8 V, as needed by the various components. The Arduino MCU has an onboard voltage regulator, and is not dependant on the voltage regulators. Table A.2 tabulates the current requirements at a specific voltage of the various components.



**Table A.2:** Voltage specific current consumption per component

Component	Current at 3.3 V (mA)	Current at 1.8 V (mA)
HC-05	40	
TMP006	10	
MAX30100	8	0.6
On/Off LED	10	
<b>Total</b>	<b>68</b>	<b>0.6</b>

The 3.3 V regulator should be able to handle 7.4 V from the battery as input and supply a minimum 68 mA. The 1.8 V regulator is connected to the regulated 3.3 V power and should be able to supply a minimum of 0.6 mA. A low dropout voltage is preferred. Table A.3 lists the two selected regulators and their characteristics.

**Table A.3:** Voltage regulators

Component	Voltage out (V)	Current out (mA)	Voltage in (V)
Texas Instruments' TLV1117-33CDCY	3.3	800	4.7 - 15
STMicroelectronics' LDK130M18R	1.8	300	1.9 - 5.5

### Battery and charger

A 7.4 V, 2000 mAh rechargeable LiPo battery is selected to power the Ear-Monitor. Special charging requirements are needed to ensure the safe charging of multi-cell LiPo batteries, therefore the 'Intelligent 7.4 V Lipo Charger', available from Micro Robotics, is selected to charge the battery. The charger outputs 8.4 V and up to 2 A charging current, followed by a trickle current to balance the cells.

A switching circuit is included on the headband PCB. A SPDT relay is used to switch the battery between the load (Ear-Monitor electronics) and the charger. The Figure A.2 depicts a diagram of this switching circuit. In the depicted configuration, the charger is not connected and the battery is connected to the rest of the Ear-Monitor electronics. If the charger is connected, the coil of the relay will be magnetised and the switch will toggle, disconnecting the battery from the rest of the Ear-Monitor and connecting it to the battery. A freewheeling diode is added to eliminate voltage spikes caused by switching.

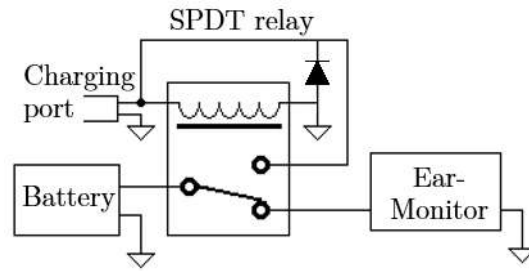


**Figure A.2:** Switching circuit diagram with the charger not connected and the battery connected to the rest of the Ear-Monitor

# Appendix B

## Printed circuit boards

### B.1 Schematic of PCB

Figure B.1 depicts a schematic of the PCB that integrates all the the electronic components. This PCB is located in the headband and has connection ports for the ear probe, Bluetooth modem, battery and charger.

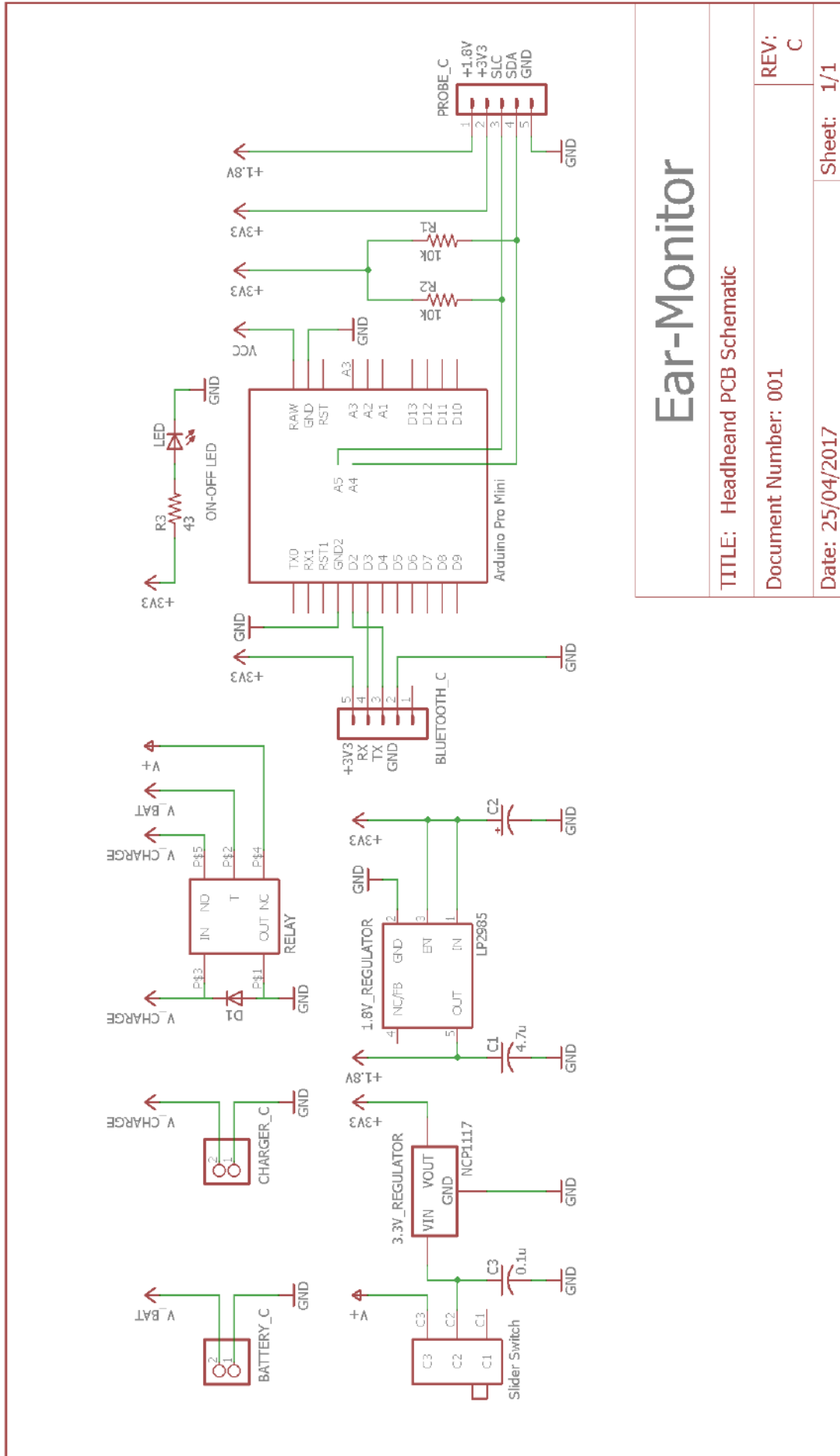


Figure B.1: Schematic of the PCB designed to integrate all the different electronic components of the Ear-Monitor

# Ear-Monitor

TITLE: Headhead PCB Schematic

Document Number: 001

REV:  
C

Date: 25/04/2017

Sheet: 1/1

## B.2 PCB layouts

A double sided PCB was designed to realise the above schematic. Figure B.2 depicts the layout of the top layer and Figure B.3 of the bottom layer. Via holes are shown in green, top copper in red and bottom copper in blue. Labels and outlines are added for the major components.

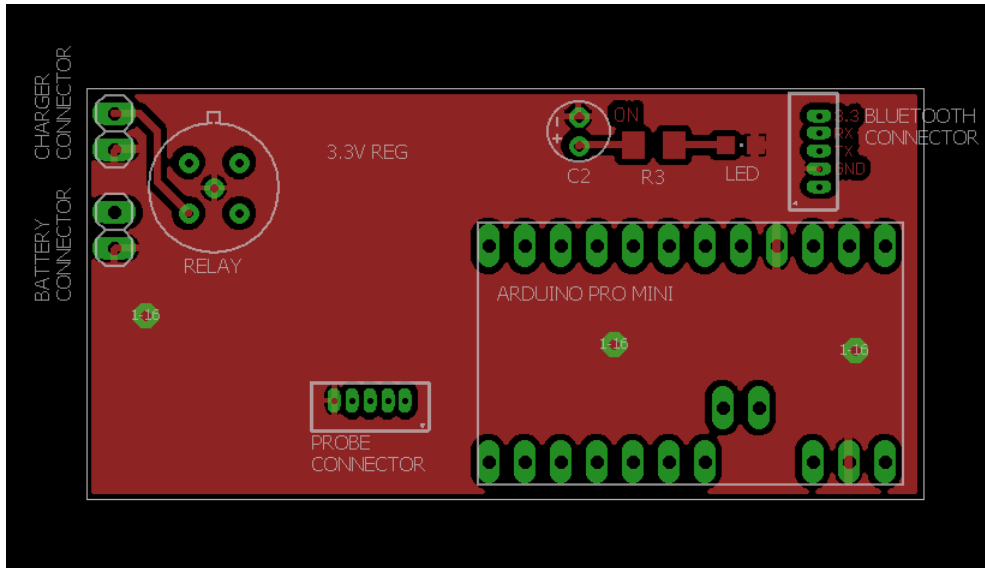


Figure B.2: Top layout of the headband PCB

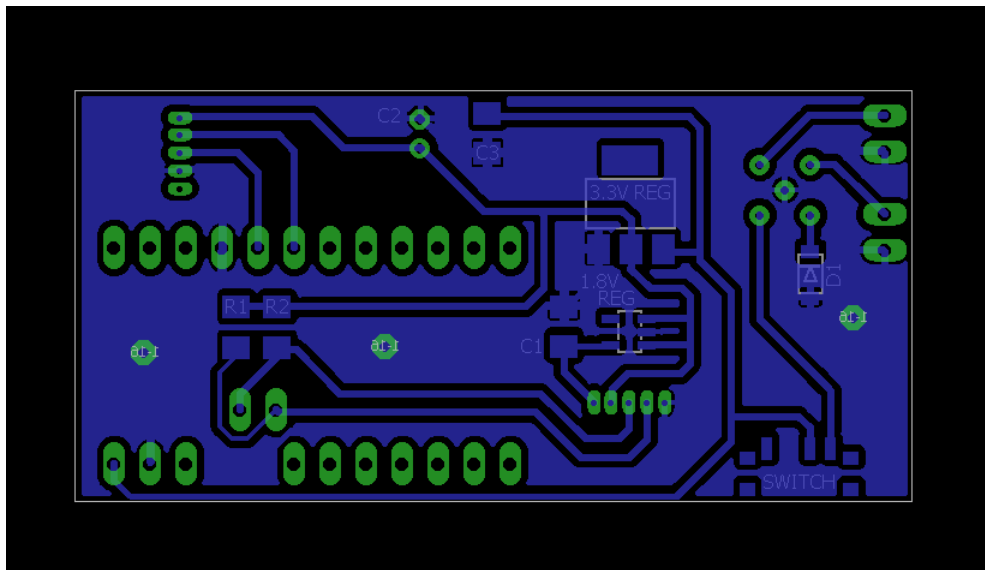


Figure B.3: Bottom layout of the headband PCB

# Appendix C

## Calibration

Data collected during the trial were used to calibrate the equations used to calculate tympanic temperature and SpO<sub>2</sub>. The calibration processes for the two different vital signs are discussed separately in this appendix.

### C.1 Temperature calibration

As discussed in Section 4.2, the TMP006 measures die temperature,  $T_{DIE}$ , and thermopile sensor voltage,  $V_{SENSOR}$ . These two measurements are used to calculate the temperature of the object,  $T_{OBJ}$ , which in the case of the Ear-Monitor is the tympanic membrane.

Each data recording session in the trial produced 15 Ear-Monitor measurements and three ET 100-A benchmark measurements. Measurements from both devices were averaged separately to get one average Ear-Monitor and one average ET 100-A measurement per session. Two different calibration approaches are discussed: the group calibration approach and the intra-participant calibration approach.

#### C.1.1 Group calibration

In this approach, five recording sessions were used to calibrate the temperature calculation equation, Equation 4.5. MATLAB's curve fitting tool was used to fit a first-order polynomial plane to the data points. The equation with calibration coefficients are shown by Equation C.1.

$$T_{OBJ} = 22.85 + 0.04803T_{DIE} - 13440V_{SENSOR} \quad (C.1)$$

This equation was applied to all Ear-Monitor temperature measurements. The advantage of the group calibration approach is that calibration is done only once and no patient-specific calibration is needed.

A box and whisker plot is depicted in Figure C.1 and illustrates the error between the ET 100-A benchmark temperature and the Ear-Monitor temperature before and after calibration for all the collected data. Improvements in accuracy and precision are clearly visible in this graphical representation of the data.

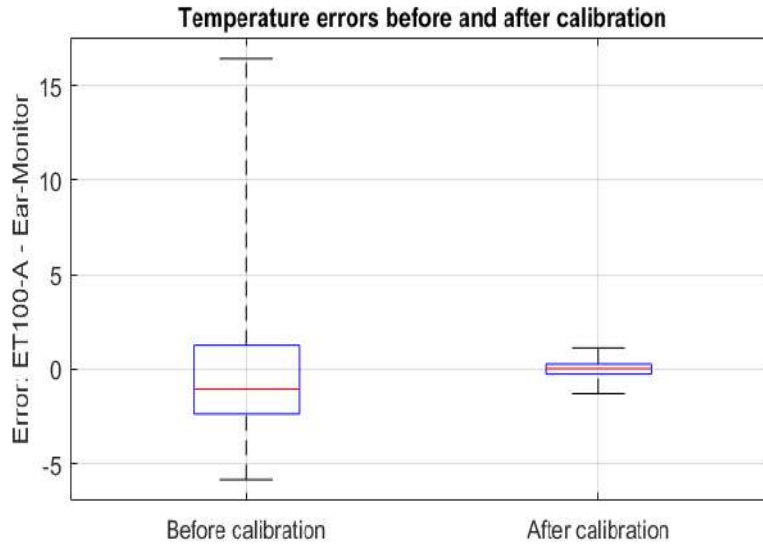


**Figure C.1:** Temperature errors before and after calibration

### C.1.2 Intra-participant calibration

In this approach, the first recording session was used to calibrate the calibration coefficients for each participant individually. The first recording session data was entered into Equation C.1 and the error between the Ear-Monitor and ET 100-A data was used to adjust Equation C.1.

The advantage of this approach is that the Ear-Monitor can adjust to patient-specific parameters, for example tympanic membrane size, the sensor's distance from the membrane and the fraction of the FOV that is occupied by the canal wall. The trade-off is that the Ear-Monitor needs to be calibrated for each participant individually. This is not a complicated process as calibration can be done in one minute and is only needed once per individual.

## C.2 SpO<sub>2</sub> calibration

According to Oak and Aroul (2015), the modulated ratio,  $R$  (Equation 4.12), is linearly related to SpO<sub>2</sub>. The relationship they propose is given by Equation C.2,

$$SpO_2 = x - m \cdot R \quad (C.2)$$

with  $x$  is equal to 110 and  $m$  equal to 25. The relationship varies for different pulse oximeters, and the calibration parameters for the MAX30100 in the Ear-Monitor were calculated empirically through experimentation. Equation C.2 was used as a starting point and the gradient,  $m$ , was constrained to be larger or equal to 15 in order to ensure  $R$ 's weight in the calculated SpO<sub>2</sub> value. The remaining calibration parameter,  $x$ , was systematically incremented until the desired fit was achieved. Equation C.3 describes the relationship between  $R$  and SpO<sub>2</sub> selected for the Ear-Monitor.

$$SpO_2 = 106.32 - 15 \cdot R \quad (C.3)$$



# Appendix D

## Proof of ethical approval



UNIVERSITEIT • STELLENBOSCH • UNIVERSITY  
for knowledge • vir kennis • for knowledge • partners

### Approved with Stipulations New Application

27-June-2017

**Ethics Reference #:** M16/09/038

**Title:** Monitoring core temperature, heart rate, respiratory rate and EEG through a wireless ear probe

Dear Mr Andre Bestbier,

The **Response to Defferal** received on **15 May 2017**, was reviewed by members of **Health Research Ethics Committee (HREC) 2** via **expedited** review procedures on **27-June-2017**.

Please note the following information about your approved research protocol:

Protocol Approval Period: **27-June-2017 – 26-June-2018**.

The Stipulations of your ethics approval are as follows:

1. **Please remove the word "neonate" on page 1 of the synopsis under "participant consent" (last line of paragraph 1);**
2. **In the 1st paragraph of the informed consent form under "what is this study all about", there is an incomplete sentence "the idea is to"...please complete the sentence or remove it;**
3. **Please change the word "devise" to "device" in the 2nd paragraph of the informed consent form under "what is this study all about";**
4. **Please change the word "health" to "healthy" in the informed consent form under "Why have you been invited to participate".**

Please remember to use your **protocol number (M16/09/038)** on any documents or correspondence with the HREC concerning your research protocol.

Please note that the HREC has the prerogative and authority to ask further questions, seek additional information, require further modifications, or monitor the conduct of your research and the consent process.

**After Ethical Review:**

Please note a template of the progress report is obtainable on [www.sun.ac.za/rds](http://www.sun.ac.za/rds) and should be submitted to the Committee before the year has expired.

The Committee will then consider the continuation of the project for a further year (if necessary). Annually a number of projects may be selected randomly for an external audit.

Translation of the consent document to the language applicable to the study participants should be submitted.

Federal Wide Assurance Number: 00001372

Institutional Review Board (IRB) Number: IRB0005240 for HREC1



Fakulteit Geneeskunde en Gesondheidswetenskappe  
Faculty of Medicine and Health Sciences



Afdeling Navorsingsontwikkeling en -Steun • Research Development and Support Division



UNIVERSITEIT • STELLENBOSCH • UNIVERSITY  
 jou kennisvermoë • your knowledge partner

Institutional Review Board (IRB) Number: IRB0005239 for HREC2

The Health Research Ethics Committee complies with the SA National Health Act No. 61 of 2003 as it pertains to health research and the United States Code of Federal Regulations Title 45 Part 46. This committee abides by the ethical norms and principles for research, established by the Declaration of Helsinki and the South African Medical Research Council Guidelines as well as the Guidelines for Ethical Research: Principles, Structures and Processes 2015 (Departement of Health).

#### Provincial and City of Cape Town Approval

Please note that for research at a primary or secondary healthcare facility, permission must still be obtained from the relevant authorities (Western Cape Departement of Health and/or City Health) to conduct the research as stated in the protocol. Contact persons are Ms Claudette Abrahams at Western Cape Departement of Health ([healthres@pgwc.gov.za](mailto:healthres@pgwc.gov.za); Tel: +27 21 483 9907) and Dr Helene Visser at City Health ([Helene.Visser@capetown.gov.za](mailto:Helene.Visser@capetown.gov.za); Tel: +27 21 400 3981). Research that will be conducted at any tertiary academic institution requires approval from the relevant hospital manager. Ethics approval is required BEFORE approval can be obtained from these health authorities.

We wish you the best as you conduct your research.

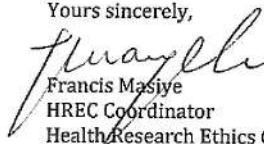
For standard HREC forms and documents, please visit: [www.sun.ac.za/rds](http://www.sun.ac.za/rds)

If you have any questions or need further assistance, please contact the HREC office at 021 938 9677.

#### Included Documents:

Investigator's Declaration Form\_PR Fourie  
 Investigator's Declaration Form\_A Bestbier  
 CV\_PR Fourie  
 CV\_A Bestbier  
 Protocol Synopsis  
 Protocol  
 Informed consent form  
 New Application form  
 Clinical Trials Checklist  
 Description of Study Site  
 Insurance on Clinical Trials  
 Flow Chart  
 Physical Examination Check  
 Proof of GCP  
 Recruitment Email

Yours sincerely,

  
 Francis Masjye  
 HREC Coordinator  
 Health Research Ethics Committee

STELLENBOSCH UNIVERSITY  
 Health Research Ethics Committee

27 JUN 2017

STELLENBOSCH UNIVERSITEIT  
 Gesondheidsnavorsing Etieskomitee



Fakulteit Geneeskunde en Gesondheidswetenskappe  
 Faculty of Medicine and Health Sciences



Afdeling Navorsingsontwikkeling en -Steun • Research Development and Support Division

Posbus/PO Box 241 • Cape Town 8000 • Suid-Afrika/South Africa  
 Tel: +27 (0) 21 938 9677





UNIVERSITEIT • STELLENBOSCH • UNIVERSITY  
jou kennisennoot • your knowledge partner

## INVESTIGATOR RESPONSIBILITIES Protection of Human Research Participants

Some of the responsibilities investigators have when conducting research involving human participants are listed below:

1. **Conducting the Research:** You are responsible for making sure that the research is conducted according to the HREC approved research protocol. You are also responsible for the actions of all your co-investigators and research staff involved with this research.
2. **Participant Enrolment:** You may not recruit or enrol participants prior to the HREC approval date or after the expiration date of HREC approval. All recruitment materials for any form of media must be approved by the HREC prior to their use. If you need to recruit more participants than was noted in your HREC approval letter, you must submit an amendment requesting an increase in the number of participants.
3. **Informed Consent:** You are responsible for obtaining and documenting effective informed consent using **only** the HREC approved consent documents, and for ensuring that no human participants are involved in research prior to obtaining their informed consent. Please give all participants copies of the signed consent documents. Keep the originals in your secured research files for at least fifteen (15) years.
4. **Continuing Review:** The HREC must review and approve all HREC approved research protocols at intervals appropriate to the degree of risk but not less than once per year. There is **no grace period**. Prior to the date on which the HREC approval of the research expires, **it is your responsibility to submit the continuing review report in a timely fashion to ensure a lapse in HREC approval does not occur**. If HREC approval of your research lapses, you must stop new participant enrolment, and contact the HREC Office immediately.
5. **Amendments and Changes:** If you wish to amend or change any aspect of your research (such as research design, interventions or procedures, number of participants, participant population, informed consent document, instruments, surveys or recruiting material), you must submit the amendment to the HREC for review using the current Amendment Form. You **may not initiate** any amendments or changes to your research without first obtaining written HREC review and approval. The **only exception** is when it is necessary to eliminate apparent immediate hazards to participants and the HREC should be immediately informed of this necessity.
6. **Adverse or Unanticipated Events:** Any serious adverse events, participant complaints, and all unanticipated problems that involve risks to participants or others, as well as any research-related injuries, occurring at this institution or at other performance sites must be reported to the HREC within **five (5) days** of discovery of the incident. You must also report any instances of serious or continuing problems, or non-compliance with the HREC's requirements for protecting human research participants. The only exception to this policy is that the death of a research participant must be reported in accordance with the Stellenbosch University Health Research Ethics Committee Standard Operating Procedures  
[www.sun25.sun.ac.za/portal/page/portal/Health\\_Sciences/English/Centres%20and%20Institutions/Research\\_Development\\_Support/Ethics/Application\\_package](http://www.sun25.sun.ac.za/portal/page/portal/Health_Sciences/English/Centres%20and%20Institutions/Research_Development_Support/Ethics/Application_package). All reportable events should be submitted to the HREC using the Serious Adverse Event Report Form.
7. **Research Record Keeping:** You must keep the following research-related records, at a minimum, in a secure location for a minimum of fifteen years; the HREC approved research protocol and all amendments; all informed consent documents; recruiting materials; continuing review reports; adverse or unanticipated events; and all correspondence from the HREC.
8. **Reports to the MCC and Sponsor:** When you submit the required annual report to the MCC or you submit a required report to your Sponsor, you must provide a copy of that report to the HREC. You may submit the report at the time of continuing HREC review.
9. **Provisions of Emergency Medical Care:** When a physician provides emergency medical care to a participant without prior HREC review and approval, to the extent permitted by law, such activities will not be recognized as research nor will the data obtained by any of such activities be used in support of research.
10. **Final Reports:** When you have completed (no further participant enrolment, interactions, interventions or data analysis) or stopped work on your research, you must submit a Final Report to the HREC.
11. **On-Site Evaluations, MCC Inspections or Audits:** If you are notified that your research will be reviewed or audited by the MCC, the Sponsor, any other external agency or any internal group, you must inform the HREC immediately of the impending audit/evaluation.



Fakulteit Geneeskunde en Gesondheidswetenskappe  
Faculty of Medicine and Health Sciences



Afdeling Navorsingsontwikkeling en -Steun / Research Development and Support Division

# Appendix E

## Detailed Results

### E.1 PhysioNet beat detection

The beat detection algorithm of the Ear-Monitor is tested on PPG data from the open-source MIMIC Database on PhysioNet.org (Goldberger *et al.*, 2000). Results from random ten-minute segments from 14 different patients are tabulated in Table E.1. All values represent number of beats.

**Table E.1:** Results of the beat detection algorithm on the PhysioNet data

Record No.	Actual No. Beats	False Positives	False negatives
039	1337	0	0
041	1030	1	7
055	1021	0	0
211	891	2	8
212	845	0	15
216	763	0	1
218	697	0	1
219	720	0	0
221	776	0	4
224	863	0	0
230	871	7	36
237	777	2	17
240	816	1	2
252	594	0	0

## E.2 Core temperature

Temperature results for each trial participant are tabulated in Table E.2. The calibration group method is labelled A and the intra-participant calibration method as B. The temperature values are recording session averages with standard errors indicated in brackets. All values are in °C.

**Table E.2:** Temperature results

Participant No.	ET 100-A Temp	Ear-Monitor Temp A	Error A	Ear-Monitor Temp B	Error B	Ear-Monitor standard error
2a	36.33	37.63	-1.29	-	-	±0.0043
2b	36.37	37.57	-1.21	36.08	0.28	±0.0017
3a	37.65	37.54	0.11	-	-	±0.0031
3b	37.40	37.67	-0.27	37.58	-0.18	±0.0172
4a	38.30	37.37	0.93	-	-	±0.0012
4b	38.55	37.44	1.11	38.17	0.38	±0.0014
6a	38.35	37.80	0.55	-	-	±0.0032
6b	37.60	37.76	-0.16	38.11	-0.51	±0.0015
7a	37.03	37.31	-0.28	-	-	±0.0008
7b	37.00	37.34	-0.34	36.86	0.14	±0.0016
8a	38.40	38.13	0.27	-	-	±0.0072
8b	38.50	38.03	0.47	38.10	0.40	±0.0009
9a	37.55	37.53	0.02	-	-	±0.0005
9b	37.40	37.54	-0.14	37.36	0.04	±0.0007
10a	37.95	37.70	0.25	-	-	±0.0031
10b	38.10	37.73	0.37	37.77	0.33	±0.0007
11a	37.50	37.52	-0.02	-	-	±0.0006
11b	37.60	37.50	0.10	37.27	0.33	±0.0051
12a	38.50	38.51	-0.01	-	-	±0.021
12b	37.70	38.18	-0.48	37.97	-0.27	±0.0028
13a	38.05	38.02	0.03	-	-	±0.012
13b	37.53	37.92	-0.39	37.75	-0.22	±0.0016
14a	38.00	37.73	0.27	-	-	±0.001
14b	37.95	37.75	0.20	37.82	0.13	±0.0004
15a	37.65	37.58	0.07	-	-	±0.0033
15b	37.30	37.55	-0.25	37.42	-0.12	±0.0008
16a	37.90	37.90	0.00	-	-	±0.0016
16b	37.50	37.93	-0.43	37.73	-0.23	±0.0038

### E.3 Trial data beat detection

The beat detection algorithm is tested on data collected from participants during the trial period. Results for each participant is tabulated in Table E.3. All values represent number of beats.

**Table E.3:** Results of the beat detection algorithm on the trial data

Participant No.	No. Nexus-10 Beats	No. Ear-Monitor Beats	False Positives	False Negatives	% Correct
1a	150	150	0	0	100
1b	148	148	0	0	100
2a	116	108	2	10	93.1
2b	116	106	1	11	91.4
3a	136	136	0	0	100
3b	138	138	0	0	100
4a	132	132	0	0	100
4b	133	132	0	1	99.2
5a	181	181	0	0	100
5b	188	187	0	1	99.5
6a	120	120	0	0	100
6b	127	127	0	0	100
7b	144	144	0	0	100
7c	140	140	0	0	100
8a	163	163	0	0	100
8b	164	163	0	1	99.4
9a	149	149	0	0	100
9b	146	142	0	4	97.3
10a	146	146	0	0	100
10c	146	146	0	0	100
11a	131	131	0	0	100
11b	131	131	0	0	100
12a	144	144	0	0	100
12b	137	137	0	0	100
13a	169	163	0	6	96.45
13b	169	162	0	7	95.86
14a	168	168	0	0	100
14b	170	170	0	0	100
15a	149	149	0	0	100
15c	149	149	0	0	100
16a	154	151	1	4	98.05
16b	159	152	6	13	95.6

## E.4 Respiratory rate

Respiratory results for each trial participant are tabulated in Table E.4. All values represent number of breaths.

**Table E.4:** Respiratory rate results

Participant No.	No. Nexus-10 Breaths	No. Ear-Monitor Breaths	Error
1a	30	30	0
1b	23	22	1
2a	27	22	5
2b	27	22	5
3a	28	25	3
3b	25	25	0
4a	28	29	-1
4b	28	27	1
5a	24	33	-9
5b	24	44	-20
6a	34	29	5
6b	32	30	2
7b	28	29	-1
7c	26	26	0
8a	29	27	2
8b	29	32	-3
9a	42	31	11
9b	43	29	14
10a	31	29	2
10b	32	32	0
11a	29	28	1
11b	29	28	1
12a	32	26	6
12b	34	33	1
13a	30	39	-9
13b	28	43	-15
14a	22	22	0
14b	23	24	-1
15a	32	32	0
15c	30	33	-3
16a	29	28	1
16b	35	33	2



## E.5 Blood oxygen saturation

SpO<sub>2</sub> results for each trial participant are tabulated in Table E.5. All values are in percentage (%).

**Table E.5:** SpO<sub>2</sub> results

Participant No.	SureSigns VM1 SpO <sub>2</sub>	Ear-Monitor SpO <sub>2</sub>	Error
1a	96.38	99.08	2.70
1b	97.00	98.41	1.41
2a	100.00	100.00	0.00
2b	100.00	100.00	0.00
3a	100.00	98.03	-1.97
3b	99.97	98.26	-1.71
4a	98.83	99.59	0.77
4b	98.98	98.79	-0.20
5a	98.21	98.62	0.41
5b	98.13	98.63	0.50
6a	97.07	99.21	2.14
6b	97.00	98.75	1.75
7b	100.00	98.86	-1.14
7c	100.00	99.63	-0.37
8a	99.14	99.40	0.26
8b	98.33	98.69	0.36
9a	99.21	98.11	-1.10
9b	98.99	95.27	-3.73
10a	99.67	99.85	0.19
10c	99.38	99.90	0.52
11a	99.22	100.00	0.78
11b	99.75	99.92	0.17
12a	99.98	98.54	-1.44
12b	100.00	98.61	-1.39
13a	98.98	98.40	-0.59
13b	98.33	98.49	0.15
14a	99.34	99.17	-0.17
14b	99.21	98.08	-1.13
15a	99.25	99.86	0.61
15c	98.76	99.97	1.21
16a	99.88	98.08	-1.80
16b	99.91	95.65	-4.25

# List of References

- Alvord, L.S. and Farmer, B.L. (1997). Anatomy and orientation of the human external ear. *Journal-American academy of audiology*, vol. 8, pp. 383–390.
- Aoyagi, T. (2003). Pulse oximetry: its invention, theory, and future. *Journal of anesthesia*, vol. 17, no. 4, pp. 259–266.
- Aziz, O., Lo, B., King, R., Darzi, A. and Yang, G.-Z. (2006). Pervasive body sensor network: an approach to monitoring the post-operative surgical patient. In: *Wearable and Implantable Body Sensor Networks, 2006. BSN 2006. International Workshop on*, pp. 4–7. IEEE.
- Bagha, S. and Shaw, L. (2011). A real time analysis of PPG signal for measurement of SpO<sub>2</sub> and pulse rate. *International journal of computer applications*, vol. 36, no. 11, pp. 45–50.
- Bheema lingaiah, T., Hanumesh Kumar, D. and Nagaraja, C. (2013). Measurement of Pulse rate and SpO<sub>2</sub> using Pulse Oximeter developed using LabVIEW. *Journal of Electrical and Electronics Engineering*, vol. 8.
- Blahd, W. (2016 09). WebMD Sleep Apnea. [Online] Available at: <http://www.webmd.com/sleep-disorders/sleep-apnea/sleep-apnea>, [Accessed 4 March 2016].
- Bragi (2017). Meet the Dash Pro. [Online] Available at: <https://www.bragi.com/thedashpro>, [Accessed 21 Mei 2017].
- Buske, O., Neils, C. and Regnier, M. (2009). *Heartbeat: Design and Development of a Headphone*. Master's thesis, University of Washington.
- Chan, E.D., Chan, M.M. and Chan, M.M. (2013). Pulse oximetry: understanding its basic principles facilitates appreciation of its limitations. *Respiratory medicine*, vol. 107, no. 6, pp. 789–799.
- Chan, V. and Underwood, S. (2005 11). *A Single-Chip Pulsoximeter Design Using the MSP430*. Texas Instruments. Rev. Feb 2012.
- Charbek, E. (2015 08). Medscape Normal Vital Vigns. [Online] Available at: <http://emedicine.medscape.com/article/2172054-overview>, [Accessed 8 June 2017].

- Cicchetti, D.V. (1994). Guidelines, criteria, and rules of thumb for evaluating normed and standardized assessment instruments in psychology. *Psychological assessment*, vol. 6, no. 4, p. 284.
- Clifton, D., Douglas, J.G., Addison, P.S. and Watson, J.N. (2007). Measurement of respiratory rate from the photoplethysmogram in chest clinic patients. *Journal of clinical monitoring and computing*, vol. 21, no. 1, pp. 55–61.
- Cosinuss (2017a). Cosinuss One. [Online] Available at: <https://www.cosinuss.com/en/products/one>, [Accessed 11 March 2017].
- Cosinuss (2017b). Degree. [Online] Available at: <https://www.degree-fever-assistant.com>, [Accessed 11 March 2017].
- Curtin, A. (2012 08). Absorption spectra of oxygenated hemoglobin (HbO<sub>2</sub>) and deoxygenated hemoglobin (Hb) for red and infrared wavelengths. [Online] Available at: [https://en.wikipedia.org/wiki/Pulse\\_oximetry#/media/File:Oxy\\_and\\_Deoxy\\_Hemoglobin\\_Near-Infrared\\_absorption\\_spectra.png](https://en.wikipedia.org/wiki/Pulse_oximetry#/media/File:Oxy_and_Deoxy_Hemoglobin_Near-Infrared_absorption_spectra.png), [Accessed 31 June 2016].
- Da He, D., Winokur, E.S., Heldt, T. and Sodini, C.G. (2010). The ear as a location for wearable vital signs monitoring. In: *Engineering in Medicine and Biology Society (EMBC), 2010 Annual International Conference of the IEEE*, pp. 6389–6392. IEEE.
- DeMeulenaere, S. (2007). Pulse oximetry: uses and limitations. *The Journal for Nurse Practitioners*, vol. 3, no. 5, pp. 312–317.
- DerSarkissian, C. (2016). Flu or Cold Symptoms? [Online] Available at: <http://www.webmd.com/cold-and-flu/cold-guide/flu-cold-symptoms>, [Accessed 9 November 2016].
- Dexter Research Centre (2004). ST60 Micro-TO & ST60R Micro-TO. [Online] Available at: [https://dexterresearch.com/?module=Resources&event=Download&downloadID=131&fno=1&filename=st60\\_microto.pdf](https://dexterresearch.com/?module=Resources&event=Download&downloadID=131&fno=1&filename=st60_microto.pdf), [Accessed 28 March 2016].
- Doctor online (2016). Ear Anatomy. [Online] Available at: <http://www.edoctoronline.com/medical-atlas.asp?c=4&id=21693>, [Accessed 29 August 2017].
- Duun, S., Haahr, R.G., Birkelund, K., Raahauge, P., Petersen, P., Dam, H., Nørgaard, L. and Thomsen, E.V. (2007). A novel ring shaped photodiode for reflectance pulse oximetry in wireless applications. In: *Sensors, 2007 IEEE*, pp. 596–599. IEEE.
- Elgendi, M., Norton, I., Brearley, M., Abbott, D. and Schuurmans, D. (2013). Systolic peak detection in acceleration photoplethysmograms measured from emergency responders in tropical conditions. *PLoS One*, vol. 8, no. 10, p. e76585.

- Encyclopædia Britannica, T.E. (2015 01). External auditory canal. [Online] Available at: <https://global.britannica.com/science/external-auditory-canal>, [Accessed 21 June 2016].
- Encyclopædia Britannica, T.E.O. (2009). Spectrophotometry. [Online] Available at: <https://www.britannica.com/science/spectrophotometry>, [Accessed 18 July 2016].
- Erickson, R.S. and Kirklin, S.K. (1993). Comparison of ear-based, bladder, oral, and axillary methods for core temperature measurement. *Critical care medicine*, vol. 21, no. 10, pp. 1528–1534.
- Fahy, B., Lareau, S. and Sockrider, M. (2011). Pulse oximetry. *American Journal of Respiratory and Critical Care Medicine*, vol. 184.
- Gasim, G.I., Musa, I.R., Abdien, M.T. and Adam, I. (2013). Accuracy of tympanic temperature measurement using an infrared tympanic membrane thermometer. *BMC research notes*, vol. 6, no. 1, p. 194.
- Goldberger, A.L., Amaral, L.A.N., Glass, L., Hausdorff, J.M., Ivanov, P.C., Mark, R.G., Mietus, J.E., Moody, G.B., Peng, C.-K. and Stanley, H.E. (2000). PhysioBank, PhysioToolkit, and PhysioNet: Components of a New Research Resource for Complex Physiologic Signals. *Circulation*, vol. 101, no. 23, pp. e215–e220. Circulation Electronic Pages: <http://circ.ahajournals.org/content/101/23/e215.full> PMID:1085218; doi: 10.1161/01.CIR.101.23.e215.
- Goverdovsky, V., von Rosenberg, W., Nakamura, T., Looney, D., Sharp, D.J., Papavassiliou, C., Morrell, M.J. and Mandic, D.P. (2016). Hearables: Multimodal physiological in-ear sensing. *arXiv preprint arXiv:1609.03330*.
- Holland, K. (2016 09). Thermoregulation. [Online] Available at: <http://www.healthline.com/health/thermoregulation#overview1>, [Accessed 18 July 2016].
- Huang, C.-Y., Chan, M.-C., Chen, C.-Y. and Lin, B.-S. (2014). Novel wearable and wireless ring-type pulse oximeter with multi-detectors. *Sensors*, vol. 14, no. 9, pp. 17586–17599.
- Johansson, A. (2003). Neural network for photoplethysmographic respiratory rate monitoring. *Medical and Biological Engineering and Computing*, vol. 41, no. 3, pp. 242–248.
- Jones, D. (2010). *Biomedical Sensors*. Sensor technology series. Momentum Press. ISBN 9781606500569. [Online] Available at: <https://books.google.co.za/books?id=7cI83Y0IUTkC>.
- JRC (2013 04). COBP PHOTO REFLECTOR with RED & IR LED. [Online] Available at: [http://www.mouser.com/catalog/specsheets/NJL5501R\\_E.pdf](http://www.mouser.com/catalog/specsheets/NJL5501R_E.pdf), [Accessed 30 August 2016].

- Karaki, H. and Polyziev, V. (2014). Demystifying Thermopile IR Temp Sensors. [Online] Available at: <http://www.sensormag.com/components/demystifying-thermopile-ir-temp-sensors>, [Accessed 16 July 2016].
- Karriem-Norwood, V. (2017). Stress Symptoms. [Online] Available at: <http://www.webmd.com/balance/stress-management/stress-symptoms-effects-of-stress-on-the-body>, [Accessed 4 November 2016].
- Kennedy, S.M. (2015). An introduction to pulse oximeters: Equations and theory. *University of Wisconsin-Madison*, vol. 20.
- Khalifa, O.O., Khan, T. and HM, H. (2014). Development of wearable pulse oximetry for telehealth monitoring system. *Journal of Electrical Engineering*, vol. 14, no. 4, pp. 1–6.
- Koblenski, S. (2015). Everyday DSP for Programmers: DC and Impulsive Noise Removal. [Online] Available at: <http://sam-koblenski.blogspot.co.za/2015/11/everyday-dsp-for-programmers-dc-and.html>, [Accessed 12 September 2016].
- König, V., Huch, R. and Huch, A. (1998). Reflectance pulse oximetry—principles and obstetric application in the Zurich system. *Journal of Clinical Monitoring and Computing*, vol. 14, no. 6, pp. 403–412.
- Laskowski, E.R. (2015). What’s a normal resting heart rate? [Online] Available at: <http://www.mayoclinic.org/healthy-lifestyle/fitness/expert-answers/heart-rate/faq-20057979>, [Accessed 1 May 2017].
- Lee, H., Ko, H. and Lee, J. (2016). Reflectance pulse oximetry: Practical issues and limitations. *ICT Express*, vol. 2, no. 4, pp. 195–198.
- Lefrant, J.-Y., Muller, L., de La Coussaye, J.E., Benbabaali, M., Lebris, C., Zeitoun, N., Mari, C., Saissi, G., Ripart, J. and Eledjam, J.-J. (2003). Temperature measurement in intensive care patients: comparison of urinary bladder, oesophageal, rectal, axillary, and inguinal methods versus pulmonary artery core method. *Intensive care medicine*, vol. 29, no. 3, pp. 414–418.
- Leonard, P.A., Douglas, J.G., Grubb, N.R., Clifton, D., Addison, P.S. and Watson, J.N. (2006). A fully automated algorithm for the determination of respiratory rate from the photoplethysmogram. *Journal of clinical monitoring and computing*, vol. 20, no. 1, pp. 33–36.
- Lin, B.-S., Chou, W., Wang, H.-Y., Huang, Y.-J. and Pan, J.-S. (2013). Development of novel non-contact electrodes for mobile electrocardiogram monitoring system. *IEEE journal of translational engineering in health and medicine*, vol. 1, pp. 1–8.
- Louw, A., Cracco, C., Cerf, C., Harf, A., Duvaldestin, P., Lemaire, F. and Brochard, L. (2001). Accuracy of pulse oximetry in the intensive care unit. *Intensive care medicine*, vol. 27, no. 10, pp. 1606–1613.

- MAX30100 (2014). Pulse Oximeter and Heart-Rate Sensor IC for Wearable Health. [Online] Available at: <https://datasheets.maximintegrated.com/en/ds/MAX30100.pdf>, [Accessed 30 August 2016].
- Mayo Clinic (2017). Pneumonia. [Online] Available at: <http://www.mayoclinic.org/diseases-conditions/pneumonia>, [Accessed 3 November 2016].
- Moody, G.B., Mark, R.G., Bump, M.A., Weinstein, J.S., Berman, A.D., Mietus, J.E. and Goldberger, A.L. (1986). Clinical validation of the ECG-derived respiration (EDR) technique. *Group*, vol. 1, no. 3.
- Nitzan, M., Noach, S., Tobal, E., Adar, Y., Miller, Y., Shalom, E. and Engelberg, S. (2014). Calibration-Free Pulse Oximetry Based on Two Wavelengths in the Infrared-A Preliminary Study. *Sensors*, vol. 14, no. 4, pp. 7420–7434.
- Novatemp (2011). Accuracy is the key for tympanic temperature monitoring. [Online] Available at: [http://www.novamed-usa.com/tympanic\\_temperature\\_sensors.html](http://www.novamed-usa.com/tympanic_temperature_sensors.html), [Accessed 10 April 2017].
- Oak, S. and Aroul, P. (2015 3). *How to Design Peripheral Oxygen Saturation (SpO<sub>2</sub>) and Optical Heart Rate Monitoring (OHRM) Systems Using the AFE4403*. Texas Instruments.
- Olive, S., Twentyman, O. and Ramsay, C. (2016). Comparison of fingertip and earlobe pulse oximetry with arterial blood gas results.
- Optotherm (2017). Emissivity Table. [Online] Available at: <http://www.optotherm.com/emiss-table.htm>, [Accessed 5 June 2017].
- Park, J.-H., Jang, D.-G., Park, J.W. and Youm, S.-K. (2015). Wearable sensing of in-ear pressure for heart rate monitoring with a piezoelectric sensor. *Sensors*, vol. 15, no. 9, pp. 23402–23417.
- Pearce, J. (2002). A brief history of the clinical thermometer. *Qjm*, vol. 95, no. 4, pp. 251–252.
- Poh, M.-Z., Swenson, N.C. and Picard, R.W. (2010). Motion-tolerant magnetic earring sensor and wireless earpiece for wearable photoplethysmography. *IEEE Transactions on Information Technology in Biomedicine*, vol. 14, no. 3, pp. 786–794.
- Prawiro, E.A.P.J., Yeh, C.-I., Chou, N.-K., Lee, M.-W. and Lin, Y.-H. (2016). Integrated Wearable System for Monitoring Heart Rate and Step during Physical Activity. *Mobile Information Systems*, vol. 2016.
- Pujary, C., Savage, M. and Mendelson, Y. (2003). Photodetector size considerations in the design of a noninvasive reflectance pulse oximeter for telemedicine applications. In: *Bioengineering Conference, 2003 IEEE 29th Annual, Proceedings of*, pp. 148–149. IEEE.

- Shcherbina, A., Mattsson, C.M., Waggott, D., Salisbury, H., Christle, J.W., Hastie, T., Wheeler, M.T. and Ashley, E.A. (2017). Accuracy in wrist-worn, sensor-based measurements of heart rate and energy expenditure in a diverse cohort. *Journal of personalized medicine*, vol. 7, no. 2, p. 3.
- Shin, K., Kim, Y., Bae, S., Park, K. and Kim, S. (2009). A novel headset with a transmissive PPG sensor for heart rate measurement. In: *13th International Conference on Biomedical Engineering*, pp. 519–522. Springer.
- Sinex, J.E. (1999). Pulse oximetry: principles and limitations. *The American journal of emergency medicine*, vol. 17, no. 1, pp. 59–66.
- ST Electronics (2016a). MEMS digital output motion sensor ultra low-power high full-scale 3-axes "nano" accelerometer. [Online] Available at: <https://www.sparkfun.com/datasheets/Sensors/Accelerometer/LIS331HH.pdf>, [Accessed 20 September 2016].
- ST Electronics (2016b). MEMS audio sensor omnidirectional digital microphone. [Online] Available at: <http://www.st.com/content/ccc/resource/technical/document/datasheet/group3/10/65/67/7c/98/c2/4b/69/DM00333876/files/DM00333876.pdf/jcr:content/translations/en.DM00333876.pdf>, [Accessed 9 October 2016].
- Starboard (2016). Tympanic Temperature Sensors. [Online] Available at: <http://starboardmedical.com/tympanic-temperature-sensors>, [Accessed 10 April 2017].
- Stratton, J.R., Levy, W.C., Caldwell, J.H., Jacobson, A., May, J., Matsuoka, D. and Madden, K. (2003). Effects of aging on cardiovascular responses to parasympathetic withdrawal. *Journal of the American College of Cardiology*, vol. 41, no. 11, pp. 2077–2083.
- Strogonovs, R. (2017-03). Implementing pulse oximeter using MAX30100. [Online] Available at: <https://morf.lv/implementing-pulse-oximeter-using-max30100>, [Accessed 25 August 2016].
- Stumme, L.D., Baldini, T.H., Jonassen, E.A. and Bach, J.M. (2003). Emissivity of bone. In: *Summer Bioengineering Conference*, pp. 25–29.
- Sund-Levander, M., Forsberg, C. and Wahren, L.K. (2002). Normal oral, rectal, tympanic and axillary body temperature in adult men and women: a systematic literature review. *Scandinavian journal of caring sciences*, vol. 16, no. 2, pp. 122–128.
- Tamura, T., Maeda, Y., Sekine, M. and Yoshida, M. (2014). Wearable photoplethysmographic sensors-past and present. *Electronics*, vol. 3, no. 2, pp. 282–302.
- Tavakoli Dastjerdi, M. (2006). *An analog VLSI front end for pulse oximetry*. Ph.D. thesis, Massachusetts Institute of Technology.

- Thach, B. (2008). Tragic and sudden death. *EMBO reports*, vol. 9, no. 2, pp. 114–118.
- ThermoWorks (2017). Emissivity Table. [Online] Available at: [http://www.thermoworks.com/learning/emissivity\\_table](http://www.thermoworks.com/learning/emissivity_table), [Accessed 7 June 2017].
- Tytler, J. and Seeley, H. (1986). The Nellcor N-101 pulse oximeter. *Anaesthesia*, vol. 41, no. 3, pp. 302–305.
- Wang, I.-J., Liao, L.-D., Wang, Y.-T., Chen, C.-Y., Lin, B.-S., Lu, S.-W. and Lin, C.-T. (2010). A Wearable Mobile Electrocardiogram measurement device with novel dry polymer-based electrodes. pp. 379–384.
- Watthanawisuth, N., Lomas, T., Wisitsoraat, A. and Tuantranont, A. (2010). Wireless wearable pulse oximeter for health monitoring using ZigBee wireless sensor network. In: *Electrical Engineering/Electronics Computer Telecommunications and Information Technology (ECTI-CON), 2010 International Conference on*, pp. 575–579. IEEE.
- Winokur, E.S., Da He, D. and Sodini, C.G. (2012). A wearable vital signs monitor at the ear for continuous heart rate and pulse transit time measurements. In: *Engineering in Medicine and Biology Society (EMBC), 2012 Annual International Conference of the IEEE*, pp. 2724–2727. IEEE.
- World Health Organization (2011). Using the Pulse Oximeter. [Online] Available at: [http://www.who.int/patientsafety/safesurgery/pulse\\_oximetry/who\\_ps\\_pulse\\_oxymetry\\_tutorial2\\_advanced\\_en.pdf?ua=1](http://www.who.int/patientsafety/safesurgery/pulse_oximetry/who_ps_pulse_oxymetry_tutorial2_advanced_en.pdf?ua=1), [Accessed 14 May 2017].
- Yasuma, F. and Hayano, J.-i. (2004). Respiratory sinus arrhythmia: why does the heartbeat synchronize with respiratory rhythm? *Chest Journal*, vol. 125, no. 2, pp. 683–690.
- Zong, W., Heldt, T., Moody, G. and Mark, R. (2003). An open-source algorithm to detect onset of arterial blood pressure pulses. In: *Computers in Cardiology, 2003*, pp. 259–262. IEEE.